



Technische Universität München

Lehrstuhl für Innere Medizin II

Exploring the immune environment of pancreatic ductal adenocarcinoma

FLORIAN NEFF

Vollständiger Abdruck der von der Fakultät für Medizin der Technischen Universität München zur
Erlangung des akademischen Grades eines

DOKTORS DER NATURWISSENSCHAFTEN

genehmigten Dissertation.

Vorsitzender: Prof. Dr. Jürgen Ruland

Prüfer der Dissertation: 1. Prof. Dr. Jens Th. Siveke

2. Prof. Dr. Aphrodite Kapurniotu

Die Dissertation wurde am 21.09.2015 bei der Technischen Universität München eingereicht und
durch die Fakultät für Medizin am 25.02.2016 angenommen.

ABSTRACT

Pancreatic ductal adenocarcinoma (PDAC) ranks amongst the most aggressive cancer diseases remaining incurable to date. Tremendous research efforts have focused primarily on oncogenic signal transduction in malignant cells but failed to successfully translate into better patient prognosis. Hence, alternative approaches are desperately required to open novel therapeutic perspectives, not only to better understand malignant transformation but also to unravel interaction networks linking tumor cells to their stromal framework, the tumor microenvironment. This work aimed to dissect the impact of leukocytic tumor infiltrates, lymphocytes as well as myeloid subpopulations, on tumor development and progression and to identify putative targets for novel treatment approaches.

Oncogenic *Kras*-expressing genetically engineered mouse models (GEMMs) of PDAC were extensively studied regarding immune cell accumulation and the individual functions of specific cellular candidates. 70 % of cells isolated from murine pancreatic tumor masses were identified as leukocytes with myeloid cells being the most frequent ones found. However, potentially tumor preventive tumor-infiltrating lymphocytes (TILs) were also detected in significant amounts. Antibody-mediated depletion and genetic deletion of T and B lymphocytes revealed a fatal non-existence of basal adaptive anti-tumor immunity in PDAC. Moreover, immune checkpoint blockade by therapeutic α -B7H1 (α -PD-L1) treatment and blockade of CCR2-dependent myeloid cell recruitment emerged to be ineffective to unleash anti-tumor immune response in PDAC mice.

M2-polarized tumor-associated macrophages (TAMs) were identified the most prominent immune cell subpopulation in PDAC mice. Here, it was demonstrated, that genetic activation of Notch signaling counteracts M2-polarization of macrophages, not only in vitro but also in mouse models of spontaneous pancreatic cancer, resulting in prolonged survival of GEMMs thus highlighting reeducation of tumor-associated macrophages as a highly promising approach for future cancer immunotherapies.

ZUSAMMENFASSUNG

Das duktales Adenokarzinom des Pankreas (PDAC) zählt zu den aggressivsten und tödlichsten Krebserkrankungen und ist bis heute unheilbar. Erhebliche Forschungsanstrengungen konzentrierten sich bisher primär auf die onkogenen Signalwege maligner Zellen, spiegelten sich aber nicht in einer erheblich verbesserten Prognose für Patienten wider. Daher sind neue Forschungsanstrengungen dringend benötigt - nicht nur um die maligne Transformation nachhaltig zu verstehen, sondern auch um Interaktionsnetzwerke zwischen Tumorzellen und dem Stroma, die „Tumormikroumgebung“, aufzudecken um neue therapeutische Perspektiven zu eröffnen. Diese Arbeit zielte darauf den Einfluss leukozytischer Infiltrate, Lymphozyten und myeloische Subpopulationen auf die Tumorentwicklung und –progression zu untersuchen und mögliche Zielstrukturen für neue Behandlungsmöglichkeiten zu identifizieren.

Genetisch veränderte Mausmodelle des duktales Pankreaskarzinoms wurden auf ihre Immunzellakkumulation sowie Funktion spezifischer Subpopulationen hin untersucht. 70 % der aus murinen Pankreastumoren isolierten Zellen wurden als Leukozyten identifiziert. Von diesen stellten die myeloischen Zellen die größte Gruppe dar. Aber auch potentiell gegen Tumorzellen gerichtete tumorinfiltrierende Lymphozyten (TILs) konnten im Stroma nachgewiesen werden. Antikörpervermittelte Depletion und genetische Deletion von T und B Lymphozyten deckten eine fatale Nicht-existenz einer basalen adaptiven anti-Tumor Immunantwort auf. Darüber hinaus wurde gezeigt, dass „Immun-Checkpoint“ Blockade durch therapeutische α -B7H1 (α -PD-L1) Behandlung sowie Blockade der CCR2-abhängigen Rekrutierung myeloischer Zellen nicht ausreichen um eine anti-Tumor Immunantwort im PDAC Mausmodell zu erzeugen.

M2-polarisierte Tumor-assoziierte Makrophagen (TAMs) wurden als größte Immunzellsubpopulation in PDAC Mäusen identifiziert. Es konnte zudem gezeigt werden, dass genetische Aktivierung des Notch Signalwegs einer M2-Polarisierung von Makrophagen sowohl in vitro als auch in vivo entgegenwirkt und mit verlängertem Überleben einhergeht. Dies hebt das Konzept der Makrophagenrepolarisierung als besonders vielversprechenden Ansatzpunkt künftiger Immuntherapien hervor.

TABLE OF CONTENTS

Abstract.....	i
Table of Contents.....	iii
List of Figures.....	vi
List of Tables.....	viii
Abbreviations.....	ix
1 Introduction	1
1.1 The Pancreas.....	1
1.2 Pancreatic Tumors and Malignancies	2
1.2.1 PDAC-associated Precursor Lesions.....	2
1.2.2 Pancreatic Ductal Adenocarcinoma.....	3
1.3 Tumor-associated Leukocytes.....	5
1.3.1 Tumor-infiltrating Lymphocytes	6
1.3.1.1 B Lymphocytes.....	6
1.3.1.2 T Lymphocytes.....	8
1.3.1.3 Natural Killer Cells.....	10
1.3.2 Tumor-associated Myeloid Cells.....	10
1.3.2.1 Immature Myeloid Cells: MDSCs.....	11
1.3.2.2 Tumor-associated Macrophages: TAMs.....	12
1.3.2.3 Macrophage Polarization.....	13
1.4 The Notch Signaling Pathway.....	16
1.5 Therapeutic antitumor Immune Interventions	19
1.6 Model systems of Pancreatic Cancer.....	22
1.7 Objectives.....	24
2 Materials and Methods	25
2.1 Materials	25
2.1.1 Equipment.....	25
2.1.2 Chemicals and Enzymes.....	27
2.1.3 Buffers and Solutions.....	29
2.1.4 Culture Media.....	29
2.1.5 Primers.....	30
2.1.5.1 Genotyping Primers.....	30
2.1.5.2 qRT-PCR Primers.....	31

2.1.6 Antibodies.....	32
2.1.6.1 FC/FACS Antibodies	32
2.1.6.2 Depleting and Therapeutic Antibodies	32
2.1.6.3 Immunohistochemistry Antibodies	33
2.1.7 Recombinant Proteins and Bioactive Molecules	33
2.1.8 Mouse Strains.....	33
2.1.9 Crossed Mouse Lines.....	34
2.1.10 Software	34
2.2 Methods	35
2.2.1 Isolation, Amplification and Analysis of Nucleic Acids	35
2.2.1.1 Isolation of total RNA from Cells and Tissue.....	35
2.2.1.2 Isolation of genomic DNA from murine Tissue.....	35
2.2.1.3 Primer Design.....	35
2.2.1.4 Reverse Transcriptase Polymerase Chain Reaction	36
2.2.1.5 Quantitative Real-Time Polymerase Chain Reaction.....	36
2.2.1.6 Genotyping PCR	38
2.2.1.7 Agarose Gel Electrophoresis.....	38
2.2.2 Cell Culture Methods.....	39
2.2.2.1 Isolation of Bone Marrow-derived Cells	39
2.2.2.2 Differentiation of Bone Marrow Cells to Macrophages.....	39
2.2.2.3 Induction of Cre-dependent LoxP site Recombination in-vitro.....	40
2.2.2.4 Induction of M1-like Macrophage Polarization	40
2.2.2.5 Induction of M2-like Macrophage Polarization	40
2.2.3 Isolation of Tumor Cells from GEMM tumors.....	40
2.2.4 Flow Cytometry and Fluorescence-activated Cell Sort.....	41
2.2.4.1 Dead/live Cell Discrimination.....	42
2.2.4.2 Extracellular Staining.....	42
2.2.4.3 Intracellular Staining.....	42
2.2.5 Histology.....	43
2.2.5.1 Preparation of Paraffin-embedded Tissue	43
2.2.5.2 Hemalaun & Eosin Staining.....	43
2.2.5.3 Immunohistochemistry	44
2.2.6 Microscopy	44
2.2.6.1 Bright Field Microscopy.....	44
2.2.6.2 Fluorescence Microscopy.....	44
2.2.6.3 Digital Slide Scanning	45
2.2.7 Statistical Data Analysis	45

3 Results	46
3.1 Immune Phenotyping of KP mice	46
3.1.1 Leukocytes are the most abundant cell type in PDAC.....	46
3.1.2 M2-TAMs are predominant in PDAC stroma.....	47
3.1.3 Murine PDAC induces splenic granulocytosis.....	47
3.2 Lymphocytic Contribution to PDAC	50
3.2.1 B cells do not provide effective anti-PDAC immunity.....	50
3.2.2 T cells do not provide effective anti-PDAC immunity.....	52
3.2.3 Rag1 knock out confirms non-existence of adaptive anti-tumor immunity in PDAC.....	53
3.3 Mechanisms of Immune Suppression in KP Mice.....	55
3.3.1 TAMs and B lymphocytes but not tumor cells highly express PD-L1.....	55
3.3.2 PD-L1 blockade is not sufficient to unleash anti-tumor immune response in KP mice...	57
3.3.3 Immune evasion is independent of CCR2 recruitment.....	60
3.3.4 Notch activation counteracts IL4-induced M2 polarization.....	62
3.3.5 Rbpj knock out blocks LPS-induced M1 polarization	66
3.3.6 Notch activation reprograms M2 TAMs in vivo.....	67
4 Discussion	72
4.1 Macrophages dominate PDAC immune environments.....	72
4.2 TILs do not provide effective anti-PDAC immunity.....	75
4.3 Notch activation counteracts M2-TAM polarization.....	77
4.4 Conclusion.....	80
5 Literature.....	81
6 Appendix.....	94

LIST OF FIGURES

Figure 1.1:	The pancreas	1
Figure 1.2:	PanIN and PDAC lineage with potential cells of origin	3
Figure 1.3:	Immune infiltrates in pancreatic cancer	5
Figure 1.4:	Macrophage polarization model	15
Figure 1.5:	The Notch signaling pathway	18
Figure 1.6:	Receptors and ligands of T cell activating and inhibitory signaling..	21
Figure 3.1:	CD45 ⁺ leukocytes are the major cellular component of PDAC.....	46
Figure 3.2:	Immune phenotype of KP tumors: TAMs dominate leukocytic infiltrates.....	48
Figure 3.3:	KP tumors induce splenic granulocytosis and promote B1b cells ...	49
Figure 3.4:	PDAC-infiltrating B cells fail to shape effective anti-tumor immunity	51
Figure 3.5:	PDAC-infiltrating T cells fail to shape effective anti-tumor immunity	52
Figure 3.6:	Genetic T and B cell depletion reveals non-existence of efficient adaptive anti- tumor immunity in PDAC.....	54
Figure 3.7:	PD-L1 is preferentially expressed on B cells and TAMs.....	56
Figure 3.8:	Stromal PD-L1 expression is efficiently targetable in KP tumors.....	57
Figure 3.9:	PD-L1 blockade does not augment anti-tumor T cell response.....	58
Figure 3.10:	PD-L1 blockade promotes B1 B cells but does not affect myeloid cells.....	59
Figure 3.11:	Ccr2 knock out shifts M-MDSCs to G-MDSCs	61
Figure 3.12:	BMDMs provide a powerful platform to study macrophage biology in vitro.....	63
Figure 3.13:	Notch counteracts IL4-driven M2 macrophage polarization in vitro .	64
Figure 3.14:	Notch overexpression does not synergize with LPS in vitro	65
Figure 3.15:	LPS-induced M1 polarization depends on Notch/RBPj signaling	66
Figure 3.16:	Lyz2-Cre directs genetic Notch activation to myeloid cells.....	68
Figure 3.17:	Neither myeloid Notch overexpression nor Rbpj knock out perturb leukocyte development in healthy mice.....	69
Figure 3.18:	Notch signaling antagonizes M2 polarization in PDAC TAMs	70
Figure A.1:	Mouse crossing strategy	94
Figure A.2:	T cell gating strategy	95
Figure A.3:	NK and Treg gating strategy	96

Figure A.4: $\gamma\delta$ T cell gating strategy	97
Figure A.5: B cell gating strategy	98
Figure A.6: Myeloid cell gating strategy	99

LIST OF TABLES

Table 1:	Mechanisms contributing to tumor immune evasion.....	19
Table 2.1:	List of genotyping primers	30
Table 2.2:	List of qRT-PCR primers	31
Table 2.3:	List of FC/FACS antibodies.....	32
Table 2.4:	List of depleting and therapeutic antibodies.	32
Table 2.5:	List of immunohistochemistry antibodies.....	33
Table 2.6:	List of mouse strains.	33
Table 2.7:	List of crossed mouse lines.....	34
Table 2.8:	qRT-PCR cycle conditions.....	37
Table 2.9:	List of qRT-PCR target genes.	37
Table 2.10:	List of genotyping target genes and product sizes.	38
Table 2.11:	Gallios™ Flow Cytometer settings and used dyes.....	42

ABBREVIATIONS

°C	degree Celsius
ADAM17	A disintegrin and metalloprotease 17
ADM	Acinar ductal metaplasia
AFL	Atypical flat lesion
AP	Acute pancreatitis
APC	Allophycocyanin
approx.	approximately
ARG1	Arginase 1
BMDM	Bone marrow-derived macrophages
bp	base pairs
BP	bandpass
BSA	Bovine serum albumin
BTLA	B- and T-lymphocyte attenuator
Ccr2	Chemokine C-C motive receptor 2
CD	cluster of differentiation
cDNA	copy deoxyribonucleic acid
CRE	Causes Recombination
CSL	CBF-1/Su(H)/Lag1
CTL	Cytotoxic T lymphocytes
CTLA4	cytotoxic T-lymphocyte-associated protein 4
Cy	Cyanine
DAPI	Diamidinophenylindole
ddH ₂ O	double distilled water
DII	Delta-like
DMEM	Dulbecco`s Modified Eagle`s Medium
DNA	Deoxyribonucleic acid
dNTP	deoxyribonucleotide triphosphate
DTT	Dithiothreitol
EDTA	Ethylenediaminetetraacetic acid
EpCAM	Epithelial cell adhesion molecule
EtOH	Ethanol
FACS	Fluorescence-activated cell sorting

FC	Flow cytometry
FCS	fetal calf serum
FITC	Fluorescein
FLP	Flippase
FMO	Fluorescence minus one
FOXP3	Forkhead-Box-Protein P3
FRT	Flippase recognition target
FSF	FRT-STOP-FRT
g	gram / gravitational acceleration
GEM	genetically engineered mouse
HCl	Hydrochlorid acid
HLA	Human leukocyte antigen
hr(s)	hour(s)
i.p.	intraperitoneal
IFN γ	Interferon gamma
Ig	Immunoglobulin
IL	Interleukin
iNOS	inducible Nitric oxide synthase
IPMN	Intraductal papillary-mucinous neoplasm
JMJD3	Jumonji Domain Containing 3
k	kilo
KLF4	Krüppel-like factor 4
KRAS	Kirsten Rat Sarcoma Viral Oncogene Homolog
LAG3	Lymphocyte-activation gene 3
LoxP	locus of crossing over, bacteriophage P1
LP	longpass
LPS	Lipopolysaccharide
LSL	LoxP-STOP-LoxP
M	molar
MCN	mucinous cystic neoplasm
MCSF	Macrophage colony stimulating factor
MDSCs	Myeloid-derived suppressor cells
MGL1	Macrophage Galactose-Type Lectin-1
MHC	Major histocompatibility complex

min	minute(s)
MRC1	Mannose receptor 1
mRNA	messenger ribonucleic acid
MSR1	Macrophage scavenger receptor 1
NEAA	non-essential amino acids
NLS	Nuclear localization signal
NOS2	NO synthetase 2
Notch-IC	Notch intracellular domain
o.n.	over night
PanIN	Pancreatic intraepithelial neoplasia
PBS	Phosphate buffered saline
PD-1	Programmed cell death protein 1
PDAC	Pancreatic ductal adenocarcinoma
PD-L1	Programmed death-ligand 1
PDX1	Pancreatic and duodenal homeobox 1
PE	Phycoerythrin
PerCP	Peridinin chlorophyll
PFA	Paraformaldehyde
PI	Propidium iodide
Poly(I:C)	Polyinosinic-polycytidylic acid
PTF1A	Pancreas transcription factor 1 subunit alpha
RAG1	Recombination-activating gene 1
RBPJ	Recombination Signal-binding Protein for Immunoglobulin Kappa J Region
RNA	Ribonucleic acid
RPLPO	ribosomal protein, large, P0
rpm	rounds per minute
RPMI	Roswell Park Memorial Institute medium
RT	room temperature
SD	Standard deviation
sec	second(s)
SOCS	Suppressor of cytokine signaling proteins
TAE	Tris-acetate-EDTA
TAM	Tumor-associated macrophages

TAT	HIV-1 trans-activating protein
TCR	T cell receptor
TGFβ	Transforming growth factor beta
TIM3	T-cell immunoglobulin domain and mucin domain 3
TLR	Toll-like Receptor
TNFα	Tumor necrosis factor alpha
Tris	Tris(hydroxymethyl)aminomethane
TSC	Tenascin
VEGF	Vascular Endothelial Growth Factor
α	anti

1 INTRODUCTION

1.1 The Pancreas

The pancreas is a mixed exocrine-endocrine gland of duodenal origin. It locates in the upper abdominal cavity adjacent to duodenum and spleen. The pancreatic head (*Caput pancreatis*) topographically connects to the duodenum and its tail (*Cauda pancreatis*) to the hilum of the spleen. The pancreatic body (*Corpus pancreatis*) links both head and tail. The hormone and enzyme-producing double functionality of this organ reflects in two histologically distinct cellular compartments. First, the endocrine islets of Langerhans, round-shaped conglomerates of five different cell types required for blood glucose homeostasis and nutrient metabolism: (i) glucagon secreting α -cells (15%), (ii) insulin secreting β -cells (80%), (iii) somatostatin producing δ -cells (5%), (iv) grehlin releasing ϵ -cells, and (v) pancreatic polypeptide secreting PP-cells (2%).

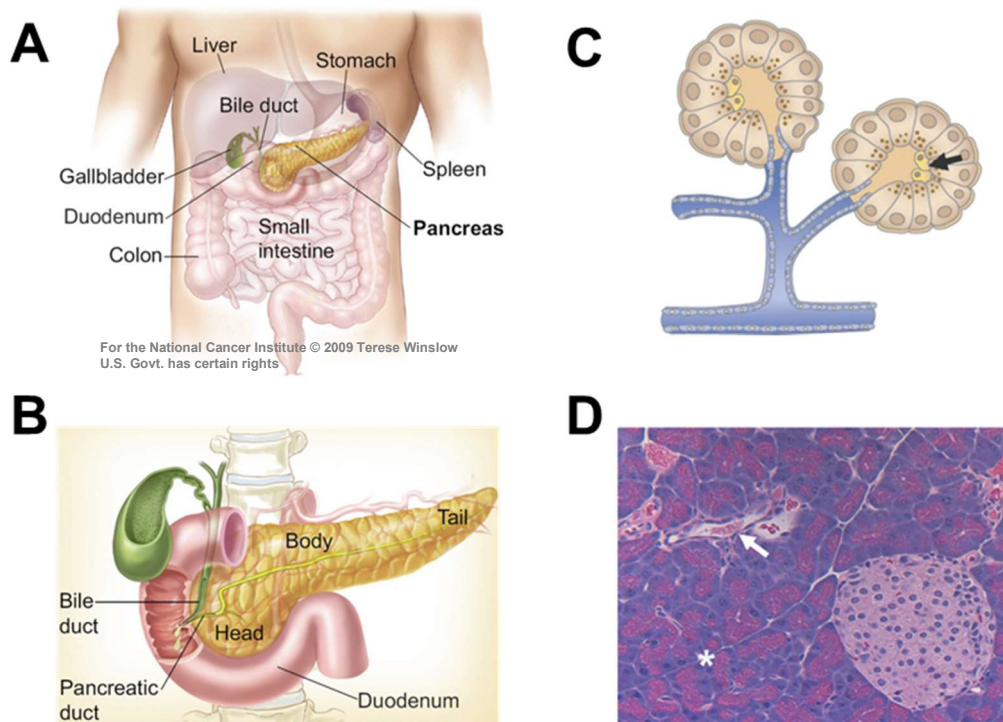


Figure 1.1: The pancreas. (A) Schematic illustration of the gastrointestinal tract in humans. (B) Anatomy of the pancreatic gland and its topographic relation to the adjacent duodenum and bile duct. (C) Organization of acinar cells and their connection to the ductal system. The arrow marks centro-acinar cells. (D) Histology of the murine pancreas presenting an Islet of Langerhans (right), acinar cells (asterix) and a duct (arrow). (A+B Permission kindly provided by T. Winslow; C+D adapted from Hezel et. al., 2009).

Second, the exocrine compartment comprising 90% of the pancreas is characterized by digestive enzymes-producing acinar cells, centro-acinar cells, which share some progenitor-like characteristics, and bicarbonate-secreting ductal cells. The latter allows for neutralization of gastric juice. (Edlund, 2002; Pan and Wright, 2011)

1.2 Pancreatic Tumors and Malignancies

The rich functional and phenotypic variety of pancreatic cell types entails the risk for pathological alterations occurring likewise multifaceted. Besides metabolic diseases (e.g. Diabetes mellitus type 1 and 2), acute and chronic pancreatitis, several types of different neoplasms, distinguishable by their histopathological appearance, are described for the pancreas. Acinar cell carcinoma, pancreatic endocrine tumors including several subtypes, cystic serous and mucinous neoplasms, solid pseudo papillary tumors, squamous cell carcinoma as well as pancreatic lymphoma constitute only a small minority of pancreatic neoplasms (Mulkeen et al., 2006). Of all diagnosed human pancreatic cancers, more than 85 % account for pancreatic ductal adenocarcinoma (PDAC) (Ryan et al., 2014). Therefore, this thesis focuses exclusively on PDAC. The term “pancreatic cancer” will be used synonymously for PDAC from here.

1.2.1 PDAC-associated Precursor Lesions

Three non-invasive precursor lesions that potentially develop to PDAC are broadly accepted although final proof for their transition to the malignant disease is missing: (1) mucinous cystic neoplasm (MCN); (2) intraductal papillary mucinous neoplasm (IPMN); and (3) pancreatic intraepithelial neoplasia (PanIN) (Hezel et al., 2006). The most abundant precursor lesion type, the PanIN lesion, is staged in PanIN1a, PanIN1b, PanIN2, and PanIN3 or newer into low grade (PanIN1 and 2) and high grade (PanIN3) PanIN lesions according to progressive dysplastic epithelial rearrangement accompanied by increasing genetic aberrations and desmoplasia (Bardeesy and DePinho, 2002). PanIN3 is classified as *carcinoma in situ*. Even though the cell of origin remains controversial, growing evidence suggests that ductal cells but also acinar cells undergoing acinar-to-ductal metaplasia (ADM) are likely to be the origin of PDAC (Habbe et al., 2008; Mazur

and Siveke, 2012; Morris et al., 2010a; Morris et al., 2010b). ADM are a common phenomenon in acute pancreatitis and murine tumor models. Additionally, atypical flat lesions (AFL) have been proposed being a further type of precursor lesion originating from the centro-acinar compartment via acinar-to-ductal metaplasia (Aichler et al., 2012). To date the cell of origin as well as the actual sequential transition of metaplastic and dysplastic precursor lesions to PDAC is still under controversial discussion among the scientific community.

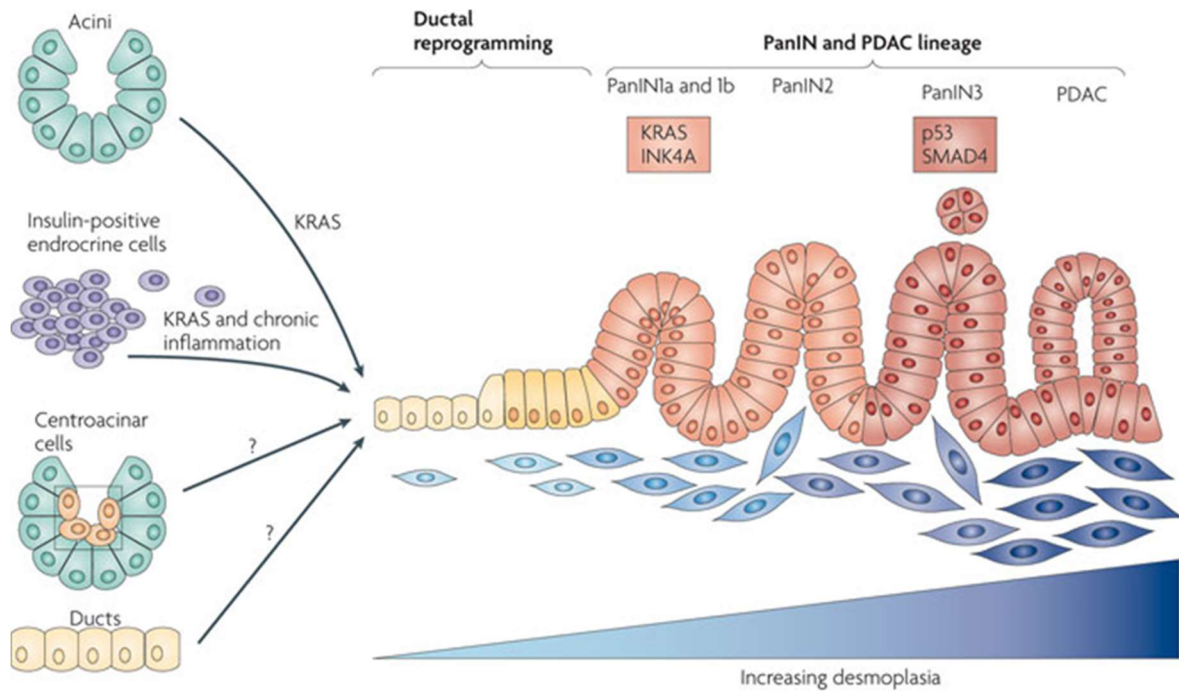


Figure 1.2: PanIN and PDAC lineage with potential cells of origin. Tumor progression model starting from differentiated endocrine or exocrine cell types resulting in pancreatic ductal adenocarcinoma. Oncogenic KRAS is highlighted as the central driver of transformation. Tumor progression is associated with increasing stroma accumulation along with increasing aberrations of epithelial architecture. (from: Morris et al., 2010b)

1.2.2 Pancreatic Ductal Adenocarcinoma

PDAC is the fourth leading cause of cancer mortality in the western world in both men and women (Jemal et al., 2008). Due to late diagnosis, frequent tumor cell dissemination and insufficient therapeutic response, the mean life expectancy is 15-18 months for patients with local and regional disease, and only 3-6 months for patients with metastatic disease. The overall 5-year-survival rate accounts for less than 5% (Vincent et al., 2011). Despite extensive research efforts, neither prognosis nor survival improved significantly during the last 20 years (Siegel et al.,

2012). Recent projections predict PDAC to be the second leading cause of cancer-related death by 2020 (Rahib et al., 2014). Therefore, novel strategies not only for earlier detection but also for more effective treatment are desperately required.

Histologically, the majority of human PDACs are well-differentiated tumors with a duct-like glandular morphology. In some cases, however, tumors form an undifferentiated, uniform cell mass with increased aggressiveness. In addition, pancreatic ductal adenocarcinoma is characterized by two outstanding hallmarks – molecularly and histologically. First, oncogenic *KRAS* mutations are detected nearly universal in advanced human PDAC (Hezel et al., 2006). Animal models with pancreas-specific expression of constitutively active *KRAS* signaling confirmed this oncogenic aberration to be sufficient for driving pancreatic cells to form PanIN lesions and to develop PDAC over time in some cases thus highlighting mutant *KRAS* as the molecular driver of PDAC development (Morris et al., 2010b). Second, from tumor initiation to carcinoma formation, PDAC development is accompanied by a progressive desmoplastic reaction (Bardeesy and DePinho, 2002) forming a highly diverse microenvironment - the stroma, that accommodates multiple different non-neoplastic tumor-associated cells of various types, origins and functions (McAllister and Weinberg, 2014). The stroma forms the extracellular and cellular tissue framework for tumor cells facilitating multiple interaction networks among themselves and cancer cells. Within the stromal compartment (1) mesenchymal cells i.e. cancer-associated fibroblasts (CAF) and pancreatic stellate cells (Hidalgo, 2010) which produce tremendous amounts of extracellular matrix proteins, in particular collagen (Apte et al., 2004; Apte et al., 2013), (2) vascular cells, and (3) infiltrating innate as well as adaptive immune cells are the most prominent ones (Chu et al., 2007). The amount of tumor-associated cells and extracellular deposit exceed the number of malignant tumor cells by far. Moreover, the immense quantities found in PDAC easily outrange those found in most other tumor types (Chu et al., 2007). The stromal compartment was taken into the center of research interests not earlier than during the recent decade. Therefore, we are just at the beginning of understanding the relevance and impact of pancreatic tumor stroma and its individual components during tumor development as well as under treatment conditions. Recent results from different laboratories provide an inconsistent and conflictive picture for pancreatic cancer (Bijlsma and van Laarhoven, 2015; Ozdemir et al., 2014;

Provenzano et al., 2012; Rhim et al., 2014; Vonlaufen et al., 2008) and other solid tumor identities (Hanahan and Coussens, 2012; Mueller and Fusenig, 2004) with regard to tumor stroma interaction.

1.3 Tumor-associated Leukocytes

Remarkably, roughly every second cell within the pancreatic tumor bulk originates from distant sources - from spleen and bone marrow (Clark et al., 2007). Owing to their enormous heterogeneity, infiltrating immune cells, which can easily be distinguished from tumor cells by expression of the pan-leukocyte cell surface marker CD45, appear to act ambivalent (Lakshmi Narendra et al., 2013; Schreiber et al., 2011) and it is subject of current research efforts under which condition they behave like “friend or foe” (Bayne et al., 2012; Beatty et al., 2011; de Visser et al., 2006; Fridman et al., 2012; Hadrup et al., 2013). Spontaneous mouse models of pancreatic cancer revealed that CD45⁺ immune infiltration is progressively accumulating from pre-invasive PanIN stage to PDAC (Clark et al., 2007). The following chapters highlight the most relevant sub-populations but do not claim to be exhaustive.

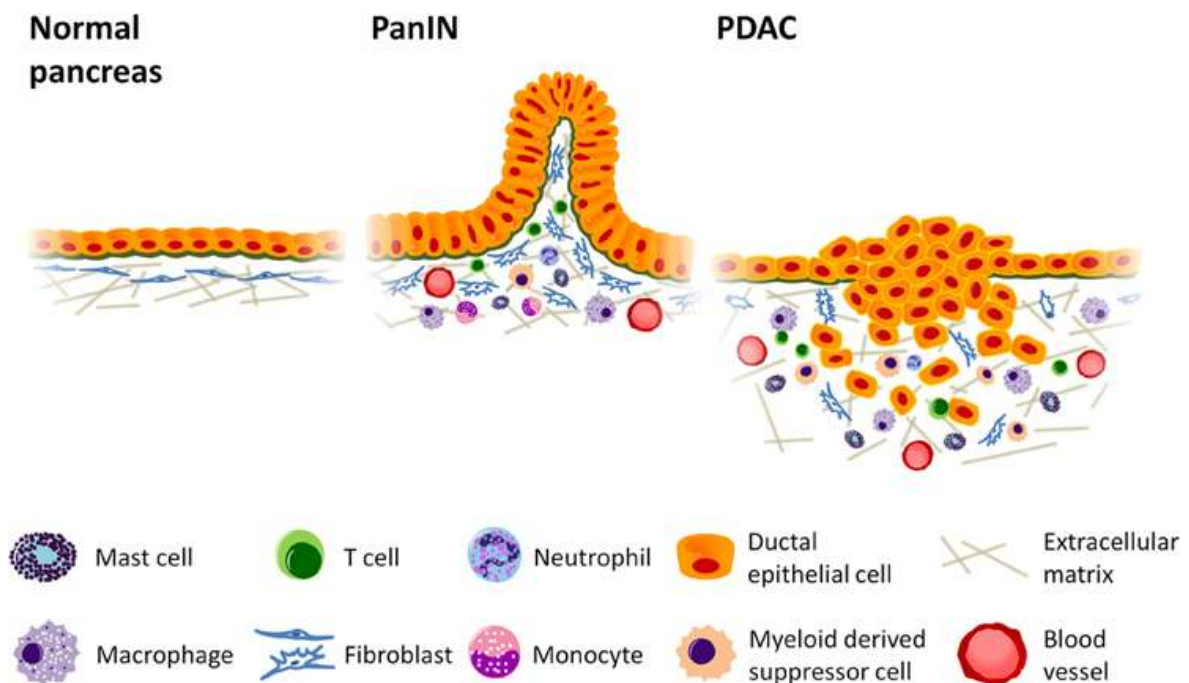


Figure 1.3: Immune infiltrates in pancreatic cancer. PanIN and PDAC formation is characterized by progressive accumulation of various adaptive and innate immune cells and a significant deposit of extracellular matrix proteins. (from: Evans and Costello, 2012)

1.3.1 Tumor-infiltrating Lymphocytes

Both human and murine PDAC are infiltrated by cellular representatives of the adaptive immune system referred to as tumor-infiltrating lymphocytes (TILs) (Clark et al., 2007; von Bernstorff et al., 2001). There is an ongoing debate, whether these infiltrating lymphocytes limit tumor growth by exerting purposive tumor cell killing and whether tumors - pancreatic cancer in particular - are providing sufficient immunogenicity to induce effective adaptive immune response or rather provide an immune privileged compartment (Blankenstein et al., 2012; Gajewski et al., 2013; Garbe et al., 2006; Vonderheide and Bayne, 2013). For a number of tumors there is evidence of robust tumor immunogenicity but the potential adaptive anti-tumor immune activation appears to be frequently prevented or shut down during disease progression by an inhibitory immune suppressive environment even in the presence of tumor antigen (Broz et al., 2014). It should be mentioned as well that TILs not exclusively consist of adaptive immune cells but also comprise a population of lymphocytes belonging to the innate immune system as it will be discussed in the following chapters.

1.3.1.1 B Lymphocytes

B cells (1) hypersecrete immunoglobulins after differentiation into plasma cells, (2) serve as professional antigen-presenters to T_H cells via MHC-II-dependent antigen presentation, (3) act as effector cells secreting a variety of cytokines and lymphotoxins regulating diverse activities of other leukocytes, and (4), may also exert granzyme B/perforin-mediated cytotoxicity (Gunderson and Coussens, 2013; Spaner, 2011). The prognostic relevance of tumor infiltrating B cells presented in current literature is inconsistent and contradictory. On the one hand, there is clear evidence for tumor suppressive B cell activity (DiLillo et al., 2010; Linnebacher and Maletzki, 2012; Nelson, 2010; Spaner, 2011). On the other hand, there is strong data suggesting B cells may even facilitate tumor progression (Affara et al., 2014; Gunderson and Coussens, 2013; Spaner, 2011).

Expression patterns of certain cell surface markers are advantageous to distinguish B cell subsets during developmental stages and in matured subsets. In adults, B cells originate from the bone marrow and functionally mature in secondary lymphoid tissue running through a continuum of developmental stages

(LeBien and Tedder, 2008). The pan-B cell marker CD19 is found on all B cells, from early immature precursors to terminally differentiated plasma cells which form the basis of humoral immunity. CD19 is therefore generally used to distinguish B cells from other lymphocytes. Once maturation and peripheral residence is established, B cells develop into certain subsets with individualized functions that are implicated in the microenvironment of tumors (Gunderson and Coussens, 2013). Whether these subsets derive from the same or distinct progenitors is controversial (LeBien and Tedder, 2008).

B1 cells

B1 cells differ phenotypically from conventional B cells by expression of CD43 and in part CD5. They preferentially reside in the peritoneum rather than the spleen. B1 cells are further sub-classified to B1a (CD5⁺) and B1b (CD5⁻) cells and are considered to be part of the innate immune system by producing natural IgM and IgA. Moreover, B1 cells function as efficient antigen-presenters and T cell activators (Renaudineau et al., 2001). The status of human B1 subclasses and their role in the tumor stroma is insufficiently characterized (LeBien and Tedder, 2008).

B2 cells

Conventional B cells are named B2 cells. In contrast to B1 cells, conventional B cells are double-negative for CD5 and CD43 and the most prominent subtype found in spleen and tumors (LeBien and Tedder, 2008).

B regulatory cells

For many decades, B cells have been investigated exclusively towards their ability to differentiate in antibody secreting cells. In recent years, a growing body of evidence emerged describing immune modulatory functions by secretion of immunosuppressive cytokines: TGF β and IL10 (LeBien and Tedder, 2008). These immune regulatory B cells are denominated B10 or regulatory B cells (B_{reg}). At present, researches could not agree on a specific marker set trustworthily identifying this immunosuppressive B cell subset (Balkwill et al., 2013). Most commonly, however, the phenotyping strategy introduced by Yanaba et al. is applied for murine tissue namely CD19⁺CD5⁺CD1d^{hi} (Yanaba et al., 2008). The

identification in humans is even more controversial (Balkwill et al., 2013). Research investigating regulatory B cell biology was performed primarily in autoimmune disease and chronic inflammatory disease. Their possible role in cancer is mostly unexplored.

1.3.1.2 T Lymphocytes

T cells are thymus-derived lymphocytes sharing the common T cell receptor (TCR) molecule complex CD3 on their cellular surface, which defines the T cell lineage, although certain TCR subunits differ between different T cell subsets. Despite this common marker several T cell subtypes differ or even oppose in function and effector properties. Classically, T cells get activated after engagement of the TCR by MHC-presented antigens and co-stimulatory signaling. Early T cell activation is traceable by CD69 expression. Once an immunological memory is established, T lymphocytes upregulate CD44. Memory T cells respond with greater intensity upon re-exposure to antigens and are usually sub-classified according to their CD62L expression state to effector memory cells (CD44^{hi}CD62L^{low}) or central memory cells (CD44^{hi}CD62L^{hi}). CD44^{low/-}CD62L^{hi} cells are considered naïve, meaning antigen unexperienced.

Cytotoxic T cells

Presence of the CD8 molecule defines cytotoxic T lymphocytes (CTL) which identify tumor cells by MHC-I presented tumor antigens. CTLs are reported to induce tumor cell death by release of granzymes and perforins. Many tumor cells, however, evade this immune response by downregulation of MHC-I (Restifo et al., 2012). Nevertheless, their presence in solid tumors is generally accepted to contribute to a favorable clinical outcome (Fridman et al., 2012; Galon et al., 2006).

T_H1, T_H2 and T_H17 cells

T helper (T_H) cells are characterized by CD4 expression representing a multifunctional subgroup of T cells. T_H1 cells produce interferon- γ , thereby promoting a pro-inflammatory, anti-tumor immune response by activating CTLs and promoting M1-like macrophage polarization. T_H2 cells counteract T_H1-mediated responses by secretion of anti-inflammatory cytokines interleukin 4 and

13. TH17 cells are detectable by expression of interleukin 17. Their specific role in neoplasms is only poorly investigated. Most studies, including those on PDAC, however, point towards a tumor promoting direction (He et al., 2010; McAllister et al., 2014) whereas others provide different evidence (Gnerlich et al., 2010). Refer to an article by Zou and Restifo for detailed review (Zou and Restifo, 2010).

Regulatory T cells

Another CD4⁺ T cell population that has attracted increased attention in recent years is the regulatory T cell (T_{reg}). T_{reg} are discriminated from other CD4⁺ T cells by expression of CD25 and the lineage-defining transcription factor FOXP3 (Schmidt et al., 2012). High tumoral T_{reg} levels are associated with poor prognosis in PDAC (Hiraoka et al., 2006) but may also act tumor-preventive in inflammation-driven carcinogenesis (Gounaris et al., 2009). The immunosuppressive function, however, is undisputed. Via direct cell-cell contact and suppressive cytokine release, regulatory T cells inhibit activation and proliferation of CD4⁺, CD8⁺ T cells, and the majority of other immune cells in the tumor microenvironment (Schmidt et al., 2012; Shevach, 2009). Refer to an article by Zou for detailed review on regulatory T cells in tumor immunity (Zou, 2006).

γδ T cells

A small fraction of T cells (approx. 5% in blood and spleen) express the γδ T cell receptor subunits instead of the αβ subunits like all other T cells and are therefore called γδ T cells (Carding and Egan, 2002). They are described to bridge the adaptive to the innate immune system (Mak and Ferrick, 1998) but their exact functionality remains incompletely understood (Carding and Egan, 2002). The distinctive feature of γδ T cells is MHC-independent non-peptide antigen-dependent activation (Constant et al., 1994; Tanaka et al., 1995; Tanaka et al., 1994). Furthermore, in the context of tumorigenesis γδ T cells are reported to develop a cytotoxic and IFNγ-producing phenotype but also exert regulatory functions by suppressing conventional αβ T cells under certain conditions (Gajewski et al., 2013). For detailed review on TCR diversity the review article by Nickolich-Zugich et al. is highly recommended (Nickolich-Zugich et al., 2004).

1.3.1.3 Natural Killer Cells

In contrast to conventional B and T cells, natural killer (NK) cells belong to a population of innate lymphoid cells. On the one hand, NK cells secrete cytokines such as IFN γ , thus promoting an adaptive T_H1 response. On the other hand, they are capable of identifying tumor cells antigen-independent and to kill those by secretion of cytotoxic mediators such as perforin and granzyme. Natural killer cells possess a wide range of diverse cell surface receptors enabling for identification and attacking of tumor cells which downregulated MHC class I molecules to evade CD8 cytotoxicity – missing-self recognition – and those with upregulated stress-induced ligands – stress-induced self-recognition (Vivier et al., 2012). In experimental models of pancreatic cancer, however, only scarce NK cell infiltrates have been reported (Clark et al., 2007).

Natural killer T cells

Natural killer T (NKT) cells are phenotypically and functionally similar to natural killer cells although they originate from the $\alpha\beta$ T cell lineage. NKT cells express a semi-invariant TCR and diverge during TCR selection from $\alpha\beta$ T cells. They have been classified into four different groups of which type I NKT cells, or invariant NKT cells (iNKT), are the most studied ones. Tumor cells that express CD1d can be directly recognized by iNKT cells and subsequently be eliminated in an NK-like cytotoxic killing procedure. Additionally, iNKT cells mediate indirect antitumor responses via IFN γ production and NK cell activation (Vivier et al., 2012). Clearly, NKT cells show adaptive as well as innate immune features (Sun et al., 2009) and there is at least some evidence for effective killing of pancreatic cancer cells under experimental conditions (Nagaraj et al., 2006).

1.3.2 Tumor-associated Myeloid Cells

All myeloid cells arise from multipotent hematopoietic stem cells in the bone marrow either developing into terminally differentiated mature myeloid cells: macrophages, dendritic (DC) cells, and granulocytes, or remain immature as monocytes or myeloid-derived suppressors cells (Gabrilovich et al., 2012). Myeloid cells are defined as such by expression of integrin- α M (CD11b) which all subsets

express except for some DC subsets. The following chapters will concentrate on the two most significant ones - macrophages and immature myeloid cells. For comprehensive review of all myeloid subsets see (Gabrilovich et al., 2012).

1.3.2.1 Immature Myeloid Cells: MDSCs

Already in the early 19th century, tumor progression was found to be associated with abnormal myeloid cell differentiation and accumulation (Talmadge and Gabrilovich, 2013). These immature cells arising from myeloid progenitors were originally described as veto cells or null cells due to a lack of expression of conventional membrane markers for lymphocytes or macrophages, but were redefined to natural suppressors (NS) later appreciating their functionality as inhibitors of T cell proliferation, antibody response and CTL induction, and, importantly, as suppressors of antitumor immune response and promoters of tumor immune evasion (Talmadge and Gabrilovich, 2013). Nomenclature was diversified again, when increased research efforts identified phenotypic heterogeneity of this cell population introducing the names immature myeloid cells (iMCs) and myeloid suppressor cells (MSCs). The terminology issue reached its final attempt for standardization in 2007, when MDSCs, myeloid-derived suppressor cells, was suggested being the preferable terminology (Gabrilovich et al., 2007) and has been widely accepted since then. Some investigators, however, continue to use the term immature myeloid cells. Although iMC does not reflect the immunosuppressive function and MDSC does not indicate the immature character in their respective terminology, both MDSCs and iMCs comprise identical cellular phenotypes and are consistently identified by their simultaneous expression of GR1 and CD11b in mice (Ostrand-Rosenberg and Sinha, 2009) and a LIN⁻CD11b⁺HLA-DR⁻CD33⁺ phenotype in humans (Gabrilovich et al., 2012).

Two MDSC subsets have been described following their heterogeneity in nuclear morphology and expression patterns of cellular markers despite GR1 and CD11b. First, monocytic-MDSCs (M-MDSCs) showing monocytic morphology and preferential expression of iNOS over arginase 1 are CD11b⁺Ly6G⁻Ly6C^{hi}GR1^{int}F4/80^{low} in mice and CD33⁺CD14⁺HLA-DR^{low/-} in humans. Second, granulocytic, pleomorphnuclear MDSCs (G-MDSCs or PMN-MDSCs), which are CD11b⁺Ly6G⁺Ly6C^{low}GR1^{hi}F4/80⁻ cells and express high levels of arginase 1. The latter is the predominant MDSC population in tumor-bearing mice (Talmadge and

Gabrilovich, 2013). In humans, G-MDSCs are LIN⁻CD11b⁺HLA-DR⁻CD33⁺ and CD15⁺ and/or CD66b⁺ (Gabrilovich et al., 2012).

Myeloid-derived suppressor cells are induced by a variety of inflammatory cytokines and subsequently attracted from the bone marrow to blood and tumor sites where they accumulate and block both innate as well as adaptive antitumor immunity through multiple mechanisms: (1) secretion of IL10 which subsequently promotes M2-like tumor-promotive macrophage polarization, (2) inhibition of CD4⁺ and CD8⁺ T cell activation by sequestering cysteine and L-arginine which is essential for T cell receptor signaling, (3) perturbing T cell homing to lymph nodes by direct cleavage of CD62L on T cells by MDSC surface-bound proteolytic ADAM17 sheddase (Ostrand-Rosenberg, 2010), and (4) antagonizing senescence in cancer cells (Di Mitri et al., 2014).

Throughout various tumor identities, MDSCs were shown to be upregulated in peripheral blood of patients and are generally linked to poor prognosis (Gabitass et al., 2011). There is also a clear implication for MDSCs in pancreatic cancer development and therapy (Gabitass et al., 2011; Greten, 2014; Porembka et al., 2012; Stromnes et al., 2014). Interestingly, the PDAC standard of care chemotherapeutic agent gemcitabine was shown to inhibit MDSC proliferation in lung and mammary cancer mouse models (Suzuki et al., 2005). Human trials on pancreatic cancer, however, showed different results (Greten, 2014). Nevertheless, animal studies have revealed delayed infiltration of MDSCs compared to macrophages with as slight upregulation in pre-invasive lesions but prominent accumulation in the malignant disease (Clark et al., 2007) emphasizing their significance in pancreatic ductal adenocarcinoma.

1.3.2.2 Tumor-associated Macrophages: TAMs

Macrophages are myeloid-derived cells of the innate immune defense. They phagocytose pathogens and dying cells, facilitate tissue remodeling during wound healing, orchestrate inflammation and stimulate adaptive immunity by antigen presentation. In a tumor setting, however, there is a considerable body of evidence that macrophages behave counter intuitive. Instead of destroying tumor cells and triggering antitumor responses by presenting tumor antigens to effector T cells, macrophages, designated as tumor-associated macrophages (TAM) in the tumoral

stroma, rather increase tumor invasion and dissemination, and suppress cancer cell-targeted immune responses suggesting that TAMs promote but not inhibit tumor progression and metastasis (Qian and Pollard, 2010; Sica et al., 2006). Nevertheless, there is at least some evidence that macrophages can kill transformed cells in vitro and may contribute to the early eradication of transformed cells (Mosser and Edwards, 2008).

Accumulation of macrophages is a very early event in the pre-invasive pancreas of genetic PDAC mice (Clark et al., 2007). TAMs can histologically be confused with MDSCs and there is some discussion whether TAMs may develop from MDSCs. But per definition TAMs are defined as mature, differentiated macrophages with a CD11b⁺F4/80⁺GR1^{-low} phenotype and are believed to derive from circulating monocytes. Both tumor-derived chemokines and cytokines are potent attractors for macrophage recruitment e.g. CC-chemokines (CCL2/MCP-1, CCL7, CCL8), vascular endothelial growth factor (VEGF), and macrophage colony stimulating factor (M-CSF) (Sica et al., 2006). Mitchem and colleagues blocked macrophage recruitment in orthotopic tumor mice of pancreatic cancer and revealed an increased antitumor T cell response, inhibition of metastasis and improved chemotherapeutic efficacy (Mitchem et al., 2013). In human PDAC patients, however, Kurahara et al. demonstrated that the absolute amount of TAMs is not predictive for survival after resection but so is their phenotype (Kurahara et al., 2011). High significance of so-called alternatively-activated or M2-polarized macrophages translated in significantly shorter patient survival. One year later another study by a different group confirmed the detrimental connection between M2 macrophages and prognosis in patients of pancreatic cancer. High numbers of M2 macrophages in PDAC patients resulted in larger tumor size, early recurrence of primary tumor and liver metastasis, and shortened survival (Yoshikawa et al., 2012). The concept of macrophage polarization is therefore subject to the next paragraph.

1.3.2.3 Macrophage Polarization

Macrophages are highly heterogeneous and display remarkable plasticity and distinct functions in response to environmental cues (Mosser and Edwards, 2008). Initially, macrophages triggered by bacterial pyrogen lipopolysaccharide (LPS), IFN γ or TNF α were described as potent pro-inflammatory drivers with strong

microbicidal capacity and high expression levels of inflammatory mediators e.g., IL1 β , IL6, IL12, TNFa, and iNOS, thus fully participating in and enhancing T_H1-type immune responses. In this context, T_H1 cells, NK cells, antigen-presenting cells, and bacterial components recognizable by Toll-like receptors (TLRs) are the major inducers of this later named M1 or classically activated macrophages (Mosser and Edwards, 2008; Sica and Mantovani, 2012). Comparable to the microbicidal activity during bacterial infection, M1 macrophages are assigned to tumoricidal capacities in cancer disease (Mosser and Edwards, 2008). De facto, however, M1-polarized macrophages are sparsely seen in tumors. Most TAMs show a squarely different or even opposing phenotype to M1 polarized macrophages earlier mentioned as M2 or alternatively activated macrophage polarization (Sica et al., 2006) that is sharing certain similarities with a third group of polarized macrophages implicated in wound-healing which are beyond the scope of this work. Classical inducers of M2 macrophage polarization are T_H2-type response mediators IL4 and IL13 which were originally considered as macrophage deactivators by downregulation of IL12 and other pro-inflammatory cytokines but emerged as strong upregulators of arginase 1 and 2, mannose receptor 1 (MRC1/CD206), several scavenger receptors, interleukin 10, Fizz1, Mgl1, and polyamines (Gordon, 2003; Sica and Mantovani, 2012; Sica et al., 2006) suggesting a strong immune suppressive and tumor promoting functionality that is also involved in angiogenesis and matrix remodeling presumably facilitating tumor dissemination and inhibition of adaptive T_H1-driven cytotoxic tumor immunity (Gordon and Martinez, 2010; Sica et al., 2006). Thus, accumulation of M2 polarized TAMs ultimately provokes tumor immune evasion.

Macrophage diversity provides severe challenge to tumor immunologists trying to dissect M1/M2 phenotypes in tumor tissue. Immunohistochemical techniques are insufficiently applicable for multi epitope analysis. The technique of choice is therefore generally multi-color flow cytometry. But unstandardized and varying marker panels used in different laboratories for a heterogeneous cell population aggravated comparability of previous research results. Moreover, intracellular effector cytokines are difficult to detect and often-used cell surface markers do not necessarily correlate with functionality. The M1 phenotype is described as CD11b⁺F4/80⁺GR1^{-/low}iNOS⁺IL12⁺CD86⁺MHCII^{hi} in mice, whereas M2

macrophages are defined as $CD11b^+F4/80^+GR1^{-/low}CD206^+CD163^+Arg1^+MHC-II^{low}IL4aR^+IL10^+$ (Gabrilovich et al., 2012).

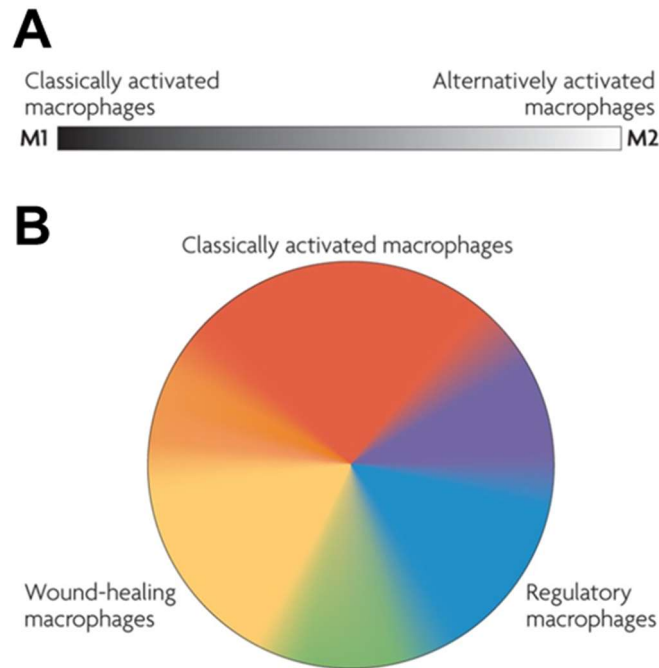


Figure 1.4: Macrophage polarization model. Macrophages display a remarkable variety of phenotypic and functional plasticity. Depending on cytokine milieu macrophages are able to express different or even opposing inflammatory mediators. First classification divided macrophages in classically activated macrophages (M1) or alternatively activated macrophages (M2). To better describe the transient and reversible character of macrophage polarization, the M1/M2 classification was transformed in a continuum of intermediates where M1 and M2 form the two extremes on a scale (A). More recently Mosser and Edwards suggested the color wheel model to better describe the multifaceted macrophage phenotypes in which M2 macrophages became subdivided in wound-healing macrophages and regulatory macrophages allowing for even more potential intermediate phenotypes (B). (from: Mosser and Edwards, 2008)

Clearly, the M1/M2 nomenclature is oversimplified because macrophages rather form a continuum of at least partially reversible intermediate phenotypes than extremes on a virtual M1/M2 scale (see Fig. 1.4) (Mosser and Edwards, 2008). The underlying molecular mechanisms of macrophage polarization and reprogramming are only partially understood but of great interest as they could provide potential starting points for future interventional strategies and novel therapeutic concepts. A considerable amount of transcriptional regulators, however, has been identified. Several groups have identified different regulatory

factors such as KLF4 (Liao et al., 2011), c-MYC (Pello et al., 2012), CRTC3 (Clark et al., 2012), SOCS3 (Qin et al., 2012), the TSC-mTOR pathway (Byles et al., 2013), and epigenetic regulators e.g. JMJD3 (Ishii et al., 2009) all ultimately integrating in IRF/STAT downstream signaling of Toll-like receptors, interferon type I and II receptors, and IL4/IL10/IL13 receptor molecules as reviewed in great detail by Sica and Mantovani (Sica and Mantovani, 2012). Another regulatory pathway important for macrophage polarization to mention is the Notch signaling pathway (Wang et al., 2010).

Notch is a key regulator in many fundamental cell fate decisions including the hematopoietic system (Amsen et al., 2009) and has been shown to be involved in myeloid cell differentiation (Cheng et al., 2014). In 2010, Wang and colleagues proposed Notch to be a master regulator of macrophage polarization (Wang et al., 2010). Two years later Xu et al. provided a mechanistic framework reporting transcriptional repression of M2-associated genes by Notch activation and upregulation of M2-associated genes via posttranslational modification of IRAK2, which is downstream of the LPS receptor TLR4 (Xu et al., 2012). The relevance of these findings to the phenotype of TAMs and its influence on tumor progression was not extensively addressed. The Notch pathway is targeted by various experimental attempts of this thesis. Therefore, the reader is offered a brief summary of the essential factors involved in canonical Notch signaling in the next chapter.

1.4 The Notch Signaling Pathway

The Notch signaling pathway is of major importance not only during development and differentiation of various cell types but also in tissue homeostasis and pathological disorders including malignancies (Andersson and Lendahl, 2014). Its components are evolutionary conserved and function as mediators of short-range cell-cell communication in fly and worm as well as in vertebrates either promoting or suppressing proliferation, cell death, acquisition of specific cell fates, or activation of differentiation (Kopan and Ilagan, 2009). Notch ligands and receptors are type I transmembrane proteins, which require the signaling cell to get in close physical proximity to activate signal transduction. The canonical Notch ligands in

vertebrates, Serrate-like (Jagged1/2) and Delta-like (Dll1, Dll3, and Dll4), differ in protein structure but all share multiple epidermal growth factor (EGF)-like repeats of which the first two are required for receptor binding (D'Souza et al., 2008). Mammals have four Notch receptor paralogs, Notch 1-4. The extracellular domains of all Notch receptors like their ligands contain 29-36 tandem EGF-like repeats of which some interact with ligand proteins. Notch proteins require three consecutive enzymatic cleaves of which the first is conducted ahead of ligand binding in most cases by furin-like convertases converting the Notch polypeptide into a heterodimer held together by non-covalent interactions. Upon ligand binding, Notch receptors are consecutively cleaved (1) extracellularly by an α -secretase complex and (2) intramembranous by the γ -secretase complex releasing the intracellular and transcriptionally active domains (Notch-IC/NIC/NICD) to the cytoplasm. The intracellular domains immediately shuttle to the nucleus where they bind to the DNA binding protein *recombination signal-binding protein 1 j-kappa* (RBPjk) thereby promoting dissociation of transcription repressors at the target gene promoter and activation of target gene expression (e.g. *heary and enhancer of split 1* (Hes1)) after recruitment of co-activating factors. It is important to note, that NICD is incapable of direct DNA-binding. Therefore, down-regulation of RBPjk or its deletion result in block of all canonical Notch-signaling (Kopan and Ilagan, 2009). The nomenclature of RBPjk is sometimes confusing. It is also called RBPj or CBF-1 in humans but was first discovered in drosophila where it is named *suppressor of Hairless* (Su(H)) or Lag1 in *C. elegans*. CSL (CBF-1/Su(H)/Lag1) is a neologism built from the first letter of all three orthologues and is used synonymously.

The above outlined signaling cascade of the Notch signaling pathway is certainly oversimplified but hereby suited to describe the principal molecular mechanisms of Notch signaling sparing the increasing knowledge of additional fine-tuning and regulatory interactions that ultimately allow for the versatile capacity of Notch signaling in variegated processes. For in-depth information on Notch regulation and non-canonical Notch signaling a review by D'Souza and colleagues and a second by Kopan and Ilagan are recommended for further reading (D'Souza et al., 2008; Kopan and Ilagan, 2009).

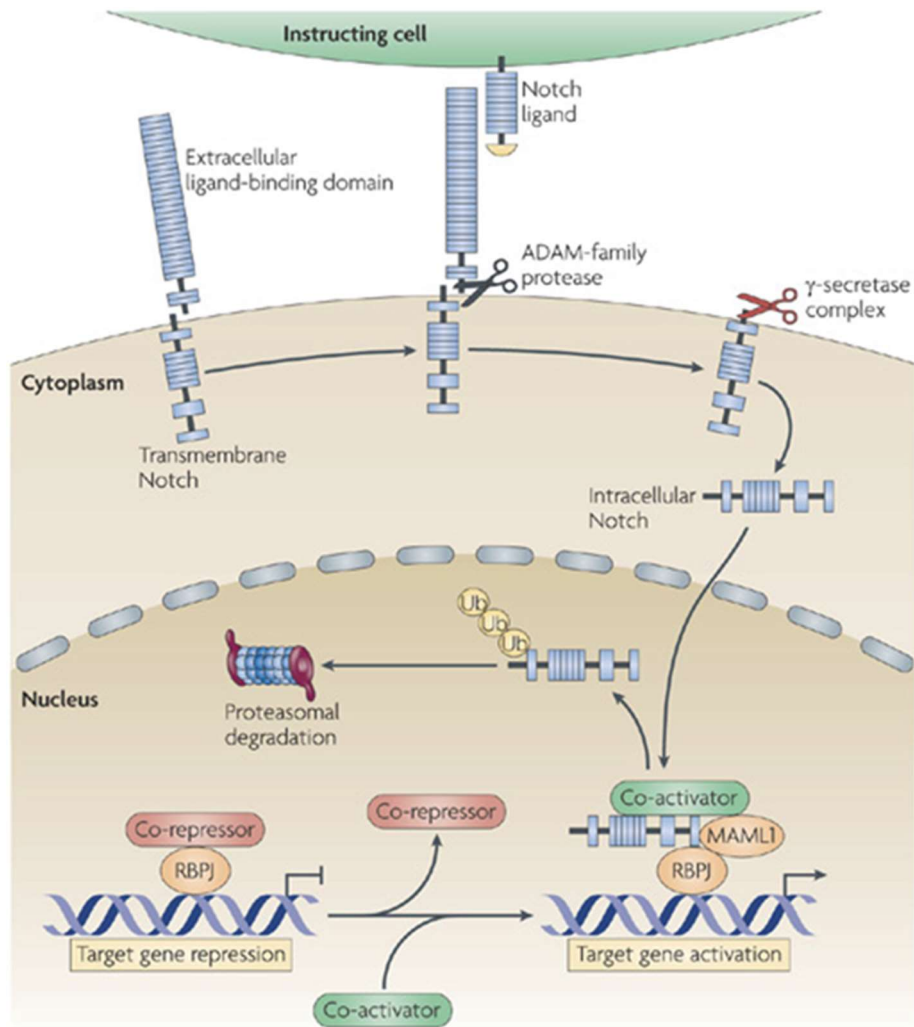


Figure 1.5: The Notch signaling pathway. Schematic description of Notch signaling from ligand binding to target gene activation. Note the central role of RBPj. Notch molecules are a family of transmembrane receptors with extracellular ligand binding domains. Ligand binding provokes consecutive cleavage of Notch receptors and nuclear shuttling of the intracellular Notch domains which subsequently require RBPj to recruit co-activating factors for target gene activation. Notch itself is incapable of direct DNA binding. In the absence of Notch, RBPj recruits transcriptional co-repressors. Notch signaling is temporally controlled by proteasomal degradation. (from Amsen et al., 2009)

1.5 Therapeutic antitumor Immune Interventions

It has already been mentioned that immune suppressive immune infiltrates as well as insufficient tumor immunogenicity are potential contributors to immune attack circumvention. These evasive mechanisms are complemented by a third type of tumor protective mechanisms: the immune checkpoints. All three, either in cooperation or independently, ultimately lead to fatal tumor immune evasion (see Tab. 1).

Immune-responses comprise powerful effector mechanisms designed for killing and eliminating infiltrating pathogens. Fulminant cytotoxic immune activation and sustained inflammation, however, are a potential threat to host tissue. Therefore, inhibitory pathways, the immune checkpoints, tightly regulate duration and amplitude of immune responses and maintain self-tolerance in order to minimize collateral tissue damage and prevent autoimmunity. Thus, immune checkpoints are crucial for effective immunity counterbalancing stimulatory signals when the immune system is responding to pathogenic infections (Pardoll, 2012). In the situation of neoplastic diseases, genetic mutations potentially provoke antigens that help the immune system to distinguish tumor cells from their normal counterparts and to initiate T cell activation specific to those tumor antigens. But there is striking evidence that tumor cells interfere with and misapply immune checkpoint pathways in order to dampen anti-tumor immune responses and to establish immune resistance (Dong et al., 2002; Parsa et al., 2007).

	cellular effectors	molecular effectors
Poor tumor immunogenicity	tumor cells	MHC-I downregulation, non-immunogenic tumor antigens
Immune checkpoint activation	tumor cells CTLs	PDL1 CTLA4, PD1, TIM3, LAG3, BTLA
Suppressive immune infiltrates	MDSCs M2-TAMs T _{H2} T cells T _{reg} B _{reg}	Arginase 1 IL10, arginase 1 IL4, IL13 IL10, TGFβ IL10

Table 1: Mechanisms contributing to tumor immune evasion.

Targeting immune checkpoints to unleash the full potential of anti-tumor immune response has therefore gained great attention during recent years. To date, for melanoma and lung cancer, these research efforts already translated in approval of therapeutic immune checkpoint inhibitors and evaluation in many other tumor types is in advanced stages of clinical trials. The two immune checkpoint molecules that have been most actively studied, *cytotoxic T-lymphocyte-associated antigen 4* (CTLA4/CD152) and *programmed cell death protein 1* (PD1/CD279) are both inhibitory receptors in immune response preferentially expressed on T cells. Blocking antibodies are used to prevent inhibitory receptor activation or to prevent potential ligands from binding. Inhibitory ligands were shown to be expressed on activated T cells, antigen presenting cells, tumor cells and many other cells of the tumor microenvironment (Nguyen and Ohashi, 2015; Pardoll, 2012). A range of B7-family members have been identified to interact with co-stimulatory and counter-regulatory inhibitory checkpoint receptors. This group includes the two known PD1 ligands PD-L1 (also known as B7H1/CD274) and PD-L2 (also known as B7-DC/CD273) of which the first has been reported to be expressed on many different tumor types including pancreatic tumors (Laheru and Jaffee, 2005). Figure 1.6 provides a simplified overview of the most relevant immune checkpoint receptors and their respective ligands but also highlights activating immune pathways involved in modulation of T cell response.

Successful therapeutic application of immune checkpoint inhibitors in melanoma and some other solid tumors were pursued by frustrating results from clinical trials for other tumors like pancreatic and colorectal cancer (Brahmer et al., 2012; Nguyen and Ohashi, 2015; Royal et al., 2010; Topalian et al., 2012) suggesting that more sophisticated combination approaches, which simultaneously target different mechanisms of tumor immune evasion (see Tab. 1), might be required for successful immunotherapies. Individually compiled strategies (1) targeting the immune suppressive microenvironment, (2) blocking immune checkpoints, plus (3) inducing tumor immunogenicity by vaccination open an expanding field of combinatorial possibilities. To avoid random choice or imprudent trial and error, in-depth analysis of tumor and immune cell interactions for each tumor identity is required but to date missing for pancreatic cancer.

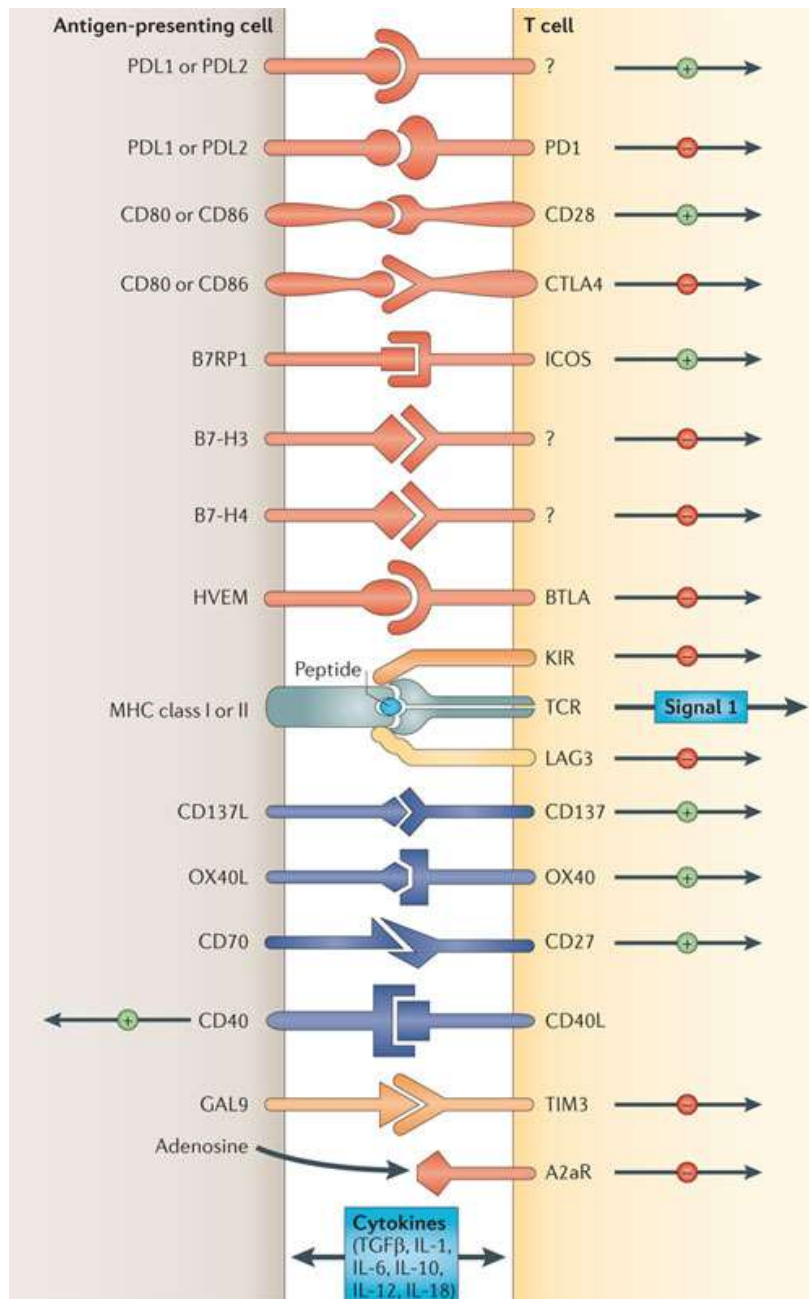


Figure 1.6: Receptors and ligands of T cell activating and inhibitory signaling. Despite MHC class I or II antigen presentation, which is the key trigger of T cell activation, tumor infiltrating T cells experience a complex fine tuning by interacting with antigen-presenting cells, tumor cells, or cells of a suppressive immune environment. Activation of the enormous variety of stimulating or inhibiting signaling mediators is depending on the immune environment and individual tumor characteristics. Inhibitory pathways form a system of immune checkpoints and are of great physiologic importance during prevention of inflammatory overshoot. Tumors frequently divert immune checkpoints from their intended use promoting fatal immune evasion. (from: Pardoll, 2012)

1.6 Model Systems of Pancreatic Cancer

Although significant progress has been achieved in understanding the molecular and cellular mechanisms of PDAC tumorigenesis, promising approaches have not yet translated sufficiently for better patient survival (Siegel et al., 2012). Therefore, highly predictable model systems are required more than ever to unravel key target structures and validate novel therapeutic strategies.

In vitro studies using either patient-derived or mouse PDAC cell lines, primary acinar explants, or even more sophisticated organoid cultures are excellent tools to cost-effectively study tumor genetics, subcellular molecular mechanisms, and to perform cancer cell-targeted drug screens but fail to recapitulate stromal complexity, angiogenesis or immune networks of the tumor microenvironment. Therefore, animal models are indispensable for addressing fundamental research questions justified by the intent to sustainably reduce human suffering. Three different types of in vivo models for pancreatic cancer are currently available: (1) chemical induction, (2) subcutaneous or orthotopic transplantation of tumor cells in rodents, and (3) genetically-engineered mouse models (GEMMs). Xenograft and GEM models are currently considered to best recapitulate human PDAC (Mazur et al., 2015).

Xenograft models use cultured pancreatic cancer cell lines or patient-derived fresh tumor isolates (PDX model) which are either subcutaneously inoculated or orthotopically transplanted in the pancreas of immune-deficient mice. Obviously, these models find a major limitation in the absence of immune infiltrates and loss of the stroma elements, both hallmarks of PDAC (Chu et al., 2007).

Identification of the *Cre/loxP* system in bacteriophage P1 in the early 1980s (Sternberg and Hamilton, 1981) opened a novel tool box for introducing tissue specific mutations, conditional gene knock-out or overexpression, of which researchers now benefit from by a plethora of GEMMs that are available today. For pancreatic cancer, multiple different GEMM lines are described (Mazur and Siveke, 2012) and the number is constantly increasing. The fundamental observation, that *KRAS* is mutated in more than 95% of human PDACs (Hezel et al., 2006), was the major breakthrough in the development of PDAC GEMMs. In one such model, one allele of the endogenous *Kras* locus has been modified to

encode a constitutively active KRAS^{G12D} protein and a regulatory *LoxP-STOP-LoxP* cassette preventing expression in the absence of CRE (Jackson et al., 2001). This *Kras*^{+/*LSL-G12D*} line was subsequently crossed to a mouse line with pancreas-specific expression of *Cre*-recombinase targeting oncogenic *Kras*^{G12D}-expression to pancreatic cells (Hingorani et al., 2003). These mice show PanIN lesions, desmoplasia and invasive PDAC faithfully resembling human disease. The pancreas-specific *Cre*-lines most frequently used are transgenic *Pdx1-Cre* and *Ptf1a/p48*^{Cre} knock-in strains. In the first construct *Cre* expression is under control of the *Pdx1* promoter, which is activated in all pancreatic progenitor cells during pancreatic development. The transgene displays a mosaic expression pattern in pancreatic tissue and off-target expression in the skin (Mazur et al., 2010). The second line, independently generated by two different researches (Kawaguchi et al., 2002; Nakhai et al., 2007), is a heterogeneous knock-in approach which directs *Cre* expression to the endogenous *Ptf1a* promoter accepting loss of one of the two functional alleles. *Ptf1a* is crucial for pancreatic organogenesis, the remaining *Ptf1a* allele, however, is sufficient for normal development. Despite the pancreas, *Ptf1a* is also expressed in the central nervous system and the retina (Nakhai et al., 2007; Obata et al., 2001).

The original model introduced by Hingorani et. al. has been diversified multiple times by addition of further mutations of interest by different laboratories but was always limited in means of simultaneous temporal and spatial control of conditional gene manipulation. Only recently, Schönhuber and colleagues introduced a dual-recombinase approach that drives pancreas-specific *Kras*^{G12D} expression under control of a *PDX1-Flp* transgene (see Fig. A.1 p 94) (Schonhuber et al., 2014). The *Flp/FRT* system acts according to the same principle and mechanism as the *Cre/LoxP* system. The recombinase is named *Flp* and the recombination sites, which differ in their sequence from *LoxP* sites, *FRT* sites providing research the unique opportunity to choose a *Cre*-line to target a second cellular compartment independently of the pancreas. This is a great advantage for approaches investigating stromal contribution to PDAC development as now e.g. myeloid cells become genetically targetable by *Lyz2-Cre* expression (Clausen et al., 1999) in spontaneous PDAC models with clear separation of differential genetic alterations in tumor and an arbitrary second tissue.

1.7 Objectives

Pancreatic ductal adenocarcinoma presents notably stroma-rich tumor masses with the majority of cellular components originating from non-tumor tissues. Among those, innate as well as adaptive immune cell infiltrates account for the predominant proportion. Yet, little is known about the underlying cellular and molecular interaction mechanisms of this tumor microenvironment. Furthermore, recent clinical immunotherapeutic trials failed in pancreatic cancer patients suggesting an even more complex and dubious biology of tumor-stroma cross-talk in PDAC compared to other solid tumors. Therefore, in-depth analysis and explicit mechanistical understanding of PDAC-associated immune cell infiltration is required to vanquish present boundaries and limitations of patient care for those suffering and dying from pancreatic cancer. To achieve this greater goal, immense collective research efforts are required.

This work intends to address four specific research aims. First, to phenotype the immune environment of pancreatic cancer in a spontaneous mouse model by quantitative determination of most relevant leukocytic subpopulations and analysis of their individual activation or effector states. Second, to investigate the specific functionality of tumor-associated B and T lymphocytes in PDAC and their implication in anti-tumor immunity. Third, to explore the impact of CCR2-dependent recruitment on myeloid cell accumulation and pancreatic cancer progression. Finally, to identify novel players and mediators of tumor immune evasion and to unravel targetable mechanisms to overcome immune suppression. The role of Notch signaling in macrophage polarization and its capacity to reprogram tumor-associated macrophages shall be explored exemplarily.

All studies of this work shall be performed in *Kras*^{G12D} GEMMs which most accurately recapitulate human disease not only genetically but also by formation of an extensive fibro-inflammatory stromal reaction phenocopying human PDAC desmoplasia.

2 MATERIALS AND METHODS

2.1 Materials

2.1.1 Equipment

ASP300S dehydrator	Leica GmbH, Solms, D
AxioCam HRc	Carl Zeiss AG, Göttingen, D
AxioCam MRm	Carl Zeiss AG, Göttingen, D
Axio Imager.A1	Carl Zeiss AG, Göttingen, D
Axiovert 200M	Carl Zeiss AG, Göttingen, D
Bond Max IHC Slide Stainer	Leica GmbH, Solms, D
Cell scraper S	TPP AG, Trasadingen, CH
Cell Star stripette 5 ml, 10 ml, 25 ml	Greiner BIO-ONE, Frickenhausen, D
Cellstar® reaction tubes 15 ml	Greiner BIO-ONE, Frickenhausen, D
Cellstar® reaction tubes 50 ml	Greiner BIO-ONE, Frickenhausen, D
Centrifuge 54150	Eppendorf GmbH, Hamburg, D
Centrifuge 5415R	Eppendorf GmbH, Hamburg, D
Centrifuge 5702 R	Eppendorf GmbH, Hamburg, D
Centrifuge 5810	Eppendorf GmbH, Hamburg, D
Drying cabinet	Heraeus GmbH, Hanau, D
Eclipse™ needle 27G x ½	BD, Franklin Lakes, NJ, USA
FACS Aria III	BD Biosciences Inc., New Jersey, USA
Falcon® Nylon mesh 100 µm	Corning Inc., Corning, NY; USA
Falcon® Nylon mesh 40 µm	Corning Inc., Corning, NY; USA
Falcon® petri dish, 10 cm	Corning Inc., Corning, NY; USA
Gallios™ Flow Cytometer	Beckman Coulter, Inc., Brea, CA, USA
Gel Documentation System	Bio-Rad GmbH, München, D
HERA cell 240	Thermo Scientific Inc., Waltham, USA
HERA safe	Thermo Scientific Inc., Waltham, USA
Leica SCN400	Leica GmbH, Solms, D
LightCycler® 480	Roche GmbH, Grenzach-Wyhlen, D
LightCycler® 480 Multiwell Plate 96	Roche Diagnostics GmbH, Mannheim, D
LightCycler® 480 Sealing Foil	Roche Diagnostics GmbH, Mannheim, D

Maxwell® 16	Promega GmbH, Mannheim, D
mC6® foam hood	Waldner GmbH, Wangen, D
Menzel SuperFrost™ Plus Slides	Thermo Scientific Inc., Waltham, USA
Microm HM 355S microtome	Thermo Scientific Inc., Waltham, USA
Microplate, 96 well ELISA U-bottom	Greiner BIO-ONE, Frickenhausen, D
Microvette® serum tube	Sarsted GmbH, Nürnbrecht, D
MR3001 magnetic stirrer	Heidolph GmbH, Schwabach, D
NanoDrop 2000 UV-Vis Spectrophotometer	Thermo Scientific Inc., Waltham, USA
Neubauer improved counting chamber	Marienfeld GmbH, Königshofen, D
Omnifix® 1 ml syringe	B.Braun Melsungen AG, Melsungen, D
Paraffin embedding machine EG 1150 H	Leica GmbH, Solms, D
Petri dish, 5 cm	Greiner BIO-ONE, Frickenhausen, D
Pipetus®	Hirschmann Laborgeräte, Eberstadt, D
Power supply 8E143	Consort
PP-Tubes, 1.3 ml 8.55/44MM	Greiner BIO-ONE, Frickenhausen, D
Primo Star microscope with 4x, 10x, 40x, 100x objectives	Carl Zeiss AG, Göttingen, D
Reaction Tubes 0.5, 1.5, and 2.0 ml	Sarsted GmbH, Nürnbrecht, D
Safe Seal-Tips® professional	Biozym Scientific GmbH, Oldendorf, D
Scalpel No. 23	Feather Safety Razor Co., Ltd, Osaka, J
Silentcrusher M	Heidolph GmbH, Schwabach, D
S-Monovette EDTA K	Sarsted GmbH, Nürnbrecht, D
Sterican® 20 G, 0,9x40mm BL/LB	B.Braun Melsungen AG, Melsungen, D
Sub-Cell® GT electrophoresis cells	Bio-Rad GmbH, München, D
Syringe 10 ml	BD Biosciences Inc., NJ, USA
T100™ Thermal Cycler	Bio-Rad GmbH, München, D
Thermomixer compact	Eppendorf GmbH, Hamburg, D
Timberline balance	Denver Instruments, Bohemia, NY, USA
Vortex-Genie2™	Scientific Industries
Water bath	GFL, Burgwedel, D

2.1.2 Chemicals and Enzymes

0.9 % NaCl, isotonic	B.Braun Melsungen AG, Melsungen, D
Accutase	Sigma-Aldrich GmbH, Steinheim, D
Agarose	Biozym Scientific GmbH, Oldendorf, D
Ammoniac, 25% solution	Merck KgaA, Darmstadt, D
Aqua ad injectabile	B.Braun Melsungen AG, Melsungen, D
ArC™ Amine reactive Bead Kit	Life Technologies Corp., NY, USA
Bond Polymer Refine Detection Kit	Leica GmbH, Solms, D
Collagenase type V	Sigma-Aldrich GmbH, Steinheim, D
DirectPCR-Tail Lysis Buffer	Peqlab GmbH, Erlangen, D
dNTPS	Sigma-Aldrich GmbH, Steinheim, D
Dulbecco's PBS, cell culture grade	Life Technologies Corp., NY, USA
EDTA	Sigma-Aldrich GmbH, Steinheim, D
Eosin	Krankenhausapotheke, MRI, München, D
Ethanol 70 % / 96% / 99,8 %	Krankenhausapotheke, MRI, München, D
FCS	Life Technologies Corp., NY, USA
Fixable Viability Dye eFluor780	eBioscience, San Diego, USA
Foxp3/Transcription Factor Buffer Set	eBioscience, San Diego, USA
Histosec® pastilles	Merck KgaA, Darmstadt, D
Hoechst 33342	Life Technologies Corp., NY, USA
Horse Serum	Biochrom AG, Berlin, D
Hydrochlorid acid, 37%	Sigma-Aldrich GmbH, Steinheim, D
Isofluran CP® 1ml/ml	CP-Pharma, Burgdorf, D
KAPA2G™ Fast HS Genotyping Mix	KAPA Biosciences Inc., Boston, USA
LightCycler® 480 SYBR Green I Master Kit	Roche GmbH, Grenzach-Wyhlen, D
LIVE/DEAD® Fixable Yellow stain	Life Technologies Corp., NY, USA
Maxwell® 16 LEV simplyRNA Tissue Kit	Promega GmbH, Mannheim, D
Mayer's hemalaun solution	Merck KgaA, Darmstadt, D
Na-Pyruvate	Biochrom AG, Berlin, D
Non-Essential Amino Acids	Biochrom AG, Berlin, D
Oligo(dT)15 Primer	Promega GmbH Mannheim, D

OneComp eBeads™	eBioscience, San Diego, USA
Paraformaldehyde 4%, ChemCruz	SantaCruz Biotech., Dallas, TX, USA
Penicillin/Streptomycin	Life Technologies Corp., NY, USA
PeqGOLD DNA Ladder Mix	Peqlab GmbH, Erlangen, D
PERTEX® mounting medium	Medite GmbH, Burgdorf, D
Propidium iodide	Clontech, Mountain View, CA; USA
Proteinase K, PCR Grade	Roche GmbH, Grenzach-Wyhlen, D
RA 1 lysis buffer	Macherey-Nagel GmbH, Düren, D
RBC Lysing Buffer	Sigma-Aldrich GmbH, Steinheim, D
RedTaq® Ready Mix™	Sigma-Aldrich GmbH, Steinheim, D
Rnase ZAP™	Sigma-Aldrich GmbH, Steinheim, D
Roti®-Histol	Carl Roth GmbH, Karlsruhe, D
RPMI-1640 high glucose	Life Technologies Corp., NY, USA
GlutaMAX™	
Saponin	Sigma-Aldrich GmbH, Steinheim, D
SUPERase IN™	Thermo Fisher Scientific, Waltham, USA
SuperScript® II Reverse	Life Technologies Corp., NY, USA
Transcriptase	
Tris-Ultra	Carl Roth GmbH, Karlsruhe, D
Tissue-Tek® O.C.T.™	Hartenstein, Würzburg, D
Trypsin	Life Technologies Corp., NY, USA
VECTASHIELD® mounting medium	Vector Labs Inc., Burlingame, USA
X-TRA-solv®	Medite GmbH, Burgdorf, D
β-mercaptoethanol	Sigma-Aldrich GmbH, Steinheim, D

2.1.3 Buffers and Solutions

Ammoniac water	500ml tap water 40 drops ammoniac
FACS Buffer	D-PBS 2% FCS
HCl-water	500 ml ddH ₂ O 2.5 ml HCl, 37%
Permeabilization buffer	D-PBS 0.5 % w/v Saponin
TAE Buffer, pH8.0	100 ml EDTA, 0.5 M 57.1 ml glacial acetic acid 242 g Tris ddH ₂ O ad 1000 ml
Tissue dissociation medium	RPMI-1640 1 mg/ml Collagenase type V

2.1.4 Culture Media

Macrophage medium	RPMI1640 high glucose GlutaMAX™ 15% FCS 5% Horse Serum 1% Non-Essential Amino Acids 1% Sodium pyruvate 1% Penicillin/Streptomycin
Macrophage differentiation medium	Macrophage medium 50 ng/ml murine M-CSF

2.1.5 Primers

2.1.5.1 Genotyping Primers

Primer	Sequence
Cre001	ACCAGCCAGCTATCAACTCG
Cre002	TTACATTGGTCCAGCCACC
Cre003	CTAGGCCACAGAATTGAAAGATCT
Cre004	GTAGGTGGAAATTCTAGCATCATCC
LysCre1	CTTGGGCTGCCAGAATTTCTC
LysCre2	TTACAGTCGGCCAGGCTGAC
LysCre3	CCCAGAAATGCCAGATTACG
mG_CCR2_mut_f	CTTGGGTGGAGAGGCTATTC
mG_CCR2_mut_r	AGGTGAGATGACAGGAGATC
mG_CCR2_wt_f	CCACAGAATCAAAGGAAATGG
mG_CCR2_wt_r	CCAATGTGATAGAGCCCTGTG
mG_FSF-Kras_4	GCGAAGAGTTTGTCTCAACC
mG_Kras_mut_UP	CCATGGCTTGAGTAAGTCTGC
mG_Kras_URP_Lp1	AGCTAATGGCTCTCAAAGGAATGTA
mG_Kras_wt_UP1	CACCAGCTTCGGCTTCCTATT
mG_p53fret_1	CAAGAGAACTGTGCCTAAGAG
mG_p53fret_2	CTTTCTAACAGCAAAGGCAAGC
mG_p53fret_3	ACTCGTGGAACAGAAACAGGCAGA
mG_Pdx_Flp_1	AGAGAGAAATTGAAACAAGTGCAGGT
mG_Pdx_Flp_2	CGTTGTAAGGGATGATGGTGAAGTC
mG_Rag1_1	AGACACAACGGCTTGCAACACAG
mG_Rag1_2	TGCCGAGAAAGTCCTTCTGCCAG
mG_Rag1_3	GTGGAATGAGTGCGAGGCCAGA
mG_RbpJ-p73	AGTTTAGGCTTTCCAAAAGGC
mG_RbpJ-p74	GTATTGCTAAGAACTTGT
mG_Rosa_Tom_1	AAGGGAGCTGCAGTGGAGTA
mG_Rosa_Tom_2	CCGAAAATCTGTGGGAAGTC
mG_Rosa_Tom_3	GGCATTAAAGCAGCGTATCC
mG_Rosa_Tom_4	CTGTTCTGTACGGCATGG
N2_IC For	CCCTTGCCCTCTATGTACCA
N2_IC Rev	ATCCCGGTCTCCGTATAGTG
p53-loxP-1	CACAAAAACAGGTAAACCCA
p53-loxP-2	AGCACATAGGAGGCAGAGAC

Table 2.1: List of genotyping primers.

2.1.5.2 qRT-PCR Primers

Primer	Sequence
qmArg1_FN_for_1	ATCGGAGCGCCTTTCTCAA
qmArg1_FN_rev_1	GGTCTCTCACGTCATACTCTGT
qmCCR2_FN_for_1	AGGGCATTGGATTCACCACA
qmCCR2_FN_rev_1	AGTATGCCGTGGATGAACTGA
qmCyphy_FN_for_1	ATGGTCAACCCCACCGTGT
qmCyphy_FN_rev_1	TTCTGCTGTCTTTGGAACCTTTGTC
qmF4/80_FN_for_1	CAGGGCAGGGATCTTGGTTA
qmF4/80_FN_rev_1	GCTGCACTCTGTAAGGACACT
qm_Hes1_F	AAAGCCTATCATGGAGAAGAGGCG
qm_Hes1_R	GGAATGCCGGGAGCTATCTTTCTT
qmIL10_FN_for1	AGGCGCTGTCATCGATTCT
qmIL10_FN_rev1	ATGGCCTTGTAGACACCTTGG
qmIL12p35_FN_for_2	TCCCGAAACCTGCTGAAGAC
qmIL12p35_FN_rev_2	CTGGTTTGGTCCCCTGTGAT
qmIL12p40_FN_for_2	GAGTGGGATGTGTCCTCAGAA
qmIL12p40_FN_rev_2	GTCCAGTCCACCTCTACAACA
qmIL1b_FN_for_1	TGCCACCTTTTACAGTGATG
qmIL1b_FN_rev_1	ATGTGCTGCTGCGAGATTTG
qmIL6_FN_for_1	ACTTCACAAGTCGGAGGCTT
qmIL6_FN_rev_1	TGCAAGTGCATCATCGTTGT
qmJmjd3_FN_for_1	CTGTAGCCCATAGGACCCAC
qmJmjd3_FN_rev_1	GTCTCCGCCTCAGTAACAGC
qmMgl1_FN_for_1	GGAAGCCAAGACTTCACACTG
qmMgl1_FN_rev_1	CTGGACGGAAACCAAGACAC
qmMrc1_FN_for_1	AACAAGAATGGTGGGCAGTC
qmMrc1_FN_rev_1	TTTGCAAAGTTGGTTCTCC
qmNos2_FN_for_1	CGTGAAGAAAACCCCTTGTGC
qmNos2_FN_rev_1	GGAACATTCTGTGCTGTCCCA
qmh_XS13_for	TGGGCAAGAACACCATGATG
qmh_XS13_rev	AGTTTCTCCAGAGCTGGGTTGT

Table 2.2: List of qRT-PCR primers.

2.1.6 Antibodies

2.1.6.1 FC/FACS Antibodies

Antigen	Conjugate	Clone	Manufacturer	Species/Isotype	Reactivity
ARG1	APC	polyclonal	R&D	Sheep IgG	Human, Mouse
B7H1(PD-L1)	PE	MIH5	eBioscience	Rat IgG2a	Mouse
CD2	APC	RPA-2.10	eBioscience	Mouse IgG1	Human
CD3ε	PE-Cy™7	145-2C11	eBioscience	Armenian Hamster IgG	Mouse
CD4	eFluor 450	GK1.5	eBioscience	Rat IgG2b	Mouse
	BD Horizon™ V450	RM4-5	BD Bioscience	Rat IgG2a	Mouse
CD5	PE	53-7.3	eBioscience	Rat IgG2a	Mouse
CD8a	FITC	53-6.7	eBioscience	Rat IgG2a	Mouse
	PerCP-Cy™5.5	53-6.7	BD Bioscience	Rat IgG2a	Mouse
CD11b	eFluor 450	M1/70	eBioscience	Rat IgG2b	Mouse
CD11c	APC	N418	eBioscience	Armenian Hamster IgG	Mouse
CD16/CD32	-	2.4G2	BD Bioscience		Mouse
CD19	APC	1D3	eBioscience	Rat IgG2a	Mouse
CD25	PE	PC61.5	eBioscience	Rat IgG1	Mouse
	PerCP-Cy™5.5	PC	BD Bioscience	Rat IgG1	Mouse
CD43	FITC	eBioR2/60	eBioscience	Rat IgM	Mouse
CD44	FITC	IM7	BD Bioscience	Rat IgG2b	Mouse
CD45	FITC, Alexa Fluor 700	30-F11	eBioscience	Rat IgG2b	Mouse
CD62L	APC	MEL-14	BD Bioscience	Rat IgG2a	Mouse
CD69	FITC	H1.2F3	BD Bioscience	Armenian Hamster IgG1	Mouse
CD138	PE-Cy™7	281-2	BioLegend	Rat IgG2a	Mouse
CD206	FITC, PerCP-Cy™5.5	C068C2	BioLegend	Rat IgG2a	Mouse
EpCAM	APC; PE	G8.8	eBioscience	Rat IgG2a	Mouse
F4/80	FITC, eFluor 450, PE-eFluor610	BM8	eBioscience	Rat IgG2a	Mouse
FOXP3	APC	FJK-16s	eBioscience	Rat IgG2a	Mouse, Rat
γδTCR	PE	eBioGL3	eBioscience	Armenian Hamster IgG	Mouse
IgM	eFluor 450	15F9	eBioscience	Rat IgG2a	Mouse
Ly6C	Alexa Fluor 488	HK1.4	eBioscience	Rat IgG2c	Mouse
Ly6G	APC	1A8-Ly6g	eBioscience	Rat IgG2a	Mouse
Ly6G (GR-1)	PE-Cy™7	RB6-8C5	eBioscience	Rat IgG2b	Mouse
NK1.1	PE	PK136	BD Bioscience	Mouse IgG2a	Mouse
NOS2	PE	CXNFT	eBioscience	Rat IgG2a	Mouse

Table 2.3: List of FC/FACS antibodies.

2.1.6.2 Depleting and Therapeutic Antibodies

Antibody	Clone	Manufacturer	Species/Isotype	Reactivity
<i>InVivo</i> Mab anti m Thy-1.2	30H12	BioXCell	Rat IgG2b	Mouse
<i>InVivo</i> Mab Rat IgG2b	LTF-2	BioXCell	Rat IgG2b	-
anti-CD20	18B12-5C2	Genentech	ms IgG2a	Mouse
IgG2a isotype control	2BS	Genentech	ms IgG2a	-
B7H1 (PD-L1)	MIH5	eBioscience	Rat IgG2a	Mouse

Table 2.4: List of depleting and therapeutic antibodies.

2.1.6.3 Immunohistochemistry Antibodies

Antigen	Clone	Manufacturer	Species/Isotype	Reactivity	Diltution
B220	RA3-6B2	BP Pharmingen	Rat IgG2a	Human, Mouse	1:3000
CD3	SP7	Zyted	Rabbit IgG	Human, Mouse	1:250
CD4	4SM95	eBioscience	Rat IgG1	Mouse	1:1000
CD45	30-F11	BP Pharmingen	Rat IgG2b	Mouse	1:300
F4/80	BM8	BMA Biomedicals	Rat IgG2a	Human, Mouse	1:120

Table 2.5: List of immunohistochemistry antibodies.

2.1.7 Recombinant Proteins and Bioactive Molecules

His-TAT-NLS-CRE	MPI of Biochemistry, Martinsried, D
IL4, murine	eBioscience, San Diego, CA, USA
LPS	Sigma-Aldrich, St. Louis, MO, USA
MCSF, murine	PELOBiotech, Martinsried, D

2.1.8 Mouse Strains

Gene	Genetic modification	Strain	Reference
<i>Ccr2</i>	deletion	<i>Ccr2^{tm1Ifc}</i>	(Boring et al., 1997)
<i>Rag1</i>	deletion	<i>Rag1^{tm1Mom}</i>	(Mombaerts et al., 1992)
<i>Rbpj</i>	<i>LoxP</i> -site knock-in	<i>Rbpj^{tm1Rsch}</i>	(Nakhai et al., 2008)
<i>Kras</i>	LSL-KrasG12D knock-in	<i>Kras^{tm4Tyj}</i>	(Jackson et al., 2001)
<i>Kras</i>	FSF-KrasG12D knock-in	<i>Kras^{tm1Dsa}</i>	(Schonhuber et al., 2014)
<i>Trp53</i>	<i>LoxP</i> -sites knock-in	<i>Trp53^{tm1Bm}</i>	(Marino et al., 2000)
<i>Trp53</i>	<i>FRT</i> -sites knock-in	<i>Trp53^{tm1.1Dgk}</i>	(Lee et al., 2012)
<i>Lyz2</i>	<i>Cre</i> knock-in	<i>Lyz2^{tm1(cre)lfo}</i>	(Clausen et al., 1999)
<i>Ptf1a</i>	<i>Cre</i> knock-in	<i>Ptf1a^{tm1(cre)Hnak}</i>	(Nakhai et al., 2007)
Pdx1-Flp	transgene	<i>Tg(Pdx1-flpo)^{Dsa}</i>	(Schonhuber et al., 2014)
Notch2	Rosa26 knock-in	<i>Gt(ROSA)26Sor^{tm2(CAG-Notch2*)Uzs}</i>	(Hampel et al., 2011)
tdTomato	Rosa26 knock-in	<i>Gt(ROSA)26Sor^{tm9(CAG-tdTomato)Hze}</i>	(Madisen et al., 2010)

Table 2.6: List of mouse strains.

2.1.9 Crossed Mouse Lines

Line	Genotype
KP	<i>Ptf1a</i> ^{+Cre} ; <i>Kras</i> ^{+LSL-G12D} ; <i>p53</i> ^{fl/fl}
KP ^{het}	<i>Ptf1a</i> ^{+Cre} ; <i>Kras</i> ^{+LSL-G12D} ; <i>p53</i> ^{+fl}
KP ^{het} ; <i>Rag1</i> ^{null}	<i>Ptf1a</i> ^{+Cre} ; <i>Kras</i> ^{+LSL-G12D} ; <i>p53</i> ^{+fl} ; <i>Rag1</i> ^{-/-}
KP; <i>Rag1</i> ^{null}	<i>Ptf1a</i> ^{+Cre} ; <i>Kras</i> ^{+LSL-G12D} ; <i>p53</i> ^{fl/fl} ; <i>Rag1</i> ^{-/-}
KP ^{het} ; <i>Ccr2</i> ^{null}	<i>Ptf1a</i> ^{+Cre} ; <i>Kras</i> ^{+LSL-G12D} ; <i>p53</i> ^{+fl} ; <i>Ccr2</i> ^{-/-}
KP; <i>Ccr2</i> ^{null}	<i>Ptf1a</i> ^{+Cre} ; <i>Kras</i> ^{+LSL-G12D} ; <i>p53</i> ^{fl/fl} ; <i>Ccr2</i> ^{-/-}
KP ^{flp,het} ; <i>Lyz2</i> ; <i>N2IC</i>	<i>Pdx1-Flp</i> ; <i>Kras</i> ^{+FSF-G12D} ; <i>p53</i> ^{+frt} ; <i>Lyz2</i> ^{+Cre} ; <i>Rosa26</i> ^{+LSL-Notch2-IC}
KP ^{flp} ; <i>Lyz2</i> ; <i>N2IC</i>	<i>Pdx1-Flp</i> ; <i>Kras</i> ^{+FSF-G12D} ; <i>p53</i> ^{frt/frt} ; <i>Lyz2</i> ^{+Cre} ; <i>Rosa26</i> ^{+LSL-Notch2-IC}
KP ^{flp,het} ; <i>Lyz2</i> ; <i>Rbpj</i>	<i>Pdx1-Flp</i> ; <i>Kras</i> ^{+FSF-G12D} ; <i>p53</i> ^{+frt} ; <i>Lyz2</i> ^{+Cre} ; <i>Rbpj</i> ^{fl/fl} ; <i>Rosa26</i> ^{+LSL-tdTomato}
KP ^{flp} ; <i>Lyz2</i> ; <i>Rbpj</i>	<i>Pdx1-Flp</i> ; <i>Kras</i> ^{+FSF-G12D} ; <i>p53</i> ^{frt/frt} ; <i>Lyz2</i> ^{+Cre} ; <i>Rbpj</i> ^{fl/fl} ; <i>Rosa26</i> ^{+LSL-tdTomato}

Table 2.7: List of crossed mouse lines.

2.1.10 Software

Axio Vision 4.8.1.0	Carl Zeiss AG, Göttingen, D
Digital Image Hub	Leica Microsystems, Nussloch, D
FACSDiva™ 7.0	BD Biosciences Inc., NJ, USA
FlowJo 7.5.5	Tree Star Inc., Ashland, OR, USA
LightCycler® 480 1.5.0, SP4, 2008	Roche, Basel, CH
NanoDrop 200 1.4.1, 2009	Thermo Scientific Inc, Waltham, MA, USA
Prism 5.0	GraphPad Software, Inc., La Jolla, CA, USA
Quantity One 4.5.2	Bio-Rad GmbH, München, D

2.2 Methods

2.2.1 Isolation, Amplification and Analysis of Nucleic Acids

2.2.1.1 Isolation of total RNA from Cells and Tissue

Cultured macrophages as well as tumor tissues were lysed in RA1 lysis buffer containing 1 % of β -mercaptoethanol in order to isolate total RNA. Cultured cells were washed twice with pre-chilled PBS before lysis and removed from cell culture dishes with a cell scraper. During necropsy, two small pieces were cut off the tumor with a scalpel and immediately homogenized in 600 μ l lysis buffer containing β -mercaptoethanol by vigorous shredding using the Heidolph Silentcrusher M. Lysates were immediately shock-frozen in liquid nitrogen and stored at -80°C . Total RNA was purified from 300 μ l lysate using the Promega Maxwell[®] 16 system according to the manufacture's manual including DNaseI digestion. The purified RNA was subsequently stored at -80°C until further analysis. To avoid sample contamination with RNAses, technical equipment and working space were cleaned with RNaseZAP[™] before RNA isolation was performed.

2.2.1.2 Isolation of genomic DNA from murine Tissue

Genomic DNA was isolated from mouse tail tips or ear punches for genotyping. Mouse biopsies were incubated in 200 μ l DirectPCR-Tail Lysis Buffer with 10 μ l Proteinase K at 55°C for 4 hours or o.n on a shaker at 600 rpm. Subsequently the enzyme was heat-inactivated at 85°C for 45 min and lysates were centrifuged for 1 min at full speed in a bench top centrifuge. Supernatant was used without further dilution for genotyping PCR or stored at 4°C for later analysis.

2.2.1.3 Primer Design

Primers for qRT-PCRs were designed using the NCBI Primer Blast website available at www.ncbi.nlm.nih.gov/tools/primer-blast and purchased from Eurofins MWG Operon GmbH, Ebersberg. Exon junction-spanning primer pairs were preferred whenever possible. The PCR products were designed with a size of ~ 100 bp. Lyophilised primers were dissolved in ddH₂O to a stock concentration of 100 μM .

2.2.1.4 Reverse Transcriptase Polymerase Chain Reaction

Purified RNA was reversely transcribed to cDNA by Superscript® II according to the manufacture's protocol. A Nanodrop UV-Vis spectrophotometer was used to determine the concentration of isolated RNA. To ensure equal input, RNAs were diluted in ddH₂O to equalize RNA amounts in each experiment. Two to three µg of purified RNA were used in a 20 µl reaction. 1 µl Oligo-(dT)₁₅ primers (500 µg/ml) were used to initialize reverse transcription and allowed for specific mRNA transcription. 1 µl of a dNTP mix (10 mM each) was added to the reaction mix which was subsequently incubated for 5 min at 60 °C to separate double-stranded loops and chilled on ice afterwards. Then, 4 µl First-Strand Buffer, 2 µl 0.1 M DTT and 1 µl RNaseOUT™ (40 units) or SUPERase IN™ (20 units) were added and annealing was performed for 5 min at 42 °C. Subsequently 200 units (1 µl) of SuperScript™ II were added and cDNA was synthesized at 42 °C for 50 min. Finally, the enzyme got inactivated by incubating the reaction mix for 15 min at 70 °C. The cDNAs were stored at -20 °C or immediately analyzed for target gene expression using qRT-PCRs.

2.2.1.5 Quantitative Real-Time Polymerase Chain Reaction

Quantification of gene expression was done by quantitative real-time (qRT) PCR on a Roche LightCycler® 480 using the LightCycler® 480 SYBR Green I Master Kit in a 96 well format. First, cDNA was diluted 1:4 in ddH₂O. 4 µl of the cDNA dilution were added per reaction. Second, primer pairs were combined in a 0.5 µM stock solution, of which 6 µl were added to each reaction (0.15 µM final concentration). Finally, 10 µl of 2X SYBR Green I Master Mix were added to every reaction completing a 20 µl reaction mix. The plate was sealed with a foil and spun down for 30 s. All real time PCR experiments were run under 58° C annealing condition and amplification was run for 45 cycles. A melting curve was implemented in each experiment to prove single product amplification. For detailed cyclor settings see Tab. 2.8. Data was analyzed using ΔC_t calculations where RPLP0 or cyclophilin A served as house keeper control for normalization. The amplification efficiency was experimentally determined or assumed as 2 (doubling each cycle). Relative mRNA expression levels compared to house keeper gene expression ($\text{efficiency}^{-\Delta C_t}$) were used for visualization when not stated differently.

	Temp.	Duration	Ramp rate
Preincubation	95 °C	5 min	4.4 °C/s
	95 °C	20 s	4.4 °C/s
Amplification (45 cycles)	58 °C	20 s	2.2 °C/s
	72 °C	20 s	4.4 °C/s
Melting curve	95 °C	5 min	4.4 °C/s
	65 °C	1 min	2.2 °C/s
	97 °C	contin.	0.1 °C/s
Cooling	37 °C	30 s	

Table 2.8: qRT-PCR cycle conditions.

Target Gene	Primer	Product size
<i>Arg1</i>	qmArg1_FN_for_1, qmArg1_FN_rev_1	118 bp
<i>Ccr2</i>	qmCCR2_FN_for_1, qmCCR2_FN_rev_1	112 bp
<i>Cyclophilin A</i>	qmCyphy_FN_for_1, qmCyphy_FN_rev_1	102 bp
<i>F4/80</i>	qmF4/80_FN_for_1, qmF4/80_FN_rev_1	113 bp
<i>Hes1</i>	qm_Hes1_F, qm_Hes1_R	106 bp
<i>IL12a (p35)</i>	qmIL12p35_FN_for_2, mIL12p35_FN_rev_2	119 bp
<i>IL12b (p40)</i>	qmIL12p40_FN_for_2, qmIL12p40_FN_rev_2	120 bp
<i>IL1β</i>	qmIL1b_FN_for_1, qmIL1b_FN_rev_1	136 bp
<i>IL6</i>	qmIL6_FN_for_1, qmIL6_FN_rev_1	111 bp
<i>Jmjd3 (Kdm6b)</i>	qmJmjd3_FN_for_1, qmJmjd3_FN_rev_1	108 bp
<i>Mgl1</i>	qmMgl1_FN_for_1, qmMgl1_FN_rev_1	111 bp
<i>Mrc1 (CD206)</i>	qmMrc1_FN_for_1, qmMrc1_FN_rev_1	128 bp
<i>Nos2</i>	qmNos2_FN_for_1, qmNos2_FN_rev_1	108 bp
<i>RPLP0</i>	qmh_XS13_for, qmh_XS13_rev	70 bp

Table 2.9: List of qRT-PCR target genes.

2.2.1.6 Genotyping PCR

Genetically engineered mice were genotype from lysed biopsies obtained from ear punches or tail tips at an average age of three weeks. 1 µl of genomic DNA lysate was added to a 20 µl PCR reaction containing each primer at 0.5 µM and 10 µl of either 2X RedTaq® Ready Mix™ (*Ptf1a^{Cre}*, *Kras^{LSL-G12D}*) or 2X KAPA2G Fast HS Genotyping Mix (all other alleles). A routine PCR program was performed with an initial DNA denaturation for 5 min at 95 °C and 38 subsequent cycles comprising 30 s denaturation at 95 °C, annealing for 30 s at 58 °C, and prolongation for 1 min at 72 °C.

Target Gene	Primer	Product wildtype	Product mutated
<i>Ccr2</i>	mG_CCR2_wt_f, mG_CCR2_wt_r, mG_CCR2_mut_f, mG_CCR2_mut_r	424 bp	280 bp
<i>Kras^{FSF-G12D}</i>	mG_Kras_WT_UP1, mG_Kras_URP_Lp1, mG_FSF-Kras_4	351 bp	270 bp
<i>Kras^{LSL-G12D}</i>	mG_Kras_wt_UP1, mG_Kras_URP_Lp1, G_Kras_mut_UP	280 bp	180 bp
<i>LSL-N2IC</i>	N2_IC For, N2_IC Rev	-	460 bp
<i>LSL-tdTomato</i>	mG_Rosa_Tom_1, mG_Rosa_Tom_2, mG_Rosa_Tom_3, mG_Rosa_Tom_4	297 bp	196 bp
<i>Lyz2^{Cre}</i>	LysCre1, LysCre2, LysCre3	350 bp	750 bp
<i>p53^{fl}</i>	p53-loxP-1, p53-loxP-2	288 bp	332 bp
<i>p53^{fret}</i>	mG_p53fret_1, mG_p53fret_2, mG-p53fret_3	258 bp	292 bp
<i>Pdx1-Flp</i>	mG_Pdx_Flp_1, mG_Pdx_Flp_2	-	620 bp
<i>Ptf1a^{Cre}</i>	Cre001, Cre002, Cre003, Cre004	324 bp	199 bp
<i>Rag1</i>	mG_Rag1_1, mG_Rag1_2, mG_Rag1_3	400 bp	300 bp
<i>Rbpj^{fl}</i>	mG_RbpJ-p73, mG_RbpJ-p74	520 bp	540 bp

Table 2.10: List of genotyping target genes and product sizes.

2.2.1.7 Agarose Gel Electrophoresis

To visualize amplified DNA fragments, genotyping PCR products were separated in a 2 % agarose/TAE buffer gel electrophoresis. 5 µl of a 1 mg/ml ethidium bromide solution were added per 100 ml gel to visualize DNA. 15 µl per sample of genotyping PCR reaction were added to a single comb pocket on the agarose gel. The approximate size of amplified DNA fragments was determined by running 10 µl of peqGOLD DNA Ladder Mix in each sample row. The chamber of a Bio-Rad Sub-Cell® chamber was filled with 1X TAE buffer and samples were separated by 100 V to 140 V. The DNA fragments were visualized under UV light and photographed in a Bio-Rad gel documentation chamber.

2.2.2 Cell Culture Methods

2.2.2.1 Isolation of Bone Marrow-derived Cells

Bone marrow was isolated from *femur* and *tibia* of mice aged between 6 and 12 weeks. Mice were anesthetized by isofluran inhalation and killed by cervical dislocation. The fur was sprayed with 70 % ethanol and a scissor was subsequently used to incise the abdominal skin while avoiding laceration of the parietal peritoneum. The fur was fully removed from the mouse body by pulling both incision margins in cranial and caudal direction. Claws, muscle tissue and *fibulae* were removed and the dissected *femur* and *tibia* were separated from the hip joint using a scissor cranial of the *trochanter maior*. Dissected bones were collected in pre-chilled PBS on ice. Afterwards the bone marrow was washed out of the bones with 5 ml pre-chilled RPMI using a syringe with an appropriately sized needle and adequate pressure. The tissue was collected in 50 ml reaction tubes on ice and dissociated by passing several times through a 20 G needle until no visible clumps remained. The supernatant was removed after spinning 5 min at 300 g, 4°C and the pellet got re-suspended in 1 ml Red Blood Cell Lysing Buffer. After incubation for 5 min at RT samples were centrifuged again under the same conditions but re-suspended in Macrophage medium containing 50 ng/ml murine M-CSF. The volume was adjusted according to the intended final cell number per dish. Cells were plated on 10 cm petri dishes to final numbers of 5×10^6 cells per dish after cell counting or bone marrow isolated from one animal was spread on 5 petri dishes alternatively.

2.2.2.2 Differentiation of Bone Marrow Cells to Macrophages

Freshly isolated bone marrow cells were differentiated to macrophages by maintaining in culture with 50 ng/ml of murine M-CSF for seven days on petri dishes. M-CSF triggers myeloid maturation to macrophages (Stanley et al., 1994). The uncoated surface of petri dishes allows attachment of highly adherent cells as macrophages while other cell types float and are washed off the plate with two cycles of PBS treatment on day 7. Macrophage phenotype and culture purity were confirmed by detection of CD11b and F4/80 expression using flow cytometry and cultured bone marrow cells were considered bone marrow-derived macrophages (BMDM) from then on.

2.2.2.3 Induction of Cre-dependent LoxP site Recombination in-vitro

Where *LoxP* site recombination was aspired, BMDM were treated with 1 μ M recombinant NLS-His-Tat-NLS-CRE protein in serum free RPMI medium 1:1 diluted in PBS o.n. On the next day culture supernatant was removed and exchanged to full macrophage medium.

2.2.2.4 Induction of M1-like Macrophage Polarization

To induce M1-like polarization of BMDMs either 1 μ g/ml LPS were added to macrophage culture medium without M-CSF for 6 hrs or o.n. to gain M1-like macrophage polarization.

2.2.2.5 Induction of M2-like Macrophage Polarization

To induce M2-like polarization of BMDMs 10 ng/ml recombinant murine IL4 were added to macrophage culture medium without M-CSF. Cells were treated for 72 hrs to achieve M2-like polarization.

2.2.3 Isolation of Tumor Cells from GEMM Tumors

Tumors got extracted entirely from the abdominal body cavity and were collected in 50 ml reaction tubes containing pre-chilled PBS. Samples were washed with fresh PBS once and subsequently minced on a petri dish using scalpels. Chopped tumor tissue was incubated in 5 to 10 ml RPMI containing 1 mg/ml collagenase type V for 45 min in a 37 °C water bath. Regular shaking ensured proper dispersion. Afterwards the digested samples were passed through a 100 μ m cell strainer to allow single cell separation. The obtained cell suspension was washed with 5 ml RPMI after spinning at 300 g for 5 min at 4 °C. Red blood cells were lysed by re-suspending the cell pellet in 2 ml RBC buffer and incubating for 5 min at RT. The lysate was again filtered by applying a 40 μ m cell strainer. Tumor cells were separated from RBC buffer by spinning at 400 g for 5 min at 4 °C and re-suspended in PBS or PBS containing 5 % FCS according to the following analysis.

2.2.4 Flow Cytometry and Fluorescence-activated Cell Sort

Multi-color flow cytometry experiments were performed on a Beckman Coulter Gallios™ flow cytometer. Three lasers (405 nm, 488 nm, and 536 nm) and ten filter sets allow for simultaneous detection of up to ten colors (see Tab. 2.11). Inter- and intra-laser beam spill over correction was automatically calculated using the FlowJo 7.5.5 software. Compensation matrices were calculated based on single stainings or OneComp compensation beads loaded independently with each antibody used in the respective staining and amine-reactive ArC™ beads for fixable viability dyes according to the manufacture's guide lines. Whenever voltage settings of photomultipliers were changed, new compensation stainings were run under the altered detection settings and a new compensation matrix was calculated. Samples were run in volumes of 100 or 200 µl and up to 600,000 counts were acquired. Un-fixed cells were measured in FACS buffer containing 2 % FCS. PBS without serum was used when fixed cells were analyzed. Cell sorting was performed on a BD FACS Aria III. All samples were incubated with CD16/32 antibody to block unspecific F_C receptor-mediated antibody binding. CD16/32 antibody was used 1:200 for 10 to 30 min before staining. In experiments where fixable live/dead stains were used, the CD16/32 block was added to the live/dead stain mix. Stainings were performed on 96 well U-bottom plates with a staining volume of 60 µl consisting of 30 µl cell suspension and 30 µl of antibody pre-dilution. All antibodies were used in a final working dilution of 1:200 except for Arg1 which was used in a final dilution of 1:50. Washing steps were conducted by spinning at 400xg for 5 min at 4° C. The supernatant was removed by quickly flipping the plate upside down and the pellet was re-suspended in 200 µl FACS buffer or PBS.

Laser	Filter (nm)	Channel	Used fluorophores
488 nm	525 BP	FL1	FITC, Alexa Fluor® 488
	575 BP	FL2	PE
	620 BP30	FL3	PI, PE-eFluor®610
	695 BP30	FL4	PerCP-Cy™5.5,
	755 LP	FL5	PE-Cy™7
536 nm	660 BP	FL6	APC
	725 BP20	FL7	Alexa Fluor® 700
	755 LP	FL8	Fixable Viability Dye 780
405 nm	450 BP50	FL9	eFluor®450, BD Horizon™ V450
	550 BP40	FL10	LIVE/DEAD® Fixable Yellow stain

Table 2.11: Gallios™ Flow Cytometer settings and used dyes.

2.2.4.1 Dead/live Cell Discrimination

To exclude dead cells from flow cytometry analysis, dead cells were stained either with Fixable Viability Dye 780 or LIVE/DEAD® Fixable Yellow stain, both diluted 1:1000 in PBS, for 30 min on ice in the dark ahead of antibody stainings. Alternatively, dead cells were marked with 5 µl of a 50 µg/ml propidium iodide (PI) stock solution immediately before measurement. A sample composed of 50 % heat-killed cells (10 min, 60° C) was used as positive control for dead cell stains.

2.2.4.2 Extracellular Staining

For staining of extracellular antigens, cells were washed as described in section 2.2.4 to remove fixable viability dyes or Fc block and incubated in FACS buffer for 20 min at 4° C in the dark. Afterwards, cells were washed twice and re-suspended in FACS buffer for analysis or fixed in case of subsequent staining of intracellular antigens.

2.2.4.3 Intracellular Staining

Whenever staining of intracellular antigens was intended, cells were fixed immediately after extracellular staining. For this purpose cells were incubated in 100 µl 2 % PFA/PBS for 10 min at RT in the dark and washed with PBS. Next, cells were permeabilized with detergent to provide antibodies excess to the cytoplasmic and nuclear compartments. Cells were re-suspended in 0.5 % Saponin/PBS and incubated for 10 min at 4° C in the dark. Antibodies were pre-diluted in permeabilization buffer to concentrations indicated in section 2.2.4 and incubated for 20-30 min at 4° C in the dark, then washed twice with

permeabilization buffer and finally re-suspended in PBS for measurement. In case of FOXP3 staining, a different protocol for intracellular staining applied. Panels containing FOXP3 were fixed and permeabilized using the eBioscience Foxp3/Transcription factor buffer set according to the manufacture's protocol. Briefly, cells were fixed for 30 min at RT in 100 µl Foxp3 Fixation buffer (diluted 1:4 with eBioscience fixation buffer diluent) and permeabilized by washing with 1X Foxp3 permeabilization buffer after fixation. Foxp3 antibody was diluted in Foxp3 permeabilization buffer and incubated with the cell suspension for 30 min at RT. Finally cells were washed twice with Foxp3 permeabilization buffer and re-suspended in PBS for measurement.

2.2.5 Histology

2.2.5.1 Preparation of Paraffin-embedded Tissue

Immediately when mice were sacrificed pancreas, spleen, lung, duodenum and liver tissue were collected in a tissue cassette and incubated in 4 % PFA/PBS at 4° C o.n. to 72 hrs. Next, the PFA-fixed samples were dehydrated o.n. in a Leica ASP300S dehydrator. Until specimens got embedded in paraffin using the Leica EG 1150 H, they were kept at 55° C. Paraffin tissue blocks were stored at RT or at -20° C before slicing. 3 µm sections were obtained on a Thermo Scientific Microm HM 355S microtome and collected in a 55° C water bath to allow for stretching. After attaching to microscope slides, paraffin sections were dried at RT o.n. or for 2 hrs in a 37° C incubator.

2.2.5.2 Hemalaun & Eosin Staining

Routine histological inspections were done based on HE stains of paraffin sections, where acidophilic hemalaun stains nuclei and basophilic eosin the cytoplasm. For HE staining, paraffin sections were incubated 3 x in Roti®-Histol for 2 min each to remove paraffin. Subsequently, the slides were treated three times with absolute ethanol for rehydration and finally twice with ddH₂O. For nuclear staining, tissue sections were kept in Mayer's hemalaun solution for 4 to 5 min and immediately washed three times with ddH₂O afterwards. Next, the slides were shortly submerged in ammonia water, twice in ddH₂O, and twice in HCl-H₂O (very

briefly), before flushing with tap water. Following a second brief incubation in ammonia water, slides were rinsed twice with ddH₂O and shortly submerged in 70 % ethanol. The cytoplasmic staining was obtained by 2 min incubation in eosin solution. Subsequently the tissue sections were submerged three times in absolute ethanol to remove excess eosin and dehydrated in Roti[®]-Histol. Cover slips were mounted on slide specimens with PERTEX[®] mounting medium. All steps were carried out at RT.

2.2.5.3 Immunohistochemistry

Immunohistochemistry staining was performed on a BD Bond Max slide stainer using the Leica Bond Polymer Refine Detection Kit according to the manufacturer's instructions. For antigen retrieval, tissue sections were pre-treated with EDTA for 30 min (B220, CD3, CD4) or enzymatically processed with Leica E1 for 10 min. Primary antibodies were incubated for 30 min at RT. When primary rat antibodies were used, sections were subsequently incubated with a rabbit anti mouse antibody (Jackson Immuno Research, 1:1000) for 20 min at RT. Next, tissue sections were incubated for 20 min at RT with HRP-conjugated goat anti rabbit (Leica Polymer). Afterwards the DAB reaction was conducted for 6 min, and slides were counterstained in hematoxylin for 5 min.

2.2.6 Microscopy

2.2.6.1 Bright Field Microscopy

Histological samples and cultured cells were analyzed by bright field microscopy on a Zeiss Axio Imager.A1 with EC Plan-Neofluar 10x 0.3 and EC Plan-Neofluar 20x 0.5 objectives. Digital images were acquired using a Zeiss AxioCam HRc camera and data was processed with AxioVision Rel. 4.8. software.

2.2.6.2 Fluorescence Microscopy

The fluorescent reporter protein tdTomato was detected via fluorescence microscopy on a Zeiss Axiovert 200M fluorescence microscope. Digital images were acquired using a Zeiss AxioCam MRm camera and processed with AxioVision Rel. 4.8. software.

2.2.6.3 Digital Slide Scanning

Histological samples were scanned on a Leica SCN400 with 4x, 10x, and 20x magnification. Images were captured using the Leica DIH software tool.

2.2.7 Statistical Data Analysis

All statistics were calculated using GraphPad Prism 5.0. Two-tailed non-parametric Mann-Whitney test was applied for all analysis except for survival data which were analyzed by Log-rank (Mantel-Cox) test. One-tailed non-parametric Mann-Whitney test was applied for knock out control experiments. p values below 0.05 were considered statistically significant.

3 RESULTS

3.1 Immune Phenotyping of KP mice

3.1.1 Leukocytes are the most abundant cell type in PDAC

Murine wild type pancreas and tumors from end-stage *Ptf1a^{+Cre};Kras^{+LSL-G12D};p53^{fl/fl}* mice (named KP thereafter) were analyzed for expression of the pan-leukocyte marker CD45. Immunohistochemistry revealed strong accumulation of CD45⁺ cells in tumor lesions compared to wild type specimens (see Fig 3.1 A+B). Moreover, flow cytometry experiments identified less than 10 % of all isolated viable cells as tumor cells (EpCAM⁺CD45⁻), whereas about 70 % accounted for leukocytes (EpCAM⁻CD45⁺). 20 % of isolated cells expressed neither EpCAM nor CD45 presumably resembling fibroblasts, stellate and endothelial cells (see Fig. 3.1 C).

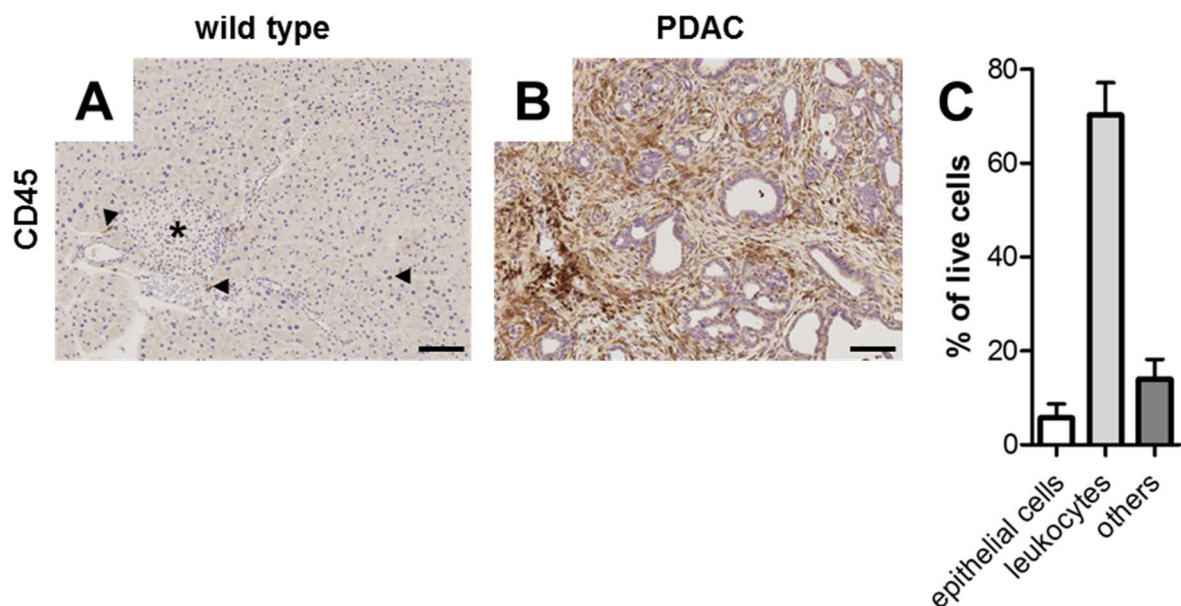


Figure 3.1: CD45⁺ leukocytes are the major cellular component of PDAC. (A+B) Representative immunohistochemistry of leukocyte antigen CD45 in wild type pancreas (A) and PDAC of end-stage KP mice (B). Scale bars represent 100 μ m; asterix marks an Islet of Langerhans; arrow heads point to few scattered positive cells. (C) Single cell suspensions were isolated from end-stage KP mice (n=5) and analyzed by flow cytometry. Percentage is given of a live cell pre-gate for epithelial cells (EpCAM⁺CD45⁻), leukocytes (EpCAM⁻CD45⁺), and other cell types (EpCAM⁻CD45⁻). Bars indicate mean and SD.

3.1.2 M2-TAMs are predominant in PDAC stroma

The majority of leukocytes isolated from KP tumors (approx. 60 %) were positive for the myeloid lineage marker molecule CD11b. 15 and 20 % express the T cell receptor molecule CD3 or the B cell marker CD19, respectively (see Fig. 3.2 A). In-depth subtype characterization found tumor-associated macrophages (TAMs), identified by a CD45⁺CD11b⁺GR1^{-/low}F4/80⁺ phenotype, as the most prominent myeloid sub-population (more than 30% of all infiltrating leukocytes) (see Fig. 3.2 B). Myeloid-derived suppressor cells accounted for 10 % of all CD45⁺ cells with a clear dominance of granulocytic over monocytic MDSCs. CD43⁻ B2 B cells represent 15 % of CD45⁺ leukocytes found in tumors. CD4⁺ helper T cells (T_H) and CD8⁺ cytotoxic T lymphocytes (CTL) made up the CD3⁺ population to equal amounts. 50 % of T_H cells and CTL were found to be negative for CD44 but positive for CD62L expression – a phenotype characterizing T cells as antigen-inexperienced or naive. 12 % of T_H cells and 5 % of CTL were identified as effector memory cells (CD44^{hi}CD62L^{low}) and approx. 5 % of both populations as central memory T cells (CD44^{hi}CD62L^{low}) (see Fig 3.2 C and D). Tumors were particularly enriched in TAMs expressing the M2-associated markers MRC1 and arginase1 (see Fig. 3.2 E). Regulatory T cells (T_{reg}), γδ T cells and natural killer (NK) cells accounted for as little as 1 % each (see Fig. 3.2 B). Despite significant amounts of CD19⁺ cells, no CD19⁺CD5⁺CD1d^{hi} B_{reg} were found in tumors or spleens (data not shown).

3.1.3 Murine PDAC induces splenic granulocytosis

Spleens of end-stage KP mice and their wild type littermates (8 weeks of age) were analyzed for tumor-induced immune cell reorganization. Spleens of tumor-bearing mice showed a significant increase of CD11b⁺ myeloid cells (5-fold) with a reduction of CD19⁺ cells compared to wild type spleens. Quantity of T cells (see Fig. 3.3 A) identified by expression of CD3e as well as T cell subtypes namely helper T cells and cytotoxic T cells and their effector states were unaffected by the presence of pancreatic neoplasms (see Fig. 3.3 B-D). The reduction of total B cells was accompanied by a relative downregulation of B1a cells and a significant relative increase in B1b cells (see Fig. 3.3 E). The profound increase of CD11b⁺ cells was due to an accumulation of GR1^{hi}F4/80⁻ cells (see Fig. 3.3 F).

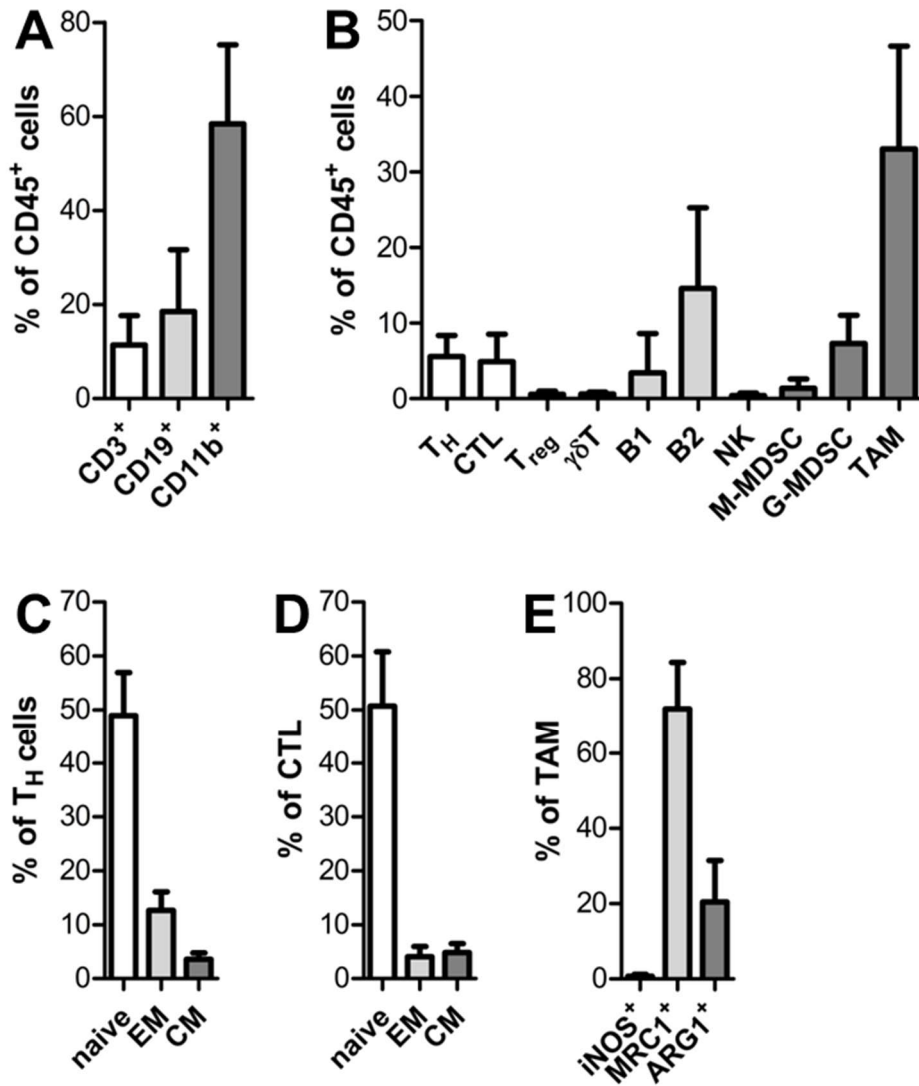


Figure 3.2: Immune phenotype of KP tumors: TAMs dominate leukocytic infiltrates. (A+B) Percentage of live CD45⁺ pre-gate for T cells (CD3), B cells (CD19) and myeloid cells (CD11b) (all **A**); CD3⁺CD4⁺CD8⁻ T cells (T_H), CD3⁺CD4⁺CD8⁺ T cells (CTL), CD3⁺CD4⁺Foxp3⁺CD25⁺ T cells (T_{reg}), CD3⁺γδTCR⁺ T cells (γδT), CD19⁺CD43⁺ B cells (B1) and CD19⁺CD43⁻ B cells (B2), NK1.1⁺ lymphocytes (NK), CD11b⁺F4/80^{-/low}GR1^{-/low}Ly6C^{hi} myeloid cells (M-MDSCs), CD11b⁺F4/80-GR1^{hi} myeloid cells (G-MDSCs) and CD11b⁺F4/80⁺GR1^{-/low} macrophages (TAM) (all **B**). **(C+D)** naive: CD44^{low}CD62L^{hi}, EM (effector memory): CD44^{hi}CD62L^{low}, CM (central memory): CD44^{hi}CD62L^{hi}. **(E)** Percentage of macrophages positive for inducible NO synthetase (NOS2⁺), mannose receptor 1 (MRC1⁺), and arginase 1 (ARG1⁺). Bars indicate mean and SD. **(A+B)** n=12, except for T_{reg} and NK (n=5), γδT (n=3), M-MDSC (n=7). **(C-E)** n=7.

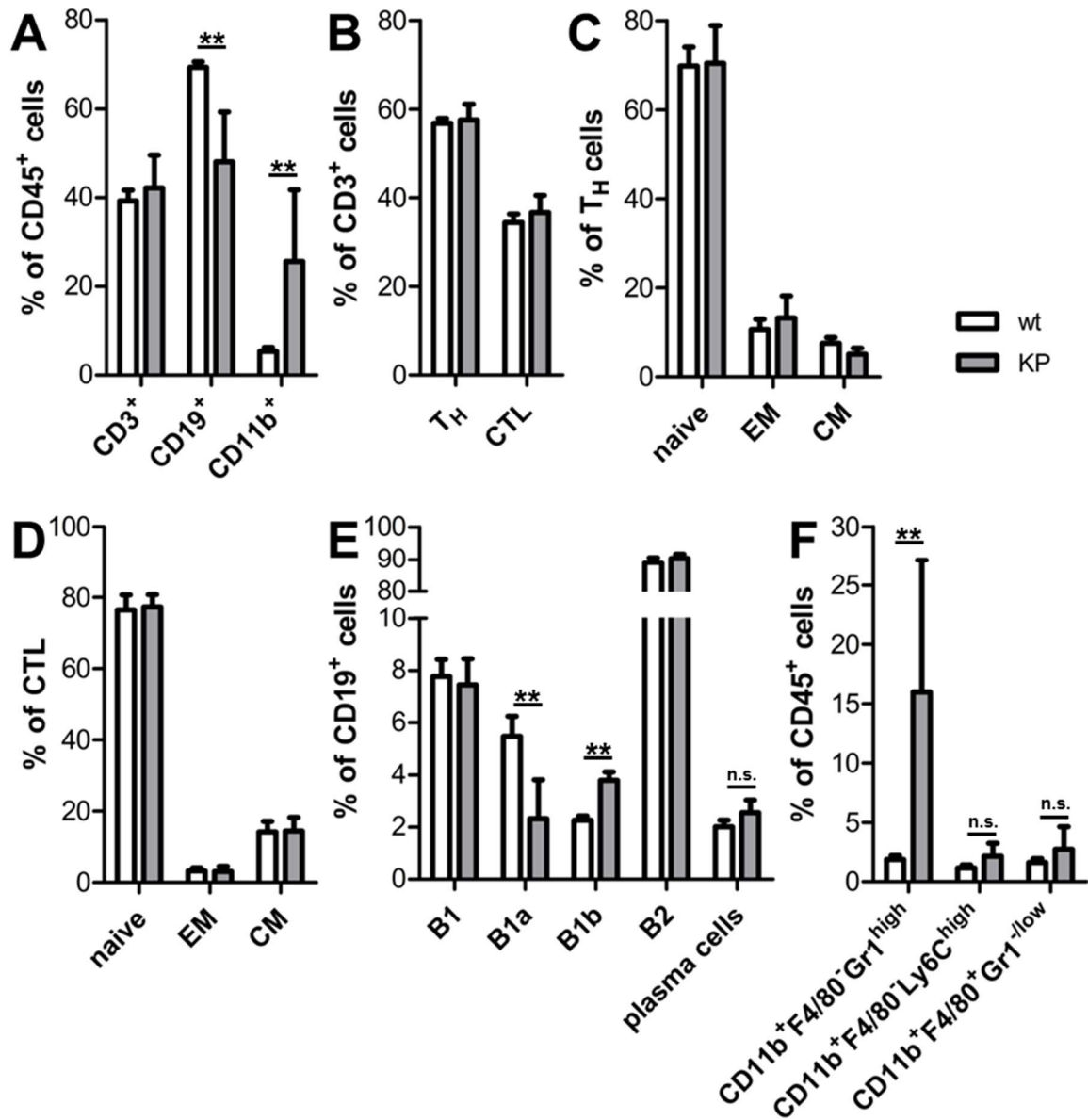


Figure 3.3: KP tumors induce splenic granulocytosis and promote B1b cells. Flow cytometry analysis of spleens from end-stage KP mice or tumor free wild type litter-mates. **(A)** Percentage of live CD45⁺ pre-gate for T cells (CD3), B cells (CD19) and myeloid cells (CD11b). **(B)** CD4⁺CD8⁻ T cells (T_H) and CD4⁺CD8⁺ T cells (CTL) in percentage of total live CD45⁺CD3⁺ T cells. **(C+D)** naive: CD44^{low}CD62L^{hi}, EM (effector memory): CD44^{hi}CD62L^{low}, CM (central memory): CD44^{hi}CD62L^{hi}. **(E)** CD43⁺ (B1), CD43⁺IgM⁺CD5⁺ (B1a), CD43⁺IgM⁺CD5⁻ (B1b), CD43⁻ (B2), CD138⁺ (plasma cells) in percentage of total live CD45⁺CD19⁺ B cells. **(F)** Myeloid subpopulations in percentage of live CD45⁺ leukocytes. Bars indicate mean and SD of n=6-7. n=4 for wt control in **(E)**. *: p<0.05, **: p<0.005, n.s.: p>0.05. wt: wild type

3.2 Lymphocytic Contribution to PDAC

A significant proportion of CD45⁺ tumor-infiltrating leukocytes were identified as T and B lymphocytes (see Fig. 3.2 A). Both cell types are potentially capable of forming adaptive anti-tumor immune response and tumor cell eradication. To test whether these TILs are limiting tumor progression and PDAC formation, tumor development was investigated in lymphocyte-depleted KP mice.

3.2.1 B cells do not provide effective anti-PDAC immunity

Using an α -CD20 antibody, B cells were efficiently depleted from KP mice. Animals were treated once a week with 10 mg/kg body weight antibody starting from two weeks of age. Successful B cell depletion was verified after the second or third injection by quantification of CD19⁺ cells in peripheral blood using flow cytometry (see Fig. 3.4 A). Efficient B lymphocyte blockade was accompanied by a relative increase of T cells in the lymphocyte population showing that α -CD20 treatment blocked specifically B cells but not other lymphocyte populations. The treatment was pursued until mice reached the final stage of disease. Spleen and tumor tissue specimens were analyzed for depletion efficacy by immunohistochemical B220 staining. As expected, spleens and tumors of treated animals were free of B cells with only some minor residual fractions in spleens whereas those animals which received isotype control injections had prominent B220 expression locating to the white pulp of the spleen and tumor stroma (see Fig. 3.4 B-E). Tumors were found macroscopically similar (see Fig. 3.4 F+G) but tumor weight to body weight ratios were significantly lower in B cell-depleted mice (see Fig. 3.4 H). The median survival of B cell free mice was reduced by 10 days (49 days vs 59) (see Fig. 3.4 I). However, no statistical significance was found for the survival difference between both groups suggesting that tumor-infiltrating B lymphocytes neither support anti-tumor immune response efficiently nor are markedly involved in tumor-promotive functions in the investigated model system of pancreatic cancer.

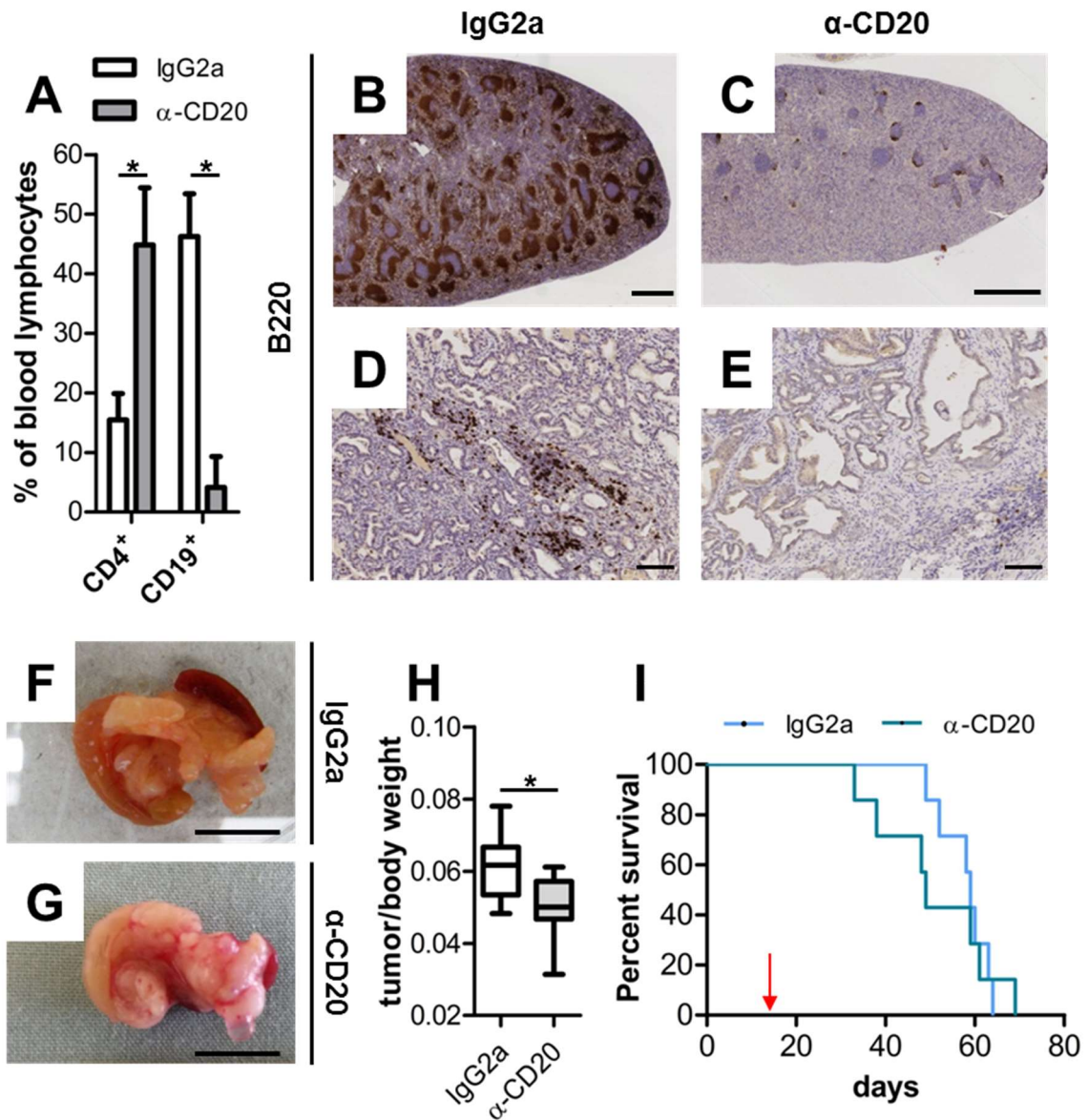


Figure 3.4: PDAC-infiltrating B cells fail to shape effective anti-tumor immunity. KP mice were intra peritoneally injected with 10 mg/kg body weight α -CD20 antibody or IgG2a control once per week from two weeks of age. **(A)** B cell depletion was monitored by flow cytometry analysis of peripheral blood from live animals during therapy (n=5 for CD4, n=3 for CD19). **(B-E)** B220 immunohistochemistry of spleens **(B+C)** and tumors of end stage animals **(D+E)** confirm efficient B lymphocyte depletion. Scale bars: 1 mm **(B+C)**, 100 μ m **(D+E)**. **(F)** Representative macroscopic image of IgG2a treated tumors with adjacent duodenum and spleen. **(G)** Representative macroscopic image of α -CD20 treated tumors with adjacent duodenum and spleen. **(F+G)** Scale bars represent 1 cm. **(H)** Box blots show ratios of tumor weight per body weight of end-stage animals on the day of euthanizing. Whiskers represent 5-95 percentiles; n=7 per group; *: p<0.05. **(I)** Survival of α -CD20 and control treated KP mice (n=7 per group). Red arrow marks therapy start. Median survival: 59 d (IgG2a controls) and 49 d (α -CD20), p=0.73.

3.2.2 T cells do not provide effective anti-PDAC immunity

To investigate the role of T cell-mediated anti-tumor immunity, T lymphocytes were depleted from KP mice from day 20 to the final stage of the disease.

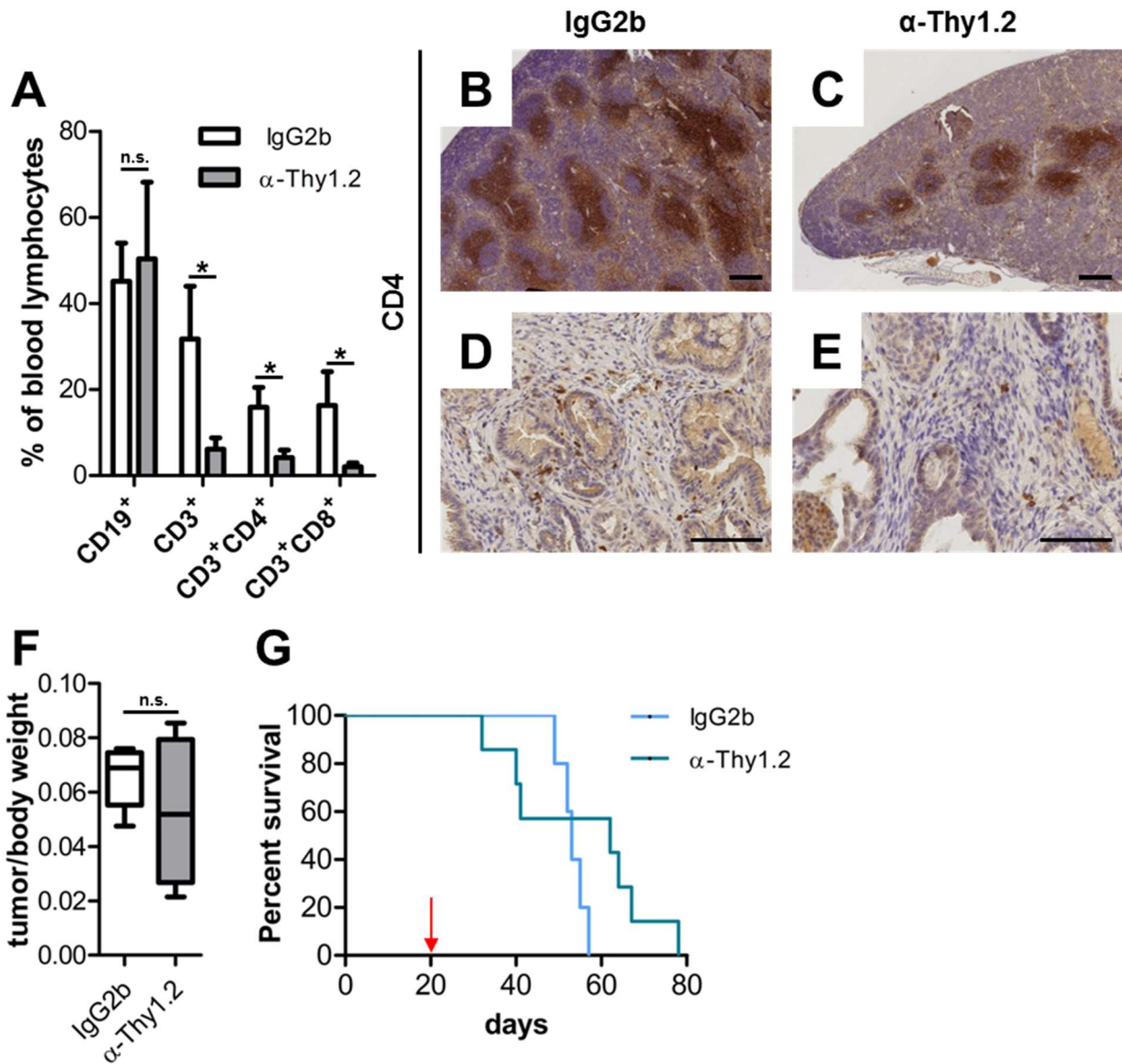


Figure 3.5: PDAC-infiltrating T cells fail to shape effective anti-tumor immunity. KP mice were intra peritoneally injected with 300 μ g α -Thy1.2 antibody per mouse three times a week starting from 20 days of age. **(A)** T cell depletion was monitored by flow cytometry analysis of peripheral blood from live animals during therapy (n=3 per group). **(B-E)** CD4 immunohistochemistry of spleens **(B+C)** and tumors of end stage animals **(D+E)**. Scale bars represent 300 μ m **(B+C)** or 100 μ m **(D+E)**. **(F)** Box blots showing tumor weight per body weight ratios of end stage animals on the day of euthanizing. Whiskers represent 5-95 percentiles of n=5 controls and n=4 α -Thy1.2-treated animals; n.s.: not significant. **(G)** Survival of α -Thy1.2 (n=7) and control treated KP mice (n=5). Red arrow marks therapy start. Median survival: 53 d (IgG2b controls) and 62 d (α -Thy1.2), p=0.238.

A T lymphocyte depleting α -Thy1.2 antibody was used to allow for T cell free tumor growth. Blood lymphocyte populations were monitored during treatment by flow cytometry (see Fig. 3.5 A). T cells (CD3⁺) were found reduced from 30 % to 5 % under α -Thy1.2 treatment effecting both CD4⁺ and CD8⁺ populations. Immunohistochemistry could confirm only partial depletion of T cells from spleen and tumor tissue (see Fig. 3.5 B-E). No difference in tumor mass relative to body weight was observed (see Fig. 3.5 F) and overall survival rates of T cell depleted mice and IgG2b control treated showed no significant discrepancy suggesting that T lymphocytes are indeed infiltrating pancreatic cancer, but incapable of effective tumor cell targeting.

3.2.3 Rag1 knock out confirms non-existence of adaptive anti-tumor immunity in PDAC

Antibody-mediated cell depletion is a time and cost-efficient tool to study tumor biology in absence of certain cellular sub-populations. This tool, however, finds its limitations in the effectiveness of depletion rate. Residual cells may interfere compensatorily thus obliterating potential effects. Therefore, a genetic mouse model lacking the *recombination-activating gene 1* (*Rag1*), was introduced to the KP mouse model of pancreatic cancer. This new generated mouse line was entitled KP;*Rag1*^{null} or KP^{het};*Rag1*^{null} depending on homozygous or heterozygous *Trp53* knock out. *Rag1*^{null} mice are incapable of developing mature B and T lymphocytes thus provided an absolutely B and T cell free tumor microenvironment, which was affirmed in this specific PDAC model via flow cytometry analysis of blood lymphocytes and immunohistochemistry (see Fig. 3.6 A and C-J, respectively). α -CD3 and α -B220 immunohistochemistry demonstrated exhaustive depletion of B and T cells from spleen and tumors in *Rag1*^{null} mice exceeding antibody-mediated B or T-cell depletion of section 3.2.1 and 3.2.2. Neither the KP^{het} nor the KP mouse model showed a difference in survival on a *Rag1*^{null} background compared to *Rag1*^{+/-} littermate controls (see Fig. 3.6 B). These results supported previous results from antibody-depletion experiments revealing no key role of adaptive anti-tumor immunity in PDAC at the tested conditions.

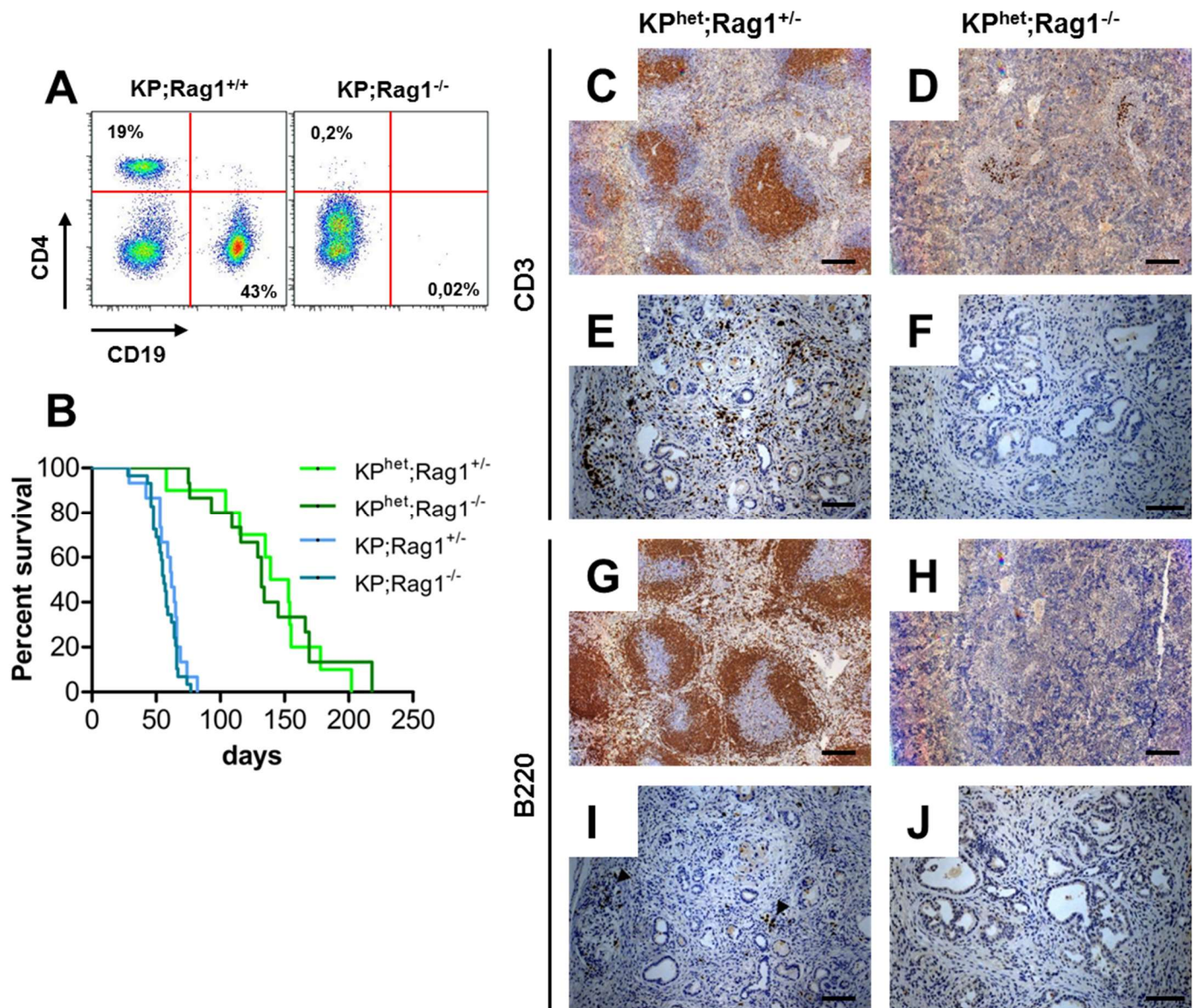


Figure 3.6: Genetic T and B cell depletion reveals non-existence of efficient adaptive anti-tumor immunity in PDAC. KP and KP^{het} mice were crossed to T and B cell free Rag1^{null} mice. **(A)** Flow cytometry analysis quantifying T (CD4) and B cells (CD19) in peripheral blood of KP and KP;Rag1^{null} mice. Relative fluorescence intensity is presented on a log-scale blot. **(B)** Survival of genetically T and B cell depleted PDAC mice (KP^{het};Rag1^{-/-}, KP;Rag1^{-/-}) and heterozygous litter mate controls (KP^{het};Rag1^{+/-}, KP;Rag1^{+/-}). Median survival: 146 d (KP^{het};Rag1^{+/-}, n=10) and 132 d (KP^{het};Rag1^{-/-}, n=15), p=0.86; 62 d (KP;Rag1^{+/-}, n=15) and 56 d (KP;Rag1^{-/-}, n=30) p=0.19. **(C-J)** Immunohistochemistry of spleens (**C+D**, **G+H**) and tumors (**E+F**, **I+J**) of end stage animals confirming efficient T (CD3) and B lymphocyte (B220) depletion. Scale bars represent 100 μm.

3.3 Mechanisms of Immune Suppression in KP Mice

Having found tumor-associated B and T cells being ineffective in combating PDAC progression, potential mechanisms of immune suppression that ultimately result in tumor immune evasion were experimentally addressed.

3.3.1 TAMs and B lymphocytes but not tumor cells highly express PD-L1

Tumors of end-stage KP mice were analyzed by flow cytometry for expression of PD-L1 (B7H1), a major inducer of CTL exhaustion and senescence via the PD-L1 receptor PD-1. PD-L1 was preferentially expressed on CD45⁺ cells. Pancreatic tumor cells (EpCAM⁺) and EpCAM⁻CD45⁻ non-tumor non-leukocyte cells showed no or only low PD-L1 expression (see Fig. 3.7 A). Next, CD45⁺ subpopulations were further analyzed for PD-L1 (see Fig. 3.7 B). T_H cells and CTL showed only low PD-L1 expression levels. CD4⁺CD8⁻ T cells, presumably consisting predominantly of $\gamma\delta$ T cells, were moderately positive for PD-L1. MDSCs were found negative, but B cells and TAMs were identified as the major source of PD-L1 in the KP mouse model of pancreatic cancer highlighting these populations as potential candidates for mediation of immune suppression in PDAC.

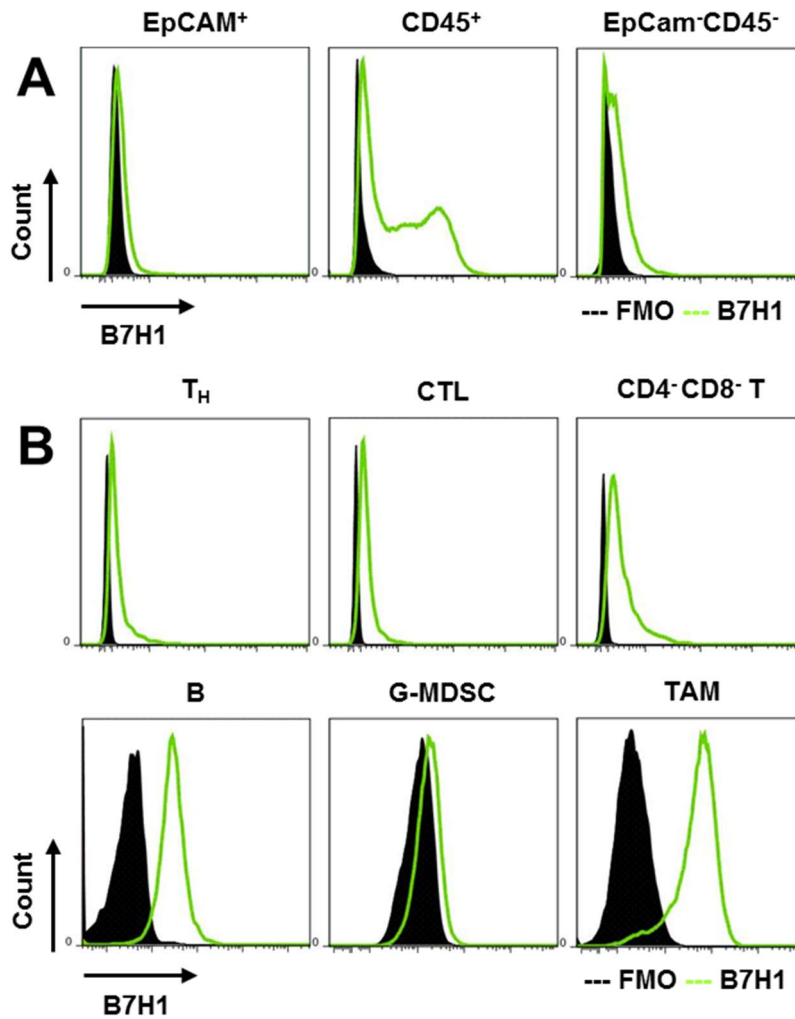


Figure 3.7: PD-L1 is preferentially expressed on B cells and TAMs. Flow cytometry analysis of end-stage KP tumors. Relative fluorescence intensity is presented on a log-scale cell count histogram. B7H1-PE (PD-L1) signal (green curve) is shown in comparison to FMO controls (filled black peak). **(A)** Tumor cells (CD45⁺EpCAM⁺), leukocytes (CD45⁺EpCAM⁻), other stroma cells (CD45⁻EpCAM⁻). **(B)** T_H: live CD45⁺CD3⁺CD4⁺CD8⁻, CTL: live CD45⁺CD3⁺CD4⁻CD8⁺, CD4⁻CD8⁻ T: live CD45⁺CD3⁺CD4⁻CD8⁻, B: live CD45⁺CD19⁺, G-MDSC: live CD45⁺CD11b⁺F4/80^{GR1^{hi}}, TAM: live CD45⁺CD11b⁺GR1^{-low}F4/80⁺.

3.3.2 PD-L1 blockade is not sufficient to unleash anti-tumor immune response in KP mice

To investigate the importance of PD-L1-mediated immune checkpoint inhibition in pancreatic cancer, KP mice with advanced PDAC were treated for one week with 3 x 150 μg $\alpha\text{-B7H1}$ antibody or the respective isotype as control starting at an age of 6.5 - 7 weeks. Mice were sacrificed one day after the last injection to check for alterations in the immune environment. B7H1 (PD-L1) was not detectable on B cells or macrophages in $\alpha\text{-B7H1}$ -treated animals anymore at the day of sacrifice indicating that the i.p. injected antibody efficiently entered the tumor microenvironment and blocked PD-L1 (see Fig. 3.8 A). $\alpha\text{-B7H1}$ treatment did not cause depletion of PD-L1 expressing cells as the proportions of major leukocyte populations, i.e. T cells, B cells, and myeloid cells remained unchanged (see Fig. 3 B).

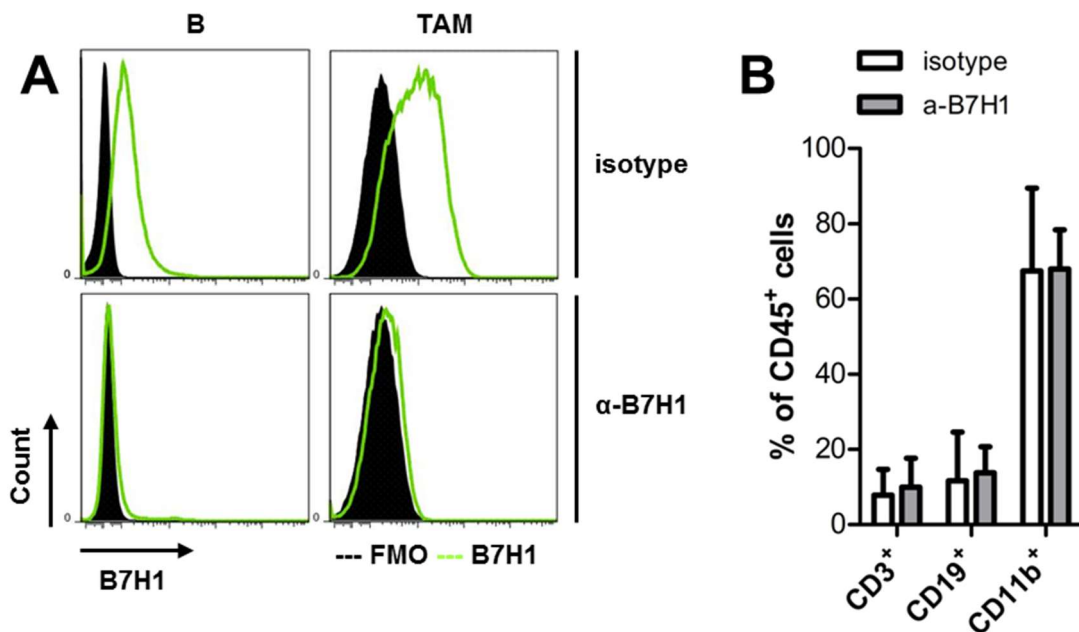


Figure 3.8: Stromal PD-L1 expression is efficiently targetable in KP tumors. Flow cytometry analysis of end-stage KP tumors from mice treated with 150 μg $\alpha\text{-B7H1}$ antibody thrice within one week starting from 6.5-7 weeks of age (n=5). Control animals received the same amount of respective isotype control (n=5). Animals were sacrificed one day after the last injection. (A) Representative image of B7H1 expression on a B cell (CD45⁺CD19⁺) or TAM (CD45⁺CD11b⁺GR1^{-low}F4/80⁺) pre-gate. Relative fluorescence intensity is presented on a log-scale cell count histogram. B7H1-PE (PD-L1) signal is shown in comparison to FMO controls. (B) Quantification of leukocyte populations in percentage of total leukocyte count (live CD45⁺ pre-gate). White bars indicate control treated samples. $\alpha\text{-B7H1}$ treatment is shown in grey. Given is mean and SD from n=5 animals per group.

To evaluate the potential effect of PD-L1 blockade on anti-tumor immune responses, effector T cell populations were quantified in tumors of α -B7H1 (PD-L1) and control treated animals. CD4⁺ helper T cell and CD8⁺ cytotoxic T cell proportions of total CD3⁺ cells turned out to be unaffected by α -B7H1 (PD-L1) treatment (see Fig. 3.9 A).

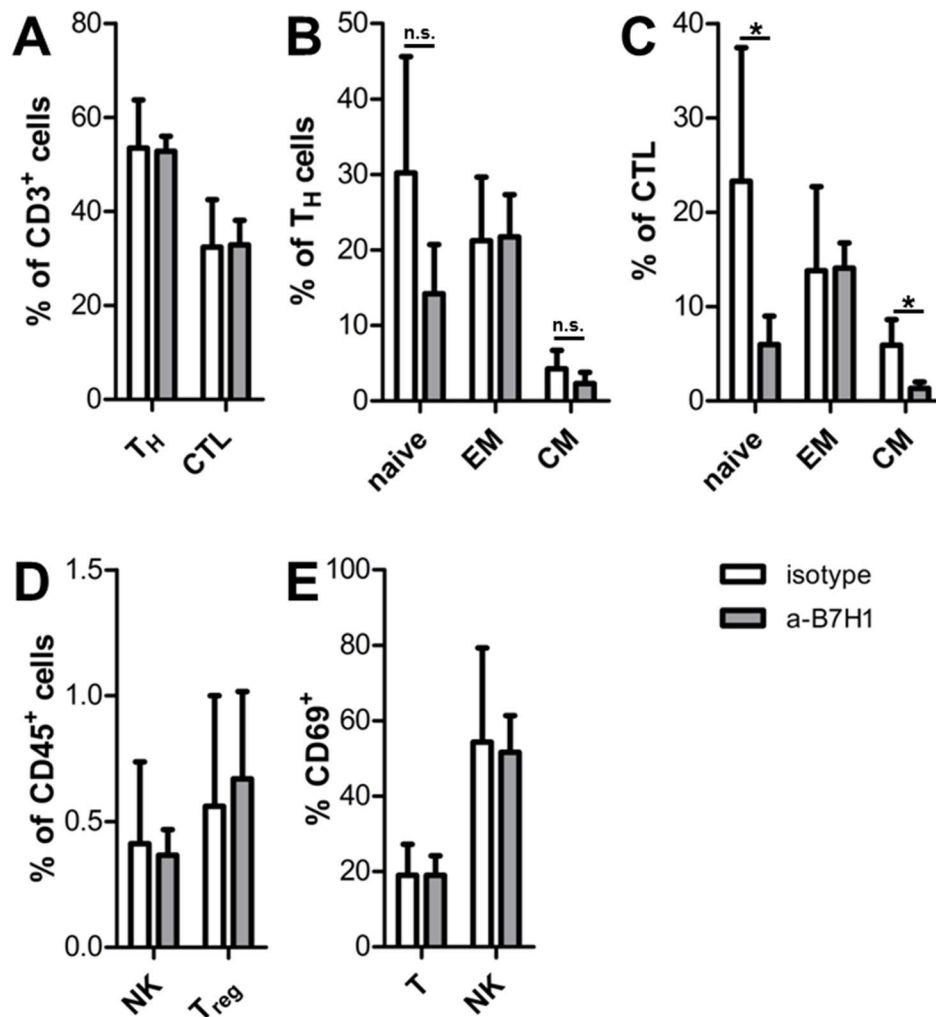


Figure 3.9: PD-L1 blockade does not augment anti-tumor T cell response. Flow cytometry analysis of end-stage KP tumors from mice treated with 150 μ g α -B7H1 antibody thrice within one week starting from 6.5-7 weeks of age (n=5). Control animals received the same amount of respective isotype control (n=5). Animals were sacrificed one day after the last injection. White bars indicate control treated samples. α -B7H1 treatment is shown in grey. Given is mean and SD from n=5 animals per group. **(A)** T_H: CD4⁺CD8⁻, CTL: CD4⁻CD8⁺ percentage of live CD45⁺CD3⁺ pregate. **(B+C)** naive: CD44^{low}CD62L^{hi}, EM (effector memory): CD44^{hi}CD62L^{low}, CM (central memory): CD44^{hi}CD62L^{hi}. **(D)** NK: NK1.1⁺ lymphocytes, T_{reg}: CD3⁺CD4⁺CD25⁺Foxp3⁺ in percentage of total live CD45⁺ cells. **(E)** CD69⁺ cells of total T cells (T: live CD45⁺CD3⁺) or total NK cells (NK: live CD45⁺NK1.1⁺ lymphocytes).

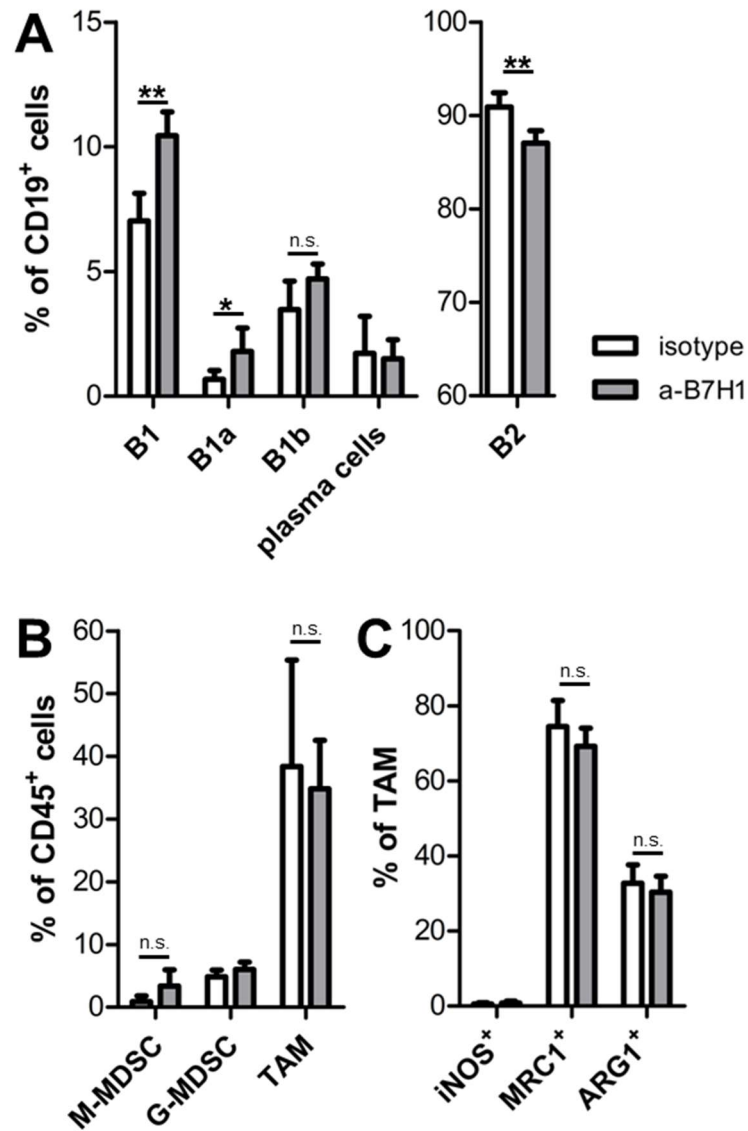


Figure 3.10: PD-L1 blockade promotes B1 B cells but does not affect myeloid cells. Flow cytometry analysis of end-stage KP tumors from mice treated with 150 μ g α -B7H1 antibody thrice within one week starting from 6.5-7 weeks of age ($n=5$). Control animals received the same amount of respective isotype control ($n=5$). Animals were sacrificed one day after the last injection. **(A)** CD43⁺ (B1), CD43⁺IgM⁺CD5⁺ (B1a), CD43⁺IgM⁺CD5⁻ (B1b), CD138⁺ (plasma cells), CD43⁻ (B2) cells, in percentage of total live CD45⁺CD19⁺ B cells. **(B)** M-MDSC (CD11b⁺F4/80^{-/low}GR1^{-/low}Ly6C^{hi}), G-MDSC (CD11b⁺F4/80-GR1^{hi}), TAM (CD11b⁺F4/80⁺GR1^{-/low}) in percentage of total live CD45⁺ cells. **(C)** Positive macrophages in percentage of total TAMs. Bars indicate mean and SD. *: $p < 0.05$, **: $p < 0.005$, n.s.: $p > 0.05$.

However, both helper and cytotoxic T cells showed reduced numbers of naive subpopulations (CD44^{low}CD62L^{hi}) but no increase in CD44^{hi} effector cells (see Fig. 3.9 B+C). Numbers of NK and regulatory T cells as well as T and NK cell activation measured by expression of the early activation marker CD69 remained unaffected (see Fig. 3.9 D+E) by PD-L1 blockade suggesting no effective anti-tumor T cell activation by PD-L1 blockade in KP mice.

Next, B lymphocytes were investigated in α -B7H1 (PD-L1) treated tumors. B1 cells were significantly increased in α -B7H1 treated tumors and showed a 50 % upregulation compared to isotype treated KP mice, which was mainly due to an increase of B1a rather than B1b cells (see Fig. 3.10 A). B2 cells, on the other hand, were significantly reduced in mice with PD-L1 inhibition. No difference on tumor-associated antigen producing plasma cells identified by CD138 expression was detected.

Myeloid subpopulations, i.e. M-MDSCs, G-MDSCs and TAMs accumulated to the same extend in treated and control tumors (see Fig. 3.10 B). Macrophage polarization determined by intracellular staining of NOS2, MRC1, and ARG1 was unaffected by PD-L1 blockade and remained unaltered with a strong M2 phenotype (see Fig. 3.10 C).

Taken together, PD-L1 blocking experiments suggest that PD-L1 blockade is not sufficient to unleash anti-tumor immune response in KP mice with advanced PDAC.

3.3.3 Immune evasion is independent of CCR2 recruitment

Tumor-associated macrophages form the most prominent leukocyte subset in KP tumors and their phenotypic characteristics strongly suggest an immune suppressive and tumor promoting functionality (see Fig. 3.2 B+E). The molecular and cellular mechanisms underlying TAM accumulation in PDAC is largely unknown. Therefore, a major myeloid cell recruitment signaling cascade, the CCL2-CCR2 axis, was disrupted by genetic ablation of *Ccr2* (Boring et al., 1997) which was crossed into the KP model. *Ccr2* knock out in KP;*Ccr2*^{null} mice was confirmed by gene expression quantification (see Fig. 3.11 A) but was not found to influence the expression levels of macrophage marker F4/80 in tumor tissue (see Fig. 3.12 B) suggesting that TAMs do not depend on CCR2-mediated recruitment.

However, KP;*Ccr2*^{null} mice showed significantly increased numbers of G-MDSCs. M-MDSCs, in contrast, were almost completely obliterated in tumors of KP;*Ccr2*^{null} mice (see Fig. 3.11 C). Somewhat surprising, these effects did not translate in altered tumor development or survival in KP mice (see Fig. 3.11 D).

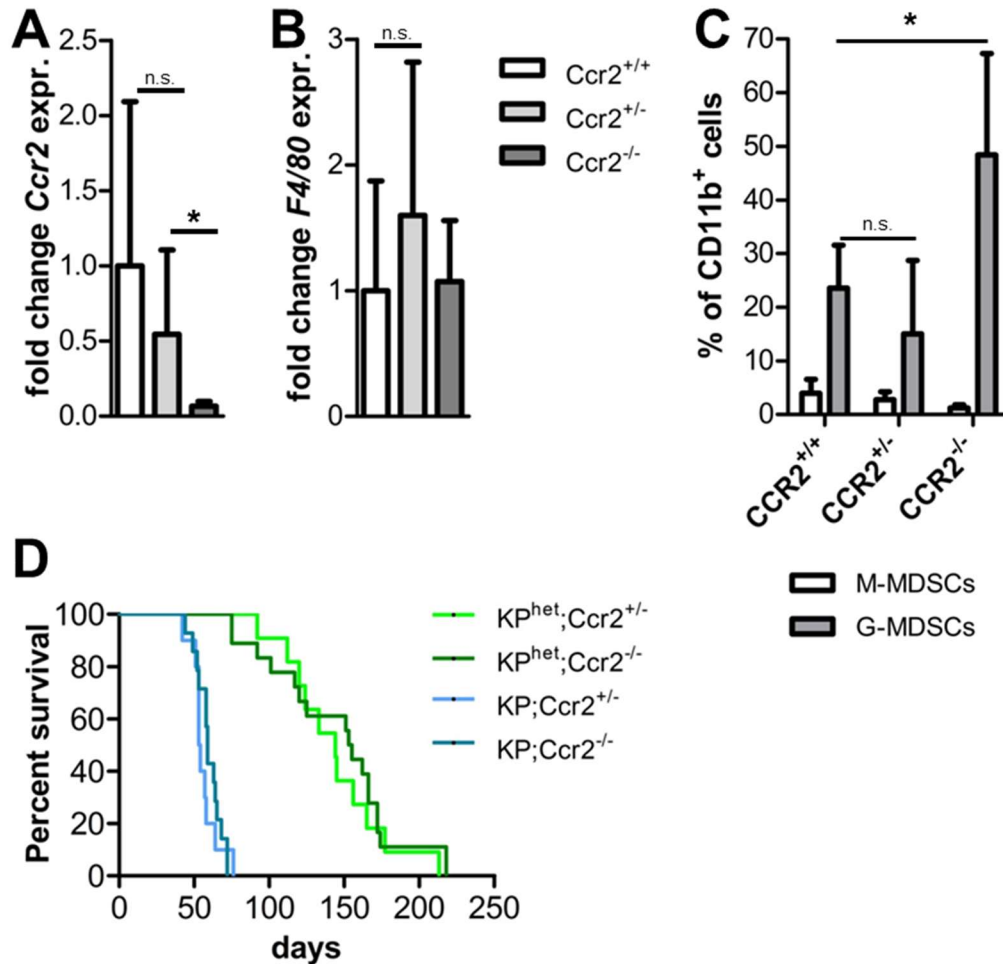


Figure 3.11: Ccr2 knock out shifts M-MDSCs to G-MDSCs. KP and KP^{het} mice were crossed to a *Ccr2*^{null} mouse line. Gene expression of *Ccr2* (A) and *F4/80* (B) in *Ccr2* knock out, heterozygous or wild type KP^{het} mice was quantified by qRT-PCR from RNA isolated from tumor tissue (n=3). (C) Flow cytometry analysis of tumor infiltrating MDSCs in KP mice (n=15) compared to KP mice with homozygous (n=5) or heterozygous *Ccr2* deletion (n=5). Bars indicate mean and SD. (D) Survival of *Ccr2*^{null} PDAC mice (KP^{het}; *Ccr2*^{-/-}, KP; *Ccr2*^{-/-}) and heterozygous litter mate controls (KP^{het}; *Ccr2*^{+/-}, KP; *Ccr2*^{+/-}). Median survival: 144 d (KP^{het}; *Ccr2*^{+/-}, n=11) and 154 d (KP^{het}; *Ccr2*^{-/-}, n=18), p=0.51; 53.5 d (KP; *Ccr2*^{+/-}, n=10) and 59 d (KP; *Ccr2*^{-/-}, n=14) p=0.43. *: p<0.05, n.s: p>0.05.

3.3.4 Notch activation counteracts IL4-induced M2

polarization

Since M2-polarized macrophages were identified as the predominant cell type in the microenvironment of KP tumors (see chapter 3.1.2), cultures of bone marrow-derived macrophages (BMDM) were established to study effects of Notch pathway manipulation on macrophage polarization. After eight days in M-CSF containing medium, bone marrow-derived cultures displayed a macrophage-like phenotype by expression of both CD11b and F4/80 (see Fig. 3.12 A). Hence, they are referred to as BMDM from here on. To test the ability of BMDMs to undergo CRE-mediated recombination, BMDM isolated from Rosa26 *LoxP-STOP-LoxP-tdTomato* reporter mice were treated with recombinant NLS-TAT-CRE in cell culture. Approx. 95 % of cells successfully underwent genetic *loxP*-site recombination as determined by tdTomato fluorescence detected by flow cytometry and fluorescence microscopy (see Fig. 3.12 B).

Next, BMDM isolated from Rosa26 *LoxP-STOP-LoxP-N2IC(-hCD2)* mice were pretreated with recombinant CRE protein or control medium and subsequently challenged for 72 hrs with IL4 to induce M2 polarization. In this model CRE recombinase excises a transcriptional STOP-cassette resulting in constitutive expression of transcriptionally active Notch and human CD2, a co-expressed reporter molecule. IL4 alone strongly induces M2-associated gene expression (*Mrc1*, *Mgl1*, and *Arg1*), whereas expression levels of M1 genes were undetectable by qRT-PCR (see Fig. 3.13 A). CRE-dependent activation of Notch signaling in CRE-only treated cells resulted in significant downregulation of baseline M2-gene expression and basal induction of M1 genes (IL1 β , IL6, IL12b). CRE-dependent activation of Notch signaling was confirmed by the co-expressed human CD2, which is traceable by flow cytometry (see Fig. 3.13 B). The stark upregulation of *Mrc1*, *Mgl1* and *Arg1* expression in IL4 treated BMDM was significantly diminished in IL4 treated cells with previous CRE treatment as demonstrated by mRNA (see Fig. 2.13 A) expression levels as well as protein levels measured by flow cytometry (see Fig. 3.13 C), thus indicating that Notch activation counteracts IL4 induced M2 polarization.

To explore the effect of Notch overexpression in a M1 situation, BMDM were stimulated for 6 hrs or o.n. with LPS resulting in a strong induction of Nos2, IL1 β , IL6, IL12a, and IL12b (see Fig. 3.14 A). Combination of Notch overexpression and LPS stimulation, however, did not translate in further augmentation of M1 gene expression or further downregulation of M2-associated genes (see Fig. 3.14 A+B).

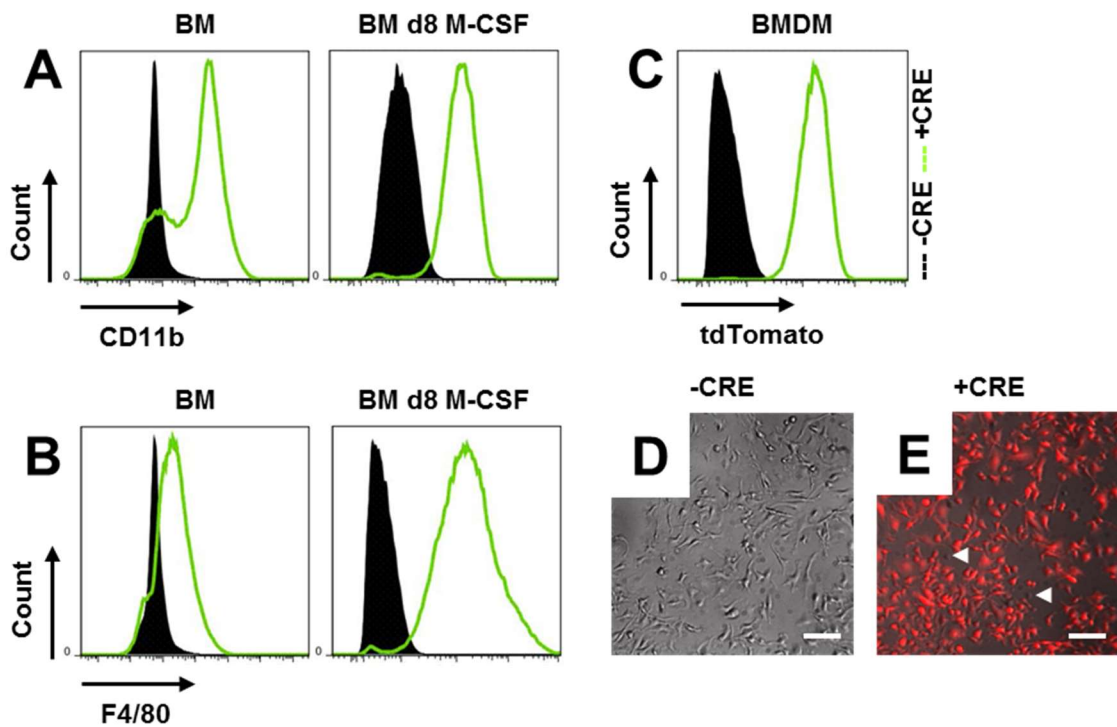


Figure 3.12: BMDMs provide a powerful platform to study macrophage biology in vitro. (A-C) Flow cytometry analysis of bone marrow (BM) or bone marrow-derived macrophages (BMDM). Relative fluorescence intensity is presented on a log-scale cell count histogram. Fresh bone marrow and bone marrow cells cultured for 8 days in macrophage medium containing 50 ng/ml M-CSF and analyzed for expression of macrophage markers. CD11b-eFluor450 (A) or F4/80-FITC signal (B) (green curves) are shown in comparison to respective isotype controls (filled peaks). Bone marrow cells cultured with M-CSF were called BMDM from day 8 in vitro. (C-E) BMDM isolated from *Rosa26 LoxP-STOP-LoxP-tdTomato* reporter mice were incubated over night with 1 μ M recombinant NLS-TAT-CRE and analyzed for tdTomato fluorescence on day 4 after treatment (C) Green: CRE-treated cells. Black: control treated cells. (D+E) BF/FL image overlays. Arrow heads mark few negative cells. Scale bars represent 100 μ m.

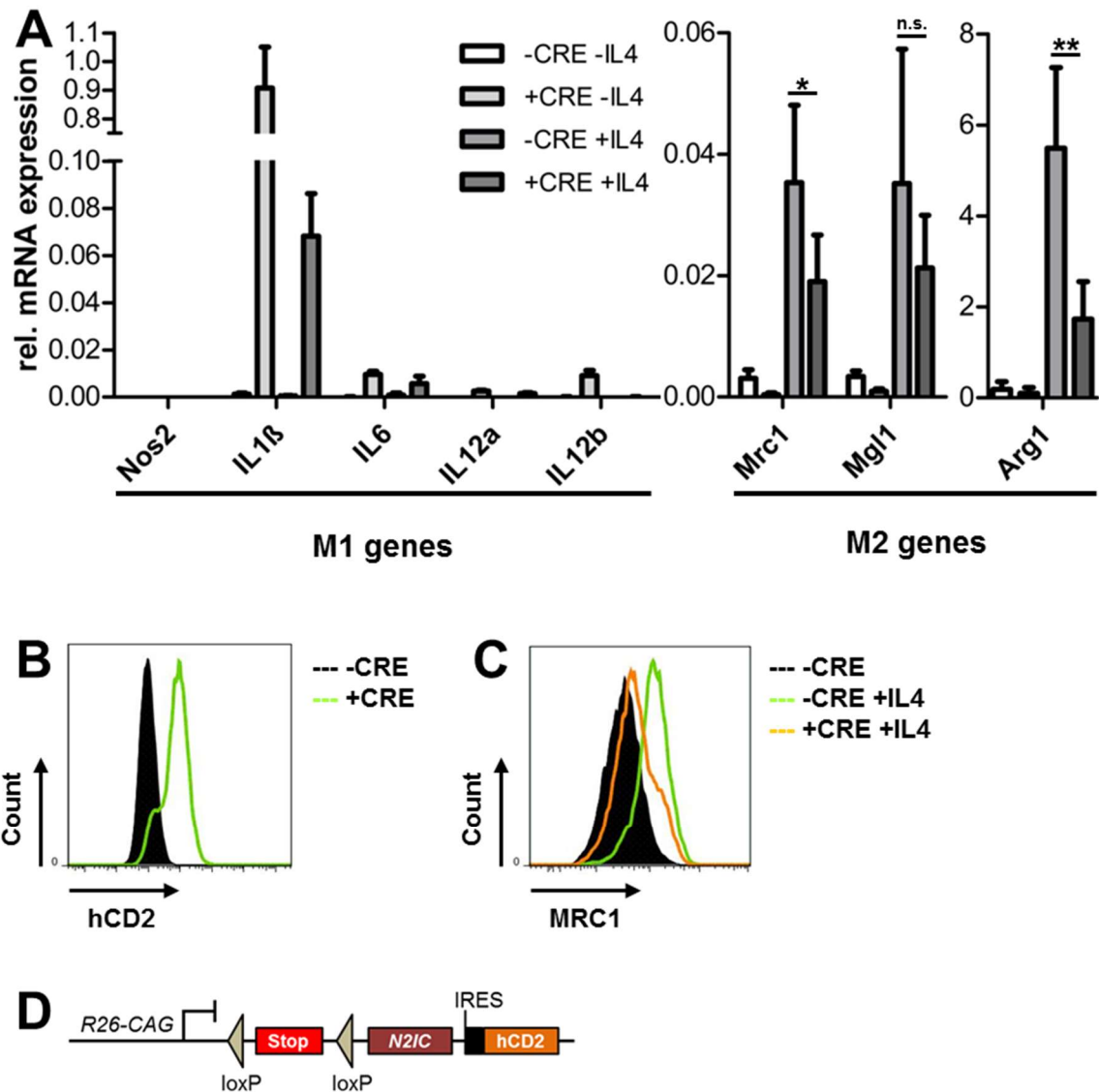


Figure 3.13: Notch counteracts IL4-driven M2 macrophage polarization in vitro. BMDM from Rosa26-LSL-N2IC were stimulated with 10ng/ml IL4 for 72 hrs with or without previous CRE treatment. **(A)** Relative expression levels of M1 and M2 marker genes determined by qRT-PCR from n=6 donor animals. Bars indicate mean and SD. *: p<0.05, **: p<0.005, n.s: p>0.05. **(B+C)** Flow cytometry analysis of BMDM. Relative fluorescence intensity is presented on a log-scale cell count histogram. Representative images of n=3 animals. **(B)** Efficient in vitro *LoxP* recombination monitored by detection of hCD2 co-expressed with N2IC. **(C)** MRC1 protein level dependent on IL4 stimulation and Notch activation on live CD11b⁺F4/80⁺ pregate. Representative blot of three independent donor animals. **(D)** Simplified description of genetic Rosa26-LSL-N2IC construct.

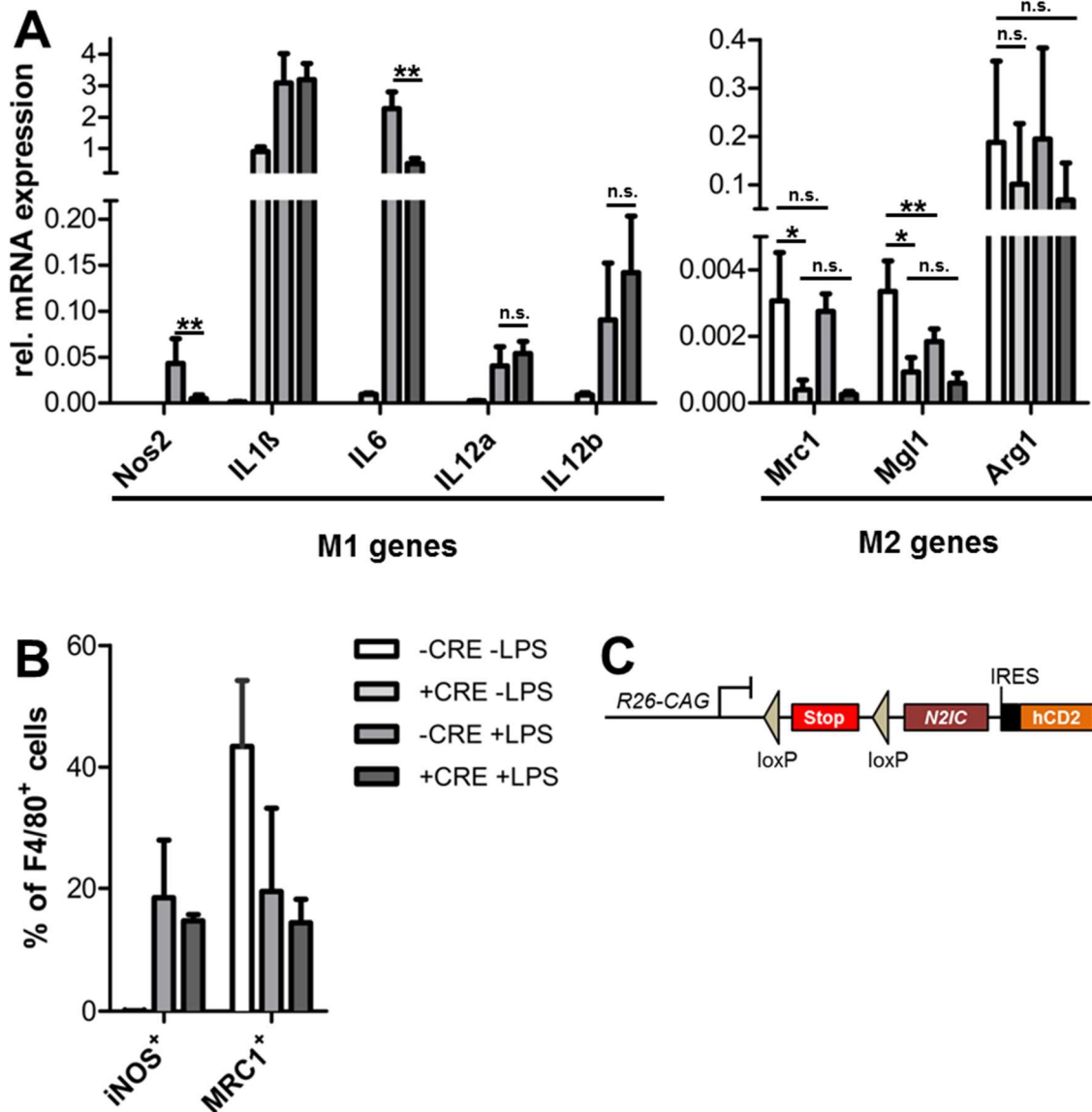


Figure 3.14: Notch overexpression does not synergize with LPS in vitro. BMDMs from Rosa26-LSL-N2IC were stimulated with 1 μ g/ml LPS for 6 hrs (A) or o.n. (B) with or without previous CRE treatment. (A) Relative mRNA expression levels of M1 and M2 marker genes determined by qRT-PCR from n=6 donor animals; (+CRE-LPS): n=3. (B) Flow cytometry analysis highlighting NOS2⁺ and MRC1⁺ cells in percentage of live F4/80⁺ BMDM. Bars indicate mean and SD. n=4. *: p<0.05, **: p<0.005, n.s.: p>0.05. (C) Simplified description of genetic Rosa26-LSL-N2IC construct.

3.3.5 Rbpj knock out blocks LPS-induced M1 polarization

The requirement of endogenous Notch signaling for either M1 or M2 macrophage polarization was the next research question to be addressed. *Rbpj^{fl/fl}* mice allow for CRE-dependent block of canonical Notch signaling. Experiments with BMDMs iso-

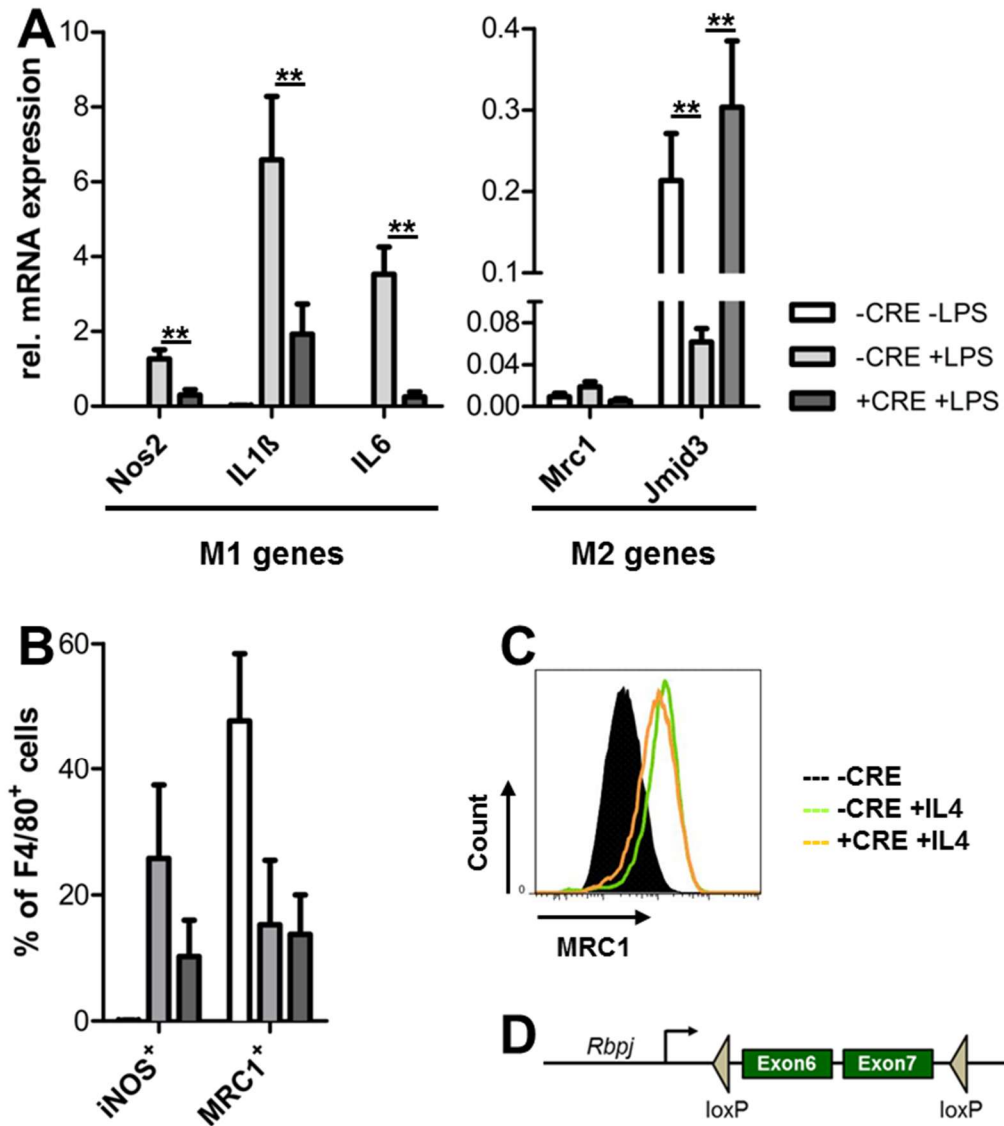


Figure 3.15: LPS-induced M1 polarization depends on Notch/RBPj signaling. BMDMs from *Rbpj^{fl/fl}* mice were stimulated with 1 μ g/ml LPS for 6 hrs (A) or o.n. (B) or with 10 ng/ml IL4 for 72 hrs (C) with or without previous CRE treatment. (A) Relative mRNA expression levels of M1 and M2 marker genes determined by qRT-PCR from n=6 donor animals. Bars indicate mean and SD. **: p<0.005, n.e: not expressed C_t>35. (B) Flow cytometry analysis highlighting NOS2⁺ and MRC1⁺ cells in percentage of live F4/80⁺ BMDM. Bars indicate mean and SD from n=4 donor animals. (C) Flow cytometry analysis showing relative fluorescence intensity presented on a log-scale cell count histogram. MRC1 expression dependent on IL4 stimulation and *Rbpj* KO of a live CD11b⁺F4/80⁺ pre-gate. Representative blot of three independent donor animals. (D) Simplified description of conditional *Rbpj^{fl/fl}* construct.

lated from those mice were performed analogously to those with LSL-N2IC BMDMs. LPS-induced M1 gene expression was significantly reduced to low levels in *Rbpj* knock out macrophages (see Fig. 3.15 A). Moreover, flow cytometry analysis revealed *Nos2* expression triggered by LPS administration down regulated in *Rbpj* KO macrophages (see Fig. 3.15 B). Both findings suggest that canonical Notch signaling is required for robust M1 polarization. Additionally, LPS-dependent *Jmjd3* downregulation, a classical M2 gene, was rescued in *Rbpj* knock out BMDMs. On the other hand, M2 polarization by IL4 measured by MRC1 protein expression is not affected by *Rbpj* knock out (see Fig. 3.15 C).

3.3.6 Notch activation reprograms M2 TAMs in vivo

Hypothesizing that Notch activation might not only promote M2 to M1 repolarization in vitro but also in myeloid cells of KP mice, a myeloid cell specific *Cre*-line (*Lyz2^{+Cre}*) was crossed to Rosa26-LSL-N2IC and *Rbpj^{fl/fl}* mice to investigate Notch-dependent macrophage polarization in vivo. First, *Lyz2*-*Cre* expression was traced with the *Rosa26-LSL-tdTomato* mouse line to quantify recombination efficiency in myeloid subsets (see Fig. 3.16 A). Approx. 80 % of CD11b⁺ myeloid cells were affected by *Lyz2*-*Cre*-dependent recombination in bone marrow and spleen. Less than 10 % of CD11b⁻ cells were observed *tdTomato* positive in bone marrow or spleen. MDSCs were differentially affected by *Lyz2*-*Cre* activity. 95 % of G-MDSCs but only around 50 % of M-MDSCs underwent *Lyz2*-*Cre*-dependent recombination.

To assure myeloid specific Notch downstream activation in *Lyz2^{+Cre};R26^{+LSL-N2IC(hC2)}* mice and blockade in *Lyz2^{+Cre};Rbpj^{fl/fl}* mice, bone marrow of respective animals was isolated and sorted according to CD11b and hCD2 expression. Population fractions were lysed and qRT-PCR from isolated RNA revealed a strong transcriptional upregulation of the Notch target gene *Hes1* in *Lyz2^{+Cre};R26^{+LSL-N2IC(hC2)}* bone marrow indicating that Notch was *Lyz2*-*Cre* dependently overexpressed as intended. Wild type and *Lyz2^{+Cre};Rbpj^{fl/fl}* mice both showed low levels of *Hes1* expression in CD11b⁺ bone marrow cells (see Fig. 3.16 C).

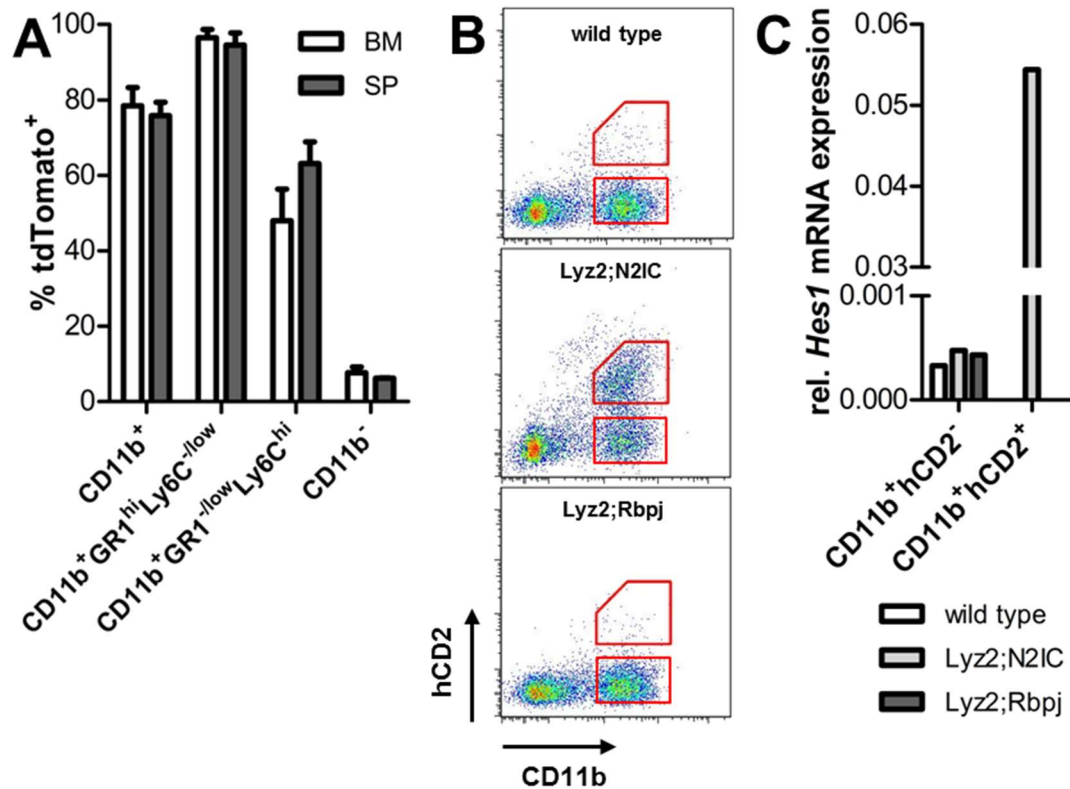


Figure 3.16: Lyz2-Cre directs genetic Notch activation to myeloid cells. (A) The Rosa26-LSL-tdTomato reporter mouse line was used to visualize Lyz2-Cre expression and recombination activity in vivo. Bars indicate tdTomato positive fractions of myeloid cells and non-myeloid cells (CD11b⁻) isolated from bone marrow (BM) and spleen (SP) and analyzed by flow cytometry. Bars indicate mean and SD from n=3 animals. (B) Bone marrow of wild type, *Lyz2^{+/Cre};R26^{+/LSL-N2IC(hCD2)}* (Lyz2;N2IC), and *Lyz2^{+/Cre};Rbpj^{fl/fl}* (Lyz2;Rbpj) mice was isolated, fluorescently labeled with α-hCD2 and α-CD11b and subsequently sorted for population specific mRNA isolation. Lower gate: CD11b⁺hCD2⁻; upper gate: CD11b⁺hCD2⁺ population. Sorted populations shown on log scale according to their relative fluorescence intensity. Cells were re-sorted to assure pure fractions. *Hes1* expression was selectively upregulated in CD11b⁺hCD2⁺ cells.

In addition, mice were analyzed for potential shifts in leukocyte subtypes of bone marrow, blood, and spleen to exclude systemic immune cell alterations by Lyz2-Cre-mediated Notch signaling manipulation. No significant abnormalities were observed between Notch overexpressing, *Rbpj* knock out, or wild type animals in myeloid or lymphoid subpopulations (see Fig. 3.17). Next, Notch signaling manipulation was introduced genetically in myeloid cells of tumor-bearing mice. For this purpose *Lyz2^{+/Cre};R26^{+/LSL-N2IC}* (Lyz2;N2IC) and *Lyz2^{+/Cre};Rbpj^{fl/fl}* (Lyz2;Rbpj) lines were crossed to the *Pdx1-Flp;Kras^{+/FRT-STOP-FRT-G12D};p53^{flr/flt}* (KP^{flp}) or *Pdx1-Flp;Kras^{+/FRT-STOP-FRT-G12D};p53^{+/flt}* (KP^{flp,hct}) PDAC mouse models. Please refer to Fig. A.1 (p 94) for details on mouse crossing strategies.

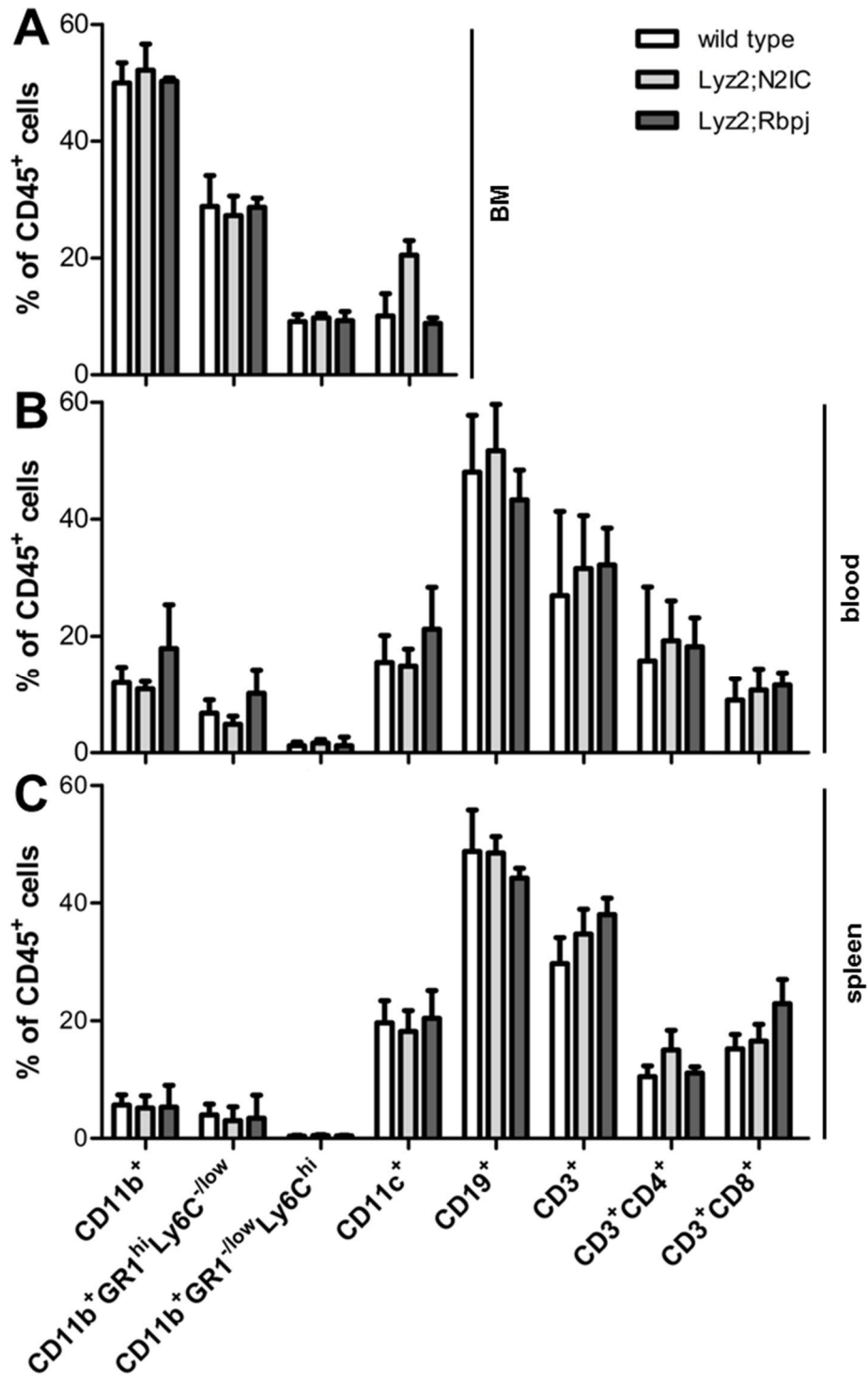


Figure 3.17: Neither myeloid Notch overexpression nor Rbpj knock out perturb leukocyte development in healthy mice. Flow cytometry analysis of bone marrow (BM), peripheral blood and spleen of 6-8 week old wild type (n=3), *Lyz2^{+/Cre};R26^{+LSL-N2IC}* (Lyz2;N2IC) (n=5), or *Lyz2^{+/Cre};Rbpj^{fl/fl}* (Lyz2;Rbpj) (n=5) mice. Quantification of positive cells is shown as percentage of a live CD45⁺ pre-gate. Bars indicate mean and SD.

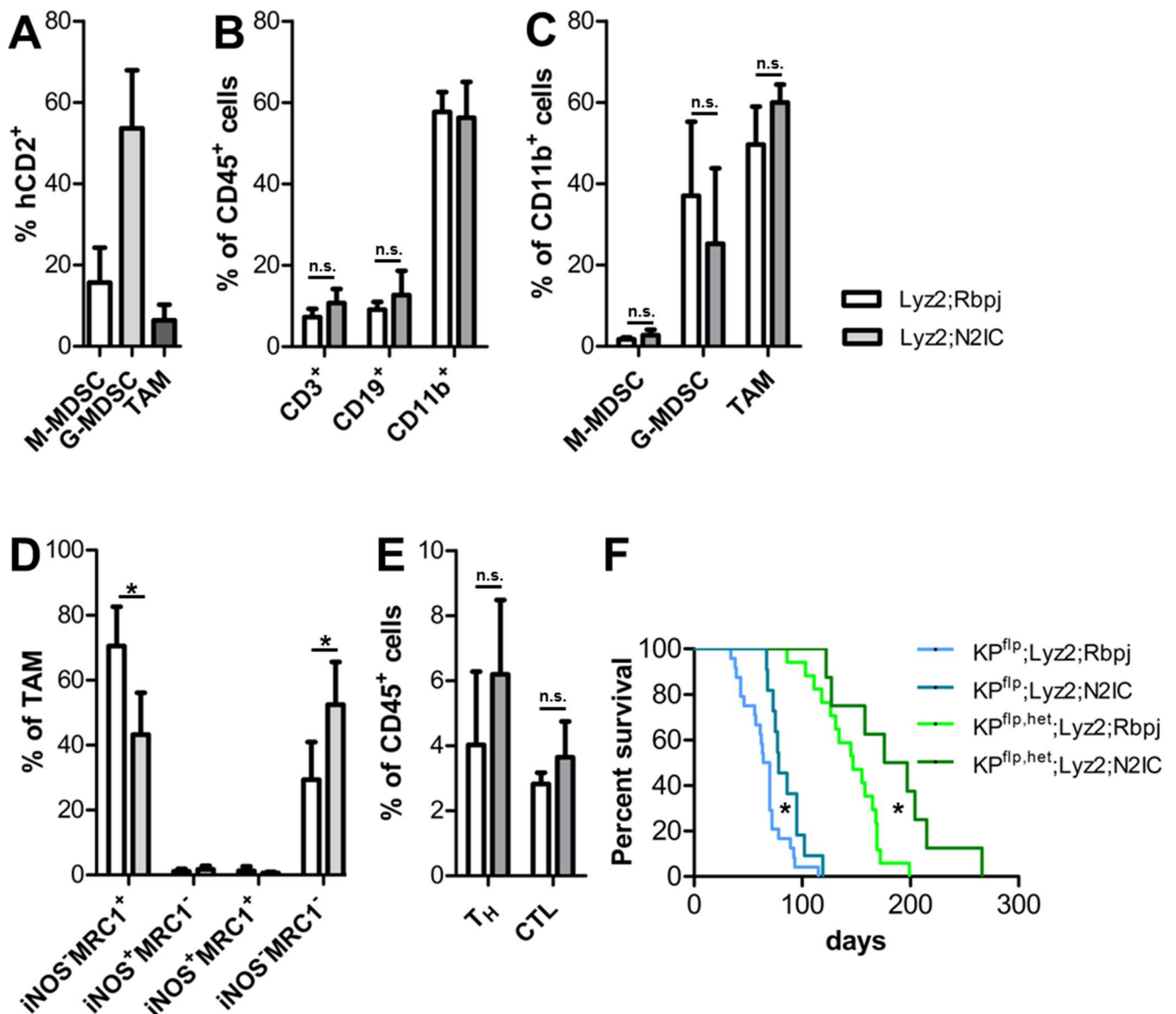


Figure 3.18: Notch signaling antagonizes M2 polarization in PDAC TAMs. Lyz2;Rbpj and Lyz2;N2IC mice were crossed to a KP^{flp} or KP^{flp,het} background. (A-E) Flow cytometry analysis of single cell suspensions. (A) Tumor suspensions of Lyz2;N2IC tumor bearing mice. Shown is percentage of cells positive for the co-expressed hCD2 reporter as percentage of the indicated myeloid population. n=5. M-MDSC: CD45⁺CD11b⁺F4/80^{-/low}GR1^{-/low}Ly6C^{hi}; G-MDSC: CD45⁺CD11b⁺F4/80^{-/low}GR1^{hi}; TAM: CD45⁺CD11b⁺F4/80⁺GR1^{-/low}. (B) Leukocyte subpopulations as percentage of total live leukocytes (CD45⁺). (C) Myeloid subpopulations as percentage of total live myeloid cells. (D) Quantification of iNOS and MRC1 expression in TAMs. iNOS⁻MRC1⁺ TAMs represent M2, iNOS⁺MRC1⁻ M1 macrophages. (E) T cell subpopulations T_H (CD3⁺CD4⁺CD8⁻) and CTL (CD3⁺CD4⁻CD8⁺) as percentage of total leukocytes. (F) Median survival: KP^{flp,het};Lyz2;Rbpj: 147 d, n=17, KP^{flp,het};Lyz2;N2IC: 186.5 d n=8, KP^{flp};Lyz2;Rbpj: 67 d, n=24, KP^{flp};Lyz2;N2IC: 78 d, n=11. Bars indicate mean and SD. *: p<0.05, n.s: p>0.05. (B,C,E) n=3-5. (D) n=6-7.

In tumor-associated myeloid cells, Lyz2-Cre activity was found in 18 % of M-MDSCs, 55 % of G-MDSCs, but only 8 % of TAMs as determined by hCD2 flow cytometry of tumor bearing Lyz2;N2IC mice (see Fig. 3.18 A). Within tumor-infiltrating leukocytes, no quantitative change in T, B, or the myeloid fractions was detected (see Fig. 3.18 B). In addition, myeloid Notch activation or blockade did not cause significant change in myeloid sub-populations (see Fig. 3.18 C). Polarization phenotyping of tumor-associated macrophages, however, revealed a significant downregulation of the MRC1 positive TAM fraction in Lyz2;N2IC tumor bearing mice compared to Lyz2;Rbpj tumor mice, indicating renunciation of M2 macrophage polarization. iNOS levels in TAMs were unaffected by myeloid Notch manipulation (see Fig. 3.18 C). To test, whether this macrophage phenotype switch leads to immune activation, tumors were analyzed for T cell infiltration. No increased influx of helper T (T_H) nor cytotoxic T cells (CTL) was detectable (see Fig. 3.18 E). However, reduction of M2 macrophage polarization translated in significant survival benefit of Lyz2;N2IC mice over Lyz2;Rbpj mice in the KP^{flp} as well as in the KP^{flp,het} PDAC mouse model system (see Fig. 3.18 F).

4 DISCUSSION

Despite extensive research efforts, the complexity and impact of the tumor immune environment on tumor progression and cancer therapies has been ignored or underestimated for decades. Novel immunotherapeutic approaches aim to unleash an immune response with the intent of attacking and eradicating malignant cells via the host's own immune defense. Such anti-tumor immune machineries have been shown to be highly effective in melanoma and lung cancer. Hence, a new perspective on non-malignant tumor components is increasingly acknowledged within the scientific community. However, in the case of pancreatic cancer, due to the repeated failures of immunotherapies, ongoing doubts have clouded our faith in them. Obviously, one can speculate that a unique, but so far unknown feature of the highly stromal microenvironment of pancreatic cancer is likely to be responsible for current barriers of immunotherapies in pancreatic cancer. Indeed, it has been reported that pancreatic cancer differs quantitatively from most other solid tumors with regards to infiltrating immune cells and tumor-associated fibroblasts (Chu et al., 2007). However, the complexity of the stromal networks goes far beyond just pure quantity as it is their precisely regulated interactions that ultimately define their behavior and outcome. This could also help to explain the intratumoral heterogeneity observed in various tumors originating from a similar genetic background.

4.1 Macrophages dominate PDAC immune environments

In this work, not only the quantity of tumor-associated immune cells was further analyzed but also the specific functions of both the adaptive as well as the innate infiltrating immune cells were investigated in detail using various experimental in vitro and in vivo systems. Flow cytometry analysis of cell suspensions isolated from PDAC of *Kras*^{G12D} tumor mice (KP mice) demonstrated that around 70 % of cells of the PDAC tumor mass account for leukocytes. These leukocytic infiltrates were found to consist of a heterogeneous assortment of various different immune cells with myeloid-derived cells forming the most significant population accounting for more than every second infiltrating leukocyte which is consistent with previous

studies in *Kras*^{G12D} mice without conditional *Trp53* deletion (Clark et al., 2007). Furthermore, it was shown that tumor-associated macrophages represent the most prominent myeloid subpopulation and, importantly, most TAMs were identified as M2-polarized macrophages which is in line with results from other tumor entities (Sica et al., 2006). M2-TAMs are linked to immune suppression, promotion of tumor progression, and poor prognosis (Kurahara et al., 2011; Sica and Mantovani, 2012). Clearly, this finding qualified TAMs for further analysis.

Three different approaches were pursued to elucidate TAM biology in pancreatic cancer. First, CCR2-dependent myeloid cell recruitment was dissected. It has been subject to ongoing debates whether TAMs originate from circulating pro-inflammatory monocytes or from tissue macrophages undergoing self-renewal (Movahedi et al., 2010). Inflammatory monocytes express the CCL2-related receptor CCR2 (Gordon and Taylor, 2005), both together forming a signaling axis commonly considered to be the major mediator of myeloid cell recruitment. Indeed pancreatic tumors are reported to express high amounts of CCL2 (Monti et al., 2003; Sanford et al., 2013). For several tumor entities, CCR2-dependent recruitment of macrophages has been linked to promotion of tumor development (Ren et al., 2012). Therefore, a genetic *Ccr2* knock out was introduced to spontaneous *Kras*^{G12D}-based PDAC mice to elucidate CCR2-dependent macrophage recruitment in pancreatic cancer. This knock out did not provoke a block in TAM accumulation in murine PDAC. In contrast, M-MDSC tumor site recruitment was blocked combined with a significant increase in G-MDSC accumulation overcompensating for the absence of M-MDSCs, an immature myeloid population showing some phenotypic overlap with circulating monocytes. This result is supported by similar findings reported from lung metastases after tail vein injection (Wolf et al., 2012) but at least partly in conflict with reports from lymphoma, melanoma, and breast cancer models (Ren et al., 2012). In terms of significance for tumor progression and overall survival, however, absence of CCR2 did not substantially affect PDAC development. Instead, the results show that tumor-associated macrophages do not rely on CCR2-dependent myeloid cell recruitment providing more evidence for monocyte independent TAM accumulation. Moreover, it was demonstrated, that tumor-infiltrating M-MDSC are not of prognostic value in PDAC, since mice developed and died from tumors similarly in absence or presence of M-MDSCs. It is important to note, that the

observed increase in G-MDSC accumulation did not aggravate tumor progression, which is surprising to some extent since elevated levels of MDSCs were described as an independent prognostic factor in humans (Gabitass et al., 2011) and there is clear evidence for G-MDSC-mediated suppression of adaptive immunity (Stromnes et al., 2014). Whether this is a species-specific difference or immune suppression simply cannot be further amplified in experimental tumor models, needs to be addressed in future studies.

Second, macrophages were identified as potential T cell in-activators via expression of PD-L1. Together with B cells, tumor-associated macrophages were identified to represent the major PD-L1 positive cell population in tumors of PDAC GEMMs. PD-L1 is a known activator of inhibitory PD-1 signal transduction, a central mediator of T cell inactivation. Hence, it was worthwhile to further analyze the role of macrophage-derived PD-L1 in pancreatic cancer immune suppression. Interestingly, PD-L1 was not found in significant amounts expressed on tumor cells, although other laboratories reported differently in human PDAC (Laheru and Jaffee, 2005). PD-L1 was blocked from binding target structures via a specific antibody in tumor-bearing mice. Analysis of the immune environment revealed that PD-L1 blockade did not promote immune cell activation. Even though the percentage of naïve helper T and cytotoxic T cells was reduced under PD-L1 blockade, no increase in T cell memory or activation markers was detectable suggesting that macrophages do not exert their immune suppressive properties via PD-L1/PD-1 signaling.

Third, tumor macrophages were successfully reprogrammed reducing tumor-promoting M2-polarization. Details on that approach will be addressed in section 4.3.

4.2 TILs do not provide effective anti-PDAC immunity

To better understand how pancreatic tumors interfere with cellular immunity, spleens of wild type and tumor-bearing mice were analyzed for their immune cell subsets. End-stage tumor mice showed an 8 x increase in CD11b⁺GR1⁺ cells accumulating in the spleen compared to tumor-free conditions. This population is generally referred to as granulocytic myeloid-derived suppressor cells. An immune suppressive phenotype of these cells could explain why T cells in spleens were qualitatively and quantitatively unperturbed in tumor hosts as they may be prevented from activation by the accumulating CD11b⁺GR1⁺ cells. Splenic B cells in contrast, were quantitatively reduced relative to total leukocytes. Within the B cell population tumors induced a shift from CD5⁺ B1a cells to CD5⁻ B1b cells, while B2 cells and plasma cells were unaffected. B1 cells are the predominant subset in the peritoneal cavity but usually rare in lymphatic organs (Renaudineau et al., 2001). In this study, they accounted for less than 10 % of all B cells in spleens of wild type mice as well as tumor-bearing mice. Whether B1a convert to B1b cells is currently not clear (Hardy, 2006) but the present results illustrate, that CD5⁻ B1 cells are clearly implicated in systemic tumor-dependent immune regulation. B cell subsets have been barely studied in models of solid tumors. From infectious disease we can assume a more innate-like immune activity of B1a but a more adaptive-oriented immune activity of B1b cells (Hardy, 2006). Future experiments need to be performed to shed light on this novel aspect of tumor-induced immune modulation.

B cells, as earlier mentioned, along with tumor-associated macrophages were found to express high amounts of PD-L1 suggesting a potential inhibitory immune function. But since highly efficient depletion of B cells as well as PD-L1 blockade did not translate in prolonged survival or immune activation, this mechanism appears to not play a major role in immune evasion of PDAC. However, it should be mentioned, that the KP mouse model is highly aggressive since homozygous loss of *Trp53* in combination with oncogenic *Kras*^{G12D} causes rapid progression from benign tumor to carcinoma. It could therefore very well be that modulating immune effects are superposed by perpetual oncogenic excitation providing only a short window until mice reach end-stage criteria. Still, PD-L1 blockade provoked alterations in tumor-infiltrating B cell subset composition. B2 cells were slightly, but

significantly reduced under α -B7H1 (PD-L1) treatment while the total B cell fraction of leukocytes was not affected. Additionally, B1a cells compensated for missing B2 cells. Results of this thesis, however, do not provide clear evidence, that PD-L1 blockade-dependent B2 to B1a shifting provokes T cell activation or induction of T cell memory as CD69⁺ and CD44^{hi} expression was not found increased in T cells. Intriguingly, PD-L1 blockade resulted in downregulation of CD62L of CTLs and T helper cells. CD62L (L-selectin) is required for T cell homing and is usually highly expressed on naïve and central memory cells, but low on effector T cells. But since no increase in CD44 or CD69 expression correlated with the downregulation of CD62L, reduction of naïve T cells cannot be definitely linked to T cell activation. It appears conceivable that PD-L1 blockade supports T cell effector state induction including CD62L downregulation, but may not be sufficient to allow for developing a full T cell effector state or T cell memory formation in pancreatic cancer as seen by missing CD69 and CD44 induction. This could help to explain, why immunotherapies targeting the PD-L1/PD-1 axis failed in patients of pancreatic cancer (Brahmer et al., 2012; Nguyen and Ohashi, 2015). Presumably, additional co-stimulatory triggers are required to achieve a robust T cell activation in pancreatic cancer. Further analyses are required to clarify at which step and by which mechanisms T cell activation is arrested under PD-L1 blockade.

Considerable amounts of adaptive immune cells including CD8⁺ T lymphocytes (CTLs), which are generally linked to better prognosis and prolonged patient survival (Fridman et al., 2012), were detected in the stroma of murine PDAC which is in contrast to findings of some other laboratories considering PDAC an immune privileged niche characterized by T cell exclusion (Beatty et al., 2015). Technical approach or used model systems are likely to be the reason for conflictive data here. Surprisingly, presence or absence of tumor-infiltrating T cells was irrelevant for tumor growth and overall survival of tumor animals. The same effect was detected for B lymphocytes providing clear evidence that T and B cells are indeed present at tumor sites, but incapable of forming an effective anti-tumor immunity in the context of pancreatic cancer illustrating that pure quantity does not incrementally imply functionality or effectiveness in anti-tumor immunity. Along this line, tumor-bearing mice did not experience increased T cell memory in spleens. Even more important, tumor-associated CTLs and T helper cells showed the same

proportion of memory T cells as in spleens of healthy littermates. These findings raise the question, whether CTLs are ineffective at PDAC tumor sites due to a non-immunogenic malignancy or missing co-stimulatory signaling potentially outbalanced by inhibitory immune suppressive signaling. Previous data provide inconsistent answers to this fundamental question (Garbe et al., 2006; Lutz et al., 2014) and it is subject to current research projects to provide convincing data addressing this question.

While regulatory T cells are often described as frequent PDAC infiltrators (Shevchenko et al., 2013), they were detected only in rare amounts in this study. This discrepancy might result from the different types of tumor models investigated. Studies specifically targeting regulatory T cells are required and will be more suited to finally clarify the actual impact of regulatory T lymphocytes on PDAC. In addition, $\gamma\delta$ T cells infiltrated tumors of the spontaneous mouse model used in this study to insignificant numbers suggesting a minor role in murine PDAC.

4.3 Notch activation counteracts M2-TAM polarization

Bone marrow-derived macrophages have proven to be a powerful tool to study macrophage polarization in vitro thus allowing for rapid analysis of various conditions. Recombinant CRE protein was efficiently used to introduce genetic activation or inactivation of Notch signaling in cultures from same donor animal. Notch signaling was found to counteract IL4-induced M2 macrophage polarization, whereas Inhibition of Notch signaling via knock out of *Rbpj* suspended LPS from inducing robust M1-polarization. Notch activation alone upregulated some but not all M1 markers to low levels, and downregulated two out of three tested M2 marker genes. Combination of Notch activation and LPS stimulation, however, did not result in a synergistic upregulation of M1 genes. Similarly, knock out of *Rbpj* could not further reinforce M2 polarization in combination with IL4. Taken together, these data suggest that activation of Notch signaling counteracts M2 polarization, whereas its blocking counteracts M1 polarization. In an initial study a different laboratory co-cultured BMDMs with a Dll1, a Notch ligand, overexpressing cell line to activate Notch signaling in BMDM (Wang et al., 2010) and found similar, but not

identical results. Wang and colleagues reported that Notch activation provides BMDMs which are more susceptible to LPS stimulation suggesting a synergistic Notch-LPS interaction. Furthermore they found some M1 gene induction by IL4 stimulated Notch-activated cells suggesting Notch to transmodulate M2 stimuli to M1 responses. It cannot be excluded in co-culture systems that additional signaling cascades are engaged compromising experimental results, a severe challenge, which genetic approaches avoid. Moreover, Wang and colleagues used a different protocol to differentiate bone marrow cells to BMDMs, which relies on GM-CSF. GM-CSF is not only described to drive dendritic cell differentiation from immature myeloid cells (van de Laar et al., 2012), but also to promote M1 polarization in macrophages (Sica et al., 2006). M-CSF, on the other hand, is not only described as macrophage maturation marker but also as inducer of M2-polarization. Thus, both studies base on different types of BMDM which could explain some discrepancy in their results. LPS was used in same concentrations, meaning differences seen in Notch-LPS synergism do not originate from LPS concentrations used. Wang and colleagues described Notch to promote M1 phenotype whereas this work sees Notch as mediator of M2 counteraction. These results are not necessarily contradictory, but more likely describing the same coin from the opposing side due to M-CSF or GM-CSF pretreatment facilitating a basal macrophage polarization which is already M2-oriented (M-CSF) or already M1-oriented (GM-CSF) at the time they were used for polarization experiments.

This work reported experiments providing striking evidence, that activation of Notch signal transduction effectively counteracts M2 macrophage polarization not only in vitro but also in vivo. Some earlier attempts to reprogram or re-polarize macrophages in experimental pancreatic cancer have reported beneficial outcome when M2 polarization was antagonized either genetically or by low-dose irradiation (Gironella et al., 2013; Klug et al., 2013). Both studies, however, face limitations of translational relevance since experiments were conducted either by orthotopic and subcutaneous tumor cell transplantation or transgenic Rt5 mouse models which do not recapitulate features of human PDAC as thoroughly as spontaneous *Kras*^{G12D}-driven PDAC mouse models. Nevertheless, their findings support the results of this study.

This study used a novel combined dual-recombinase system to genetically induce *Kras*^{G12D}-driven pancreatic tumorigenesis and myeloid specific modulation of Notch signaling demonstrating significant downregulation of M2 marker MRC1 and prolonged survival in Lyz2;N2IC tumor mice. Noteworthy, consistent with the above mentioned in vitro experiments, Notch activation counteracted M2-polarization, but did not promote upregulation of M1 phenotype. Combinatorial future approaches to not only counteract M2-polarisation, but also to induce M1-polarization will hopefully explore the full potential of anti-tumor macrophage abilities.

For recombination of *loxP*-flanked Notch1C-hCD2 target structures by Lyz2-CRE in tumor-associated macrophages an efficiency of only 8-10 % was determined while efficiency in G-MDSCs was 50 %. When this CRE-expressing line was first described in 1999 Clausen and colleagues reported 83-98 % recombination efficiency in macrophages and 100 % in granulocytes (Clausen et al., 1999). Since different reporter genes were used to quantify *loxP* recombination efficiency, comparability of results is restricted as some constructs might be more easily accessible for CRE-recombinases or reporter gene expression is differentially controlled (Liu et al., 2013). Still, having found only 8-10 % of TAMs hit by Lyz2 dependent Notch activation, data suggests that a more reliable Cre strain might provoke even stronger downregulation of M2-associated genes indicating that the full potential of macrophage reprogramming is not yet fully exhausted.

Cytotoxic T cells are often believed to function as necessary effectors of anti-tumor immunity. But, despite obvious survival benefits, no significant increase in tumor-infiltrating CTLs was detected in tumor mice with reduced M2-phenotype. Beatty and colleagues provided striking results on CD40-activated macrophages reporting that tumor regression in PDAC GEMMs did not require T cells when macrophages were tumoricidal. This suggests that therapy-induced T cell activation is not a categorical requirement for effective anti-tumor immune activation (Beatty et al., 2011). Although the exact molecular basis of the tumoricidal effectors in tumors with fostered myeloid Notch signaling requires further research efforts, current results and the study by Beatty and colleagues suggest a T cell-independent mechanism.

4.4 Conclusion

This thesis aimed to dissect the immune environment of pancreatic cancer in spontaneous PDAC mouse models. The tumor microenvironment was extensively characterized in regards to infiltrating immune cells, their activation state and functional phenotype. Related mechanisms of immune cell recruitment were addressed as well. Furthermore, a recently developed dual-recombinase approach was used to investigate genetic macrophage reprogramming in a complex in vivo tumor situation.

The results obtained from these experiments open new perspectives on PDAC-associated cellular immunity. Taken together, the present study (1) provided new evidence for monocyte-independent macrophage accumulation in PDAC, (2) identified B1 cells as novel players in pancreatic cancer immune environments, (3) provided strong evidence for a total black out of adaptive anti-tumor immunity, and (4) confirmed macrophage Notch signaling as a highly promising target to reprogram tumor-associated macrophages in vivo. Fostering effective anti-tumor innate immunity may provide a potent back up when adaptive immunity fails.

Future studies are now required to translate these novel insights in the immune environment of pancreatic cancer to therapeutic applications. Certainly, this will contribute to finally unlock current barriers to immunotherapies in pancreatic cancer, which may hopefully help to transform a deadly malignancy into a chronic, controllable disease.

5 LITERATURE

- Affara, N.I., B. Ruffell, T.R. Medler, A.J. Gunderson, M. Johansson, S. Bornstein, E. Bergsland, M. Steinhoff, Y. Li, Q. Gong, Y. Ma, J.F. Wiesen, M.H. Wong, M. Kulesz-Martin, B. Irving and L.M. Coussens. **2014**. B cells regulate macrophage phenotype and response to chemotherapy in squamous carcinomas. *Cancer Cell*. 25:809-821.
- Aichler, M., C. Seiler, M. Tost, J. Siveke, P.K. Mazur, P. Da Silva-Buttkus, D.K. Bartsch, P. Langer, S. Chiblak, A. Durr, H. Hofler, G. Kloppel, K. Muller-Decker, M. Brielmeier and I. Esposito. **2012**. Origin of pancreatic ductal adenocarcinoma from atypical flat lesions: a comparative study in transgenic mice and human tissues. *J Pathol*. 226:723-734.
- Amsen, D., A. Antov and R.A. Flavell. **2009**. The different faces of Notch in T-helper-cell differentiation. *Nat Rev Immunol*. 9:116-124.
- Andersson, E.R. and U. Lendahl. **2014**. Therapeutic modulation of Notch signalling--are we there yet? *Nat Rev Drug Discov*. 13:357-378.
- Apte, M.V., S. Park, P.A. Phillips, N. Santucci, D. Goldstein, R.K. Kumar, G.A. Ramm, M. Buchler, H. Friess, J.A. McCarroll, G. Keogh, N. Merrett, R. Pirola and J.S. Wilson. **2004**. Desmoplastic reaction in pancreatic cancer: role of pancreatic stellate cells. *Pancreas*. 29:179-187.
- Apte, M.V., J.S. Wilson, A. Lugea and S.J. Pandol. **2013**. A starring role for stellate cells in the pancreatic cancer microenvironment. *Gastroenterology*. 144:1210-1219.
- Balkwill, F., A. Montfort and M. Capasso. **2013**. B regulatory cells in cancer. *Trends Immunol*. 34:169-173.
- Bardeesy, N. and R.A. DePinho. **2002**. Pancreatic cancer biology and genetics. *Nat Rev Cancer*. 2:897-909.
- Bayne, L.J., G.L. Beatty, N. Jhala, C.E. Clark, A.D. Rhim, B.Z. Stanger and R.H. Vonderheide. **2012**. Tumor-derived granulocyte-macrophage colony-stimulating factor regulates myeloid inflammation and T cell immunity in pancreatic cancer. *Cancer Cell*. 21:822-835.
- Beatty, G.L., E.G. Chiorean, M.P. Fishman, B. Saboury, U.R. Teitelbaum, W. Sun, R.D. Huhn, W. Song, D. Li, L.L. Sharp, D.A. Torigian, P.J. O'Dwyer and R.H. Vonderheide. **2011**. CD40 agonists alter tumor stroma and show efficacy against pancreatic carcinoma in mice and humans. *Science*. 331:1612-1616.

- Beatty, G.L., R. Winograd, R.A. Evans, K.B. Long, S.L. Luque, J.W. Lee, C. Clendenin, W.L. Gladney, D.M. Knoblock, P.D. Guirnalda and R.H. Vonderheide. **2015**. Exclusion of T Cells From Pancreatic Carcinomas in Mice Is Regulated by Ly6C(low) F4/80(+) Extratumoral Macrophages. *Gastroenterology*. 149:201-210.
- Bijlsma, M.F. and H.W. van Laarhoven. **2015**. The conflicting roles of tumor stroma in pancreatic cancer and their contribution to the failure of clinical trials: a systematic review and critical appraisal. *Cancer Metastasis Rev*. 34:97-114.
- Blankenstein, T., P.G. Coulie, E. Gilboa and E.M. Jaffee. **2012**. The determinants of tumour immunogenicity. *Nat Rev Cancer*. 12:307-313.
- Boring, L., J. Gosling, S.W. Chensue, S.L. Kunkel, R.V. Farese, Jr., H.E. Broxmeyer and I.F. Charo. **1997**. Impaired monocyte migration and reduced type 1 (Th1) cytokine responses in C-C chemokine receptor 2 knockout mice. *J Clin Invest*. 100:2552-2561.
- Brahmer, J.R., S.S. Tykodi, L.Q. Chow, W.J. Hwu, S.L. Topalian, P. Hwu, C.G. Drake, L.H. Camacho, J. Kauh, K. Odunsi, H.C. Pitot, O. Hamid, S. Bhatia, R. Martins, K. Eaton, S. Chen, T.M. Salay, S. Alaparthi, J.F. Grosso, A.J. Korman, S.M. Parker, S. Agrawal, S.M. Goldberg, D.M. Pardoll, A. Gupta and J.M. Wigginton. **2012**. Safety and activity of anti-PD-L1 antibody in patients with advanced cancer. *N Engl J Med*. 366:2455-2465.
- Broz, M.L., M. Binnewies, B. Boldajipour, A.E. Nelson, J.L. Pollack, D.J. Erle, A. Barczak, M.D. Rosenblum, A. Daud, D.L. Barber, S. Amigorena, L.J. Van't Veer, A.I. Sperling, D.M. Wolf and M.F. Krummel. **2014**. Dissecting the tumor myeloid compartment reveals rare activating antigen-presenting cells critical for T cell immunity. *Cancer Cell*. 26:638-652.
- Byles, V., A.J. Covarrubias, I. Ben-Sahra, D.W. Lamming, D.M. Sabatini, B.D. Manning and T. Horng. **2013**. The TSC-mTOR pathway regulates macrophage polarization. *Nat Commun*. 4:2834.
- Carding, S.R. and P.J. Egan. **2002**. Gammadelta T cells: functional plasticity and heterogeneity. *Nat Rev Immunol*. 2:336-345.
- Cheng, P., V. Kumar, H. Liu, J.I. Youn, M. Fishman, S. Sherman and D. Gabrilovich. **2014**. Effects of notch signaling on regulation of myeloid cell differentiation in cancer. *Cancer Res*. 74:141-152.
- Chu, G.C., A.C. Kimmelman, A.F. Hezel and R.A. DePinho. **2007**. Stromal biology of pancreatic cancer. *J Cell Biochem*. 101:887-907.
- Clark, C.E., S.R. Hingorani, R. Mick, C. Combs, D.A. Tuveson and R.H. Vonderheide. **2007**. Dynamics of the immune reaction to pancreatic cancer from inception to invasion. *Cancer Res*. 67:9518-9527.

- Clark, K., K.F. MacKenzie, K. Petkevicius, Y. Kristariyanto, J. Zhang, H.G. Choi, M. Peggie, L. Plater, P.G. Pedrioli, E. McIver, N.S. Gray, J.S. Arthur and P. Cohen. **2012**. Phosphorylation of CRT3 by the salt-inducible kinases controls the interconversion of classically activated and regulatory macrophages. *Proc Natl Acad Sci U S A*. 109:16986-16991.
- Clausen, B.E., C. Burkhardt, W. Reith, R. Renkawitz and I. Forster. **1999**. Conditional gene targeting in macrophages and granulocytes using LysMcre mice. *Transgenic Res*. 8:265-277.
- Constant, P., F. Davodeau, M.A. Peyrat, Y. Poquet, G. Puzo, M. Bonneville and J.J. Fournie. **1994**. Stimulation of human gamma delta T cells by nonpeptidic mycobacterial ligands. *Science*. 264:267-270.
- D'Souza, B., A. Miyamoto and G. Weinmaster. **2008**. The many facets of Notch ligands. *Oncogene*. 27:5148-5167.
- de Visser, K.E., A. Eichten and L.M. Coussens. **2006**. Paradoxical roles of the immune system during cancer development. *Nat Rev Cancer*. 6:24-37.
- Di Mitri, D., A. Toso, J.J. Chen, M. Sarti, S. Pinton, T.R. Jost, R. D'Antuono, E. Montani, R. Garcia-Escudero, I. Guccini, S. Da Silva-Alvarez, M. Collado, M. Eisenberger, Z. Zhang, C. Catapano, F. Grassi and A. Alimonti. **2014**. Tumour-infiltrating Gr-1+ myeloid cells antagonize senescence in cancer. *Nature*. 515:134-137.
- DiLillo, D.J., K. Yanaba and T.F. Tedder. **2010**. B cells are required for optimal CD4+ and CD8+ T cell tumor immunity: therapeutic B cell depletion enhances B16 melanoma growth in mice. *J Immunol*. 184:4006-4016.
- Dong, H., S.E. Strome, D.R. Salomao, H. Tamura, F. Hirano, D.B. Flies, P.C. Roche, J. Lu, G. Zhu, K. Tamada, V.A. Lennon, E. Celis and L. Chen. **2002**. Tumor-associated B7-H1 promotes T-cell apoptosis: a potential mechanism of immune evasion. *Nat Med*. 8:793-800.
- Edlund, H. **2002**. Pancreatic organogenesis--developmental mechanisms and implications for therapy. *Nat Rev Genet*. 3:524-532.
- Evans, A. and E. Costello. **2012**. The role of inflammatory cells in fostering pancreatic cancer cell growth and invasion. *Front Physiol*. 3:270.
- Fridman, W.H., F. Pages, C. Sautes-Fridman and J. Galon. **2012**. The immune contexture in human tumours: impact on clinical outcome. *Nat Rev Cancer*. 12:298-306.

- Gabitass, R.F., N.E. Annels, D.D. Stocken, H.A. Pandha and G.W. Middleton. **2011**. Elevated myeloid-derived suppressor cells in pancreatic, esophageal and gastric cancer are an independent prognostic factor and are associated with significant elevation of the Th2 cytokine interleukin-13. *Cancer Immunol Immunother.* 60:1419-1430.
- Gabrilovich, D.I., V. Bronte, S.H. Chen, M.P. Colombo, A. Ochoa, S. Ostrand-Rosenberg and H. Schreiber. **2007**. The terminology issue for myeloid-derived suppressor cells. *Cancer Res.* 67:425; author reply 426.
- Gabrilovich, D.I., S. Ostrand-Rosenberg and V. Bronte. **2012**. Coordinated regulation of myeloid cells by tumours. *Nat Rev Immunol.* 12:253-268.
- Gajewski, T.F., H. Schreiber and Y.X. Fu. **2013**. Innate and adaptive immune cells in the tumor microenvironment. *Nat Immunol.* 14:1014-1022.
- Galon, J., A. Costes, F. Sanchez-Cabo, A. Kirilovsky, B. Mlecnik, C. Lagorce-Pages, M. Tosolini, M. Camus, A. Berger, P. Wind, F. Zinzindohoue, P. Bruneval, P.H. Cugnenc, Z. Trajanoski, W.H. Fridman and F. Pages. **2006**. Type, density, and location of immune cells within human colorectal tumors predict clinical outcome. *Science.* 313:1960-1964.
- Garbe, A.I., B. Vermeer, J. Gamrekashvili, R. von Wasielewski, F.R. Greten, A.M. Westendorf, J. Buer, R.M. Schmid, M.P. Manns, F. Korangy and T.F. Greten. **2006**. Genetically induced pancreatic adenocarcinoma is highly immunogenic and causes spontaneous tumor-specific immune responses. *Cancer Res.* 66:508-516.
- Gironella, M., C. Calvo, A. Fernandez, D. Closa, J.L. Iovanna, J. Rosello-Catafau and E. Folch-Puy. **2013**. Reg3beta deficiency impairs pancreatic tumor growth by skewing macrophage polarization. *Cancer Res.* 73:5682-5694.
- Gnerlich, J.L., J.B. Mitchem, J.S. Weir, N.V. Sankpal, H. Kashiwagi, B.A. Belt, M.R. Porembka, J.M. Herndon, T.J. Eberlein, P. Goedegebuure and D.C. Linehan. **2010**. Induction of Th17 cells in the tumor microenvironment improves survival in a murine model of pancreatic cancer. *J Immunol.* 185:4063-4071.
- Gordon, S. **2003**. Alternative activation of macrophages. *Nat Rev Immunol.* 3:23-35.
- Gordon, S. and F.O. Martinez. **2010**. Alternative activation of macrophages: mechanism and functions. *Immunity.* 32:593-604.
- Gordon, S. and P.R. Taylor. **2005**. Monocyte and macrophage heterogeneity. *Nat Rev Immunol.* 5:953-964.

- Gounaris, E., N.R. Blatner, K. Dennis, F. Magnusson, M.F. Gurish, T.B. Strom, P. Beckhove, F. Gounari and K. Khazaie. **2009**. T-regulatory cells shift from a protective anti-inflammatory to a cancer-promoting proinflammatory phenotype in polyposis. *Cancer Res.* 69:5490-5497.
- Greten, T.F. **2014**. Myeloid-derived suppressor cells in pancreatic cancer: more than a hidden barrier for antitumour immunity? *Gut.* 63:1690-1691.
- Gunderson, A.J. and L.M. Coussens. **2013**. B cells and their mediators as targets for therapy in solid tumors. *Exp Cell Res.* 319:1644-1649.
- Habbe, N., G. Shi, R.A. Meguid, V. Fendrich, F. Esni, H. Chen, G. Feldmann, D.A. Stoffers, S.F. Konieczny, S.D. Leach and A. Maitra. **2008**. Spontaneous induction of murine pancreatic intraepithelial neoplasia (mPanIN) by acinar cell targeting of oncogenic Kras in adult mice. *Proc Natl Acad Sci U S A.* 105:18913-18918.
- Hadrup, S., M. Donia and P. Thor Straten. **2013**. Effector CD4 and CD8 T cells and their role in the tumor microenvironment. *Cancer Microenviron.* 6:123-133.
- Hampel, F., S. Ehrenberg, C. Hojer, A. Draeseke, G. Marschall-Schroter, R. Kuhn, B. Mack, O. Gires, C.J. Vahl, M. Schmidt-Supprian, L.J. Strobl and U. Zimmer-Strobl. **2011**. CD19-independent instruction of murine marginal zone B-cell development by constitutive Notch2 signaling. *Blood.* 118:6321-6331.
- Hanahan, D. and L.M. Coussens. **2012**. Accessories to the crime: functions of cells recruited to the tumor microenvironment. *Cancer Cell.* 21:309-322.
- Hardy, R.R. **2006**. B-1 B cell development. *J Immunol.* 177:2749-2754.
- He, D., H. Li, N. Yusuf, C.A. Elmets, J. Li, J.D. Mountz and H. Xu. **2010**. IL-17 promotes tumor development through the induction of tumor promoting microenvironments at tumor sites and myeloid-derived suppressor cells. *J Immunol.* 184:2281-2288.
- Hezel, A.F., A.C. Kimmelman, B.Z. Stanger, N. Bardeesy and R.A. Depinho. **2006**. Genetics and biology of pancreatic ductal adenocarcinoma. *Genes Dev.* 20:1218-1249.
- Hidalgo, M. **2010**. Pancreatic cancer. *N Engl J Med.* 362:1605-1617.
- Hingorani, S.R., E.F. Petricoin, A. Maitra, V. Rajapakse, C. King, M.A. Jacobetz, S. Ross, T.P. Conrads, T.D. Veenstra, B.A. Hitt, Y. Kawaguchi, D. Johann, L.A. Liotta, H.C. Crawford, M.E. Putt, T. Jacks, C.V. Wright, R.H. Hruban, A.M. Lowy and D.A. Tuveson. **2003**. Preinvasive and invasive ductal pancreatic cancer and its early detection in the mouse. *Cancer Cell.* 4:437-450.

- Hiraoka, N., K. Onozato, T. Kosuge and S. Hirohashi. **2006**. Prevalence of FOXP3+ regulatory T cells increases during the progression of pancreatic ductal adenocarcinoma and its premalignant lesions. *Clin Cancer Res.* 12:5423-5434.
- Ishii, M., H. Wen, C.A. Corsa, T. Liu, A.L. Coelho, R.M. Allen, W.F.t. Carson, K.A. Cavassani, X. Li, N.W. Lukacs, C.M. Hogaboam, Y. Dou and S.L. Kunkel. **2009**. Epigenetic regulation of the alternatively activated macrophage phenotype. *Blood.* 114:3244-3254.
- Jackson, E.L., N. Willis, K. Mercer, R.T. Bronson, D. Crowley, R. Montoya, T. Jacks and D.A. Tuveson. **2001**. Analysis of lung tumor initiation and progression using conditional expression of oncogenic K-ras. *Genes Dev.* 15:3243-3248.
- Jemal, A., R. Siegel, E. Ward, Y. Hao, J. Xu, T. Murray and M.J. Thun. **2008**. Cancer statistics, 2008. *CA Cancer J Clin.* 58:71-96.
- Kawaguchi, Y., B. Cooper, M. Gannon, M. Ray, R.J. MacDonald and C.V. Wright. **2002**. The role of the transcriptional regulator Ptf1a in converting intestinal to pancreatic progenitors. *Nat Genet.* 32:128-134.
- Klug, F., H. Prakash, P.E. Huber, T. Seibel, N. Bender, N. Halama, C. Pfirschke, R.H. Voss, C. Timke, L. Umansky, K. Klapproth, K. Schakel, N. Garbi, D. Jager, J. Weitz, H. Schmitz-Winnenthal, G.J. Hammerling and P. Bechthold. **2013**. Low-dose irradiation programs macrophage differentiation to an iNOS(+)/M1 phenotype that orchestrates effective T cell immunotherapy. *Cancer Cell.* 24:589-602.
- Kopan, R. and M.X. Ilagan. **2009**. The canonical Notch signaling pathway: unfolding the activation mechanism. *Cell.* 137:216-233.
- Kurahara, H., H. Shinchi, Y. Mataka, K. Maemura, H. Noma, F. Kubo, M. Sakoda, S. Ueno, S. Natsugoe and S. Takao. **2011**. Significance of M2-polarized tumor-associated macrophage in pancreatic cancer. *J Surg Res.* 167:e211-219.
- Laheru, D. and E.M. Jaffee. **2005**. Immunotherapy for pancreatic cancer - science driving clinical progress. *Nat Rev Cancer.* 5:459-467.
- Lakshmi Narendra, B., K. Eshvendar Reddy, S. Shantikumar and S. Ramakrishna. **2013**. Immune system: a double-edged sword in cancer. *Inflamm Res.* 62:823-834.
- LeBien, T.W. and T.F. Tedder. **2008**. B lymphocytes: how they develop and function. *Blood.* 112:1570-1580.
- Lee, C.L., E.J. Moding, X. Huang, Y. Li, L.Z. Woodlief, R.C. Rodrigues, Y. Ma and D.G. Kirsch. **2012**. Generation of primary tumors with Flp recombinase in FRT-flanked p53 mice. *Dis Model Mech.* 5:397-402.

- Liao, X., N. Sharma, F. Kapadia, G. Zhou, Y. Lu, H. Hong, K. Paruchuri, G.H. Mahabeleshwar, E. Dalmas, N. Venteclef, C.A. Flask, J. Kim, B.W. Doreian, K.Q. Lu, K.H. Kaestner, A. Hamik, K. Clement and M.K. Jain. **2011**. Kruppel-like factor 4 regulates macrophage polarization. *J Clin Invest*. 121:2736-2749.
- Linnebacher, M. and C. Maletzki. **2012**. Tumor-infiltrating B cells: The ignored players in tumor immunology. *Oncoimmunology*. 1:1186-1188.
- Liu, J., S.G. Willet, E.D. Bankaitis, Y. Xu, C.V. Wright and G. Gu. **2013**. Non-parallel recombination limits Cre-LoxP-based reporters as precise indicators of conditional genetic manipulation. *Genesis*. 51:436-442.
- Lutz, E.R., A.A. Wu, E. Bigelow, R. Sharma, G. Mo, K. Soares, S. Solt, A. Dorman, A. Wamwea, A. Yager, D. Laheru, C.L. Wolfgang, J. Wang, R.H. Hruban, R.A. Anders, E.M. Jaffee and L. Zheng. **2014**. Immunotherapy converts nonimmunogenic pancreatic tumors into immunogenic foci of immune regulation. *Cancer Immunol Res*. 2:616-631.
- Madisen, L., T.A. Zwingman, S.M. Sunkin, S.W. Oh, H.A. Zariwala, H. Gu, L.L. Ng, R.D. Palmiter, M.J. Hawrylycz, A.R. Jones, E.S. Lein and H. Zeng. **2010**. A robust and high-throughput Cre reporting and characterization system for the whole mouse brain. *Nat Neurosci*. 13:133-140.
- Mak, T.W. and D.A. Ferrick. **1998**. The gammadelta T-cell bridge: linking innate and acquired immunity. *Nat Med*. 4:764-765.
- Marino, S., M. Vooijs, H. van Der Gulden, J. Jonkers and A. Berns. **2000**. Induction of medulloblastomas in p53-null mutant mice by somatic inactivation of Rb in the external granular layer cells of the cerebellum. *Genes Dev*. 14:994-1004.
- Mazur, P.K., B.M. Gruner, H. Nakhai, B. Sipos, U. Zimmer-Strobl, L.J. Strobl, F. Radtke, R.M. Schmid and J.T. Siveke. **2010**. Identification of epidermal Pdx1 expression discloses different roles of Notch1 and Notch2 in murine Kras(G12D)-induced skin carcinogenesis in vivo. *PLoS One*. 5:e13578.
- Mazur, P.K., A. Herner, F. Neff and J.T. Siveke. **2015**. Current methods in mouse models of pancreatic cancer. *Methods Mol Biol*. 1267:185-215.
- Mazur, P.K. and J.T. Siveke. **2012**. Genetically engineered mouse models of pancreatic cancer: unravelling tumour biology and progressing translational oncology. *Gut*. 61:1488-1500.
- McAllister, F., J.M. Bailey, J. Alsina, C.J. Nirschl, R. Sharma, H. Fan, Y. Rattigan, J.C. Roeser, R.H. Lankapalli, H. Zhang, E.M. Jaffee, C.G. Drake, F. Housseau, A. Maitra, J.K. Kolls, C.L. Sears, D.M. Pardoll and S.D. Leach. **2014**. Oncogenic Kras activates a hematopoietic-to-epithelial IL-17 signaling axis in preinvasive pancreatic neoplasia. *Cancer Cell*. 25:621-637.

- McAllister, S.S. and R.A. Weinberg. **2014**. The tumour-induced systemic environment as a critical regulator of cancer progression and metastasis. *Nat Cell Biol.* 16:717-727.
- Mitchem, J.B., D.J. Brennan, B.L. Knolhoff, B.A. Belt, Y. Zhu, D.E. Sanford, L. Belaygorod, D. Carpenter, L. Collins, D. Piwnica-Worms, S. Hewitt, G.M. Udipi, W.M. Gallagher, C. Wegner, B.L. West, A. Wang-Gillam, P. Goedegebuure, D.C. Linehan and D.G. DeNardo. **2013**. Targeting tumor-infiltrating macrophages decreases tumor-initiating cells, relieves immunosuppression, and improves chemotherapeutic responses. *Cancer Res.* 73:1128-1141.
- Mombaerts, P., J. Iacomini, R.S. Johnson, K. Herrup, S. Tonegawa and V.E. Papaioannou. **1992**. RAG-1-deficient mice have no mature B and T lymphocytes. *Cell.* 68:869-877.
- Monti, P., B.E. Leone, F. Marchesi, G. Balzano, A. Zerbi, F. Scaltrini, C. Pasquali, G. Calori, F. Pessi, C. Sperti, V. Di Carlo, P. Allavena and L. Piemonti. **2003**. The CC chemokine MCP-1/CCL2 in pancreatic cancer progression: regulation of expression and potential mechanisms of antitumorigenic activity. *Cancer Res.* 63:7451-7461.
- Morris, J.P.t., D.A. Cano, S. Sekine, S.C. Wang and M. Hebrok. **2010a**. Beta-catenin blocks Kras-dependent reprogramming of acini into pancreatic cancer precursor lesions in mice. *J Clin Invest.* 120:508-520.
- Morris, J.P.t., S.C. Wang and M. Hebrok. **2010b**. KRAS, Hedgehog, Wnt and the twisted developmental biology of pancreatic ductal adenocarcinoma. *Nat Rev Cancer.* 10:683-695.
- Mosser, D.M. and J.P. Edwards. **2008**. Exploring the full spectrum of macrophage activation. *Nat Rev Immunol.* 8:958-969.
- Movahedi, K., D. Laoui, C. Gysemans, M. Baeten, G. Stange, J. Van den Bossche, M. Mack, D. Pipeleers, P. In't Veld, P. De Baetselier and J.A. Van Ginderachter. **2010**. Different tumor microenvironments contain functionally distinct subsets of macrophages derived from Ly6C(high) monocytes. *Cancer Res.* 70:5728-5739.
- Mueller, M.M. and N.E. Fusenig. **2004**. Friends or foes - bipolar effects of the tumour stroma in cancer. *Nat Rev Cancer.* 4:839-849.
- Mulkeen, A.L., P.S. Yoo and C. Cha. **2006**. Less common neoplasms of the pancreas. *World J Gastroenterol.* 12:3180-3185.
- Nagaraj, S., C. Ziske, J. Strehl, D. Messmer, T. Sauerbruch and I.G. Schmidt-Wolf. **2006**. Dendritic cells pulsed with alpha-galactosylceramide induce anti-tumor immunity against pancreatic cancer in vivo. *Int Immunol.* 18:1279-1283.

- Nakhai, H., S. Sel, J. Favor, L. Mendoza-Torres, F. Paulsen, G.I. Duncker and R.M. Schmid. **2007**. Ptf1a is essential for the differentiation of GABAergic and glycinergic amacrine cells and horizontal cells in the mouse retina. *Development*. 134:1151-1160.
- Nakhai, H., J.T. Siveke, B. Klein, L. Mendoza-Torres, P.K. Mazur, H. Algul, F. Radtke, L. Strobl, U. Zimmer-Strobl and R.M. Schmid. **2008**. Conditional ablation of Notch signaling in pancreatic development. *Development*. 135:2757-2765.
- Nelson, B.H. **2010**. CD20+ B cells: the other tumor-infiltrating lymphocytes. *J Immunol*. 185:4977-4982.
- Nguyen, L.T. and P.S. Ohashi. **2015**. Clinical blockade of PD1 and LAG3--potential mechanisms of action. *Nat Rev Immunol*. 15:45-56.
- Nikolich-Zugich, J., M.K. Slifka and I. Messaoudi. **2004**. The many important facets of T-cell repertoire diversity. *Nat Rev Immunol*. 4:123-132.
- Obata, J., M. Yano, H. Mimura, T. Goto, R. Nakayama, Y. Mibu, C. Oka and M. Kawaichi. **2001**. p48 subunit of mouse PTF1 binds to RBP-Jkappa/CBF-1, the intracellular mediator of Notch signalling, and is expressed in the neural tube of early stage embryos. *Genes Cells*. 6:345-360.
- Ostrand-Rosenberg, S. **2010**. Myeloid-derived suppressor cells: more mechanisms for inhibiting antitumor immunity. *Cancer Immunol Immunother*. 59:1593-1600.
- Ostrand-Rosenberg, S. and P. Sinha. **2009**. Myeloid-derived suppressor cells: linking inflammation and cancer. *J Immunol*. 182:4499-4506.
- Ozdemir, B.C., T. Pentcheva-Hoang, J.L. Carstens, X. Zheng, C.C. Wu, T.R. Simpson, H. Laklai, H. Sugimoto, C. Kahlert, S.V. Novitskiy, A. De Jesus-Acosta, P. Sharma, P. Heidari, U. Mahmood, L. Chin, H.L. Moses, V.M. Weaver, A. Maitra, J.P. Allison, V.S. LeBleu and R. Kalluri. **2014**. Depletion of carcinoma-associated fibroblasts and fibrosis induces immunosuppression and accelerates pancreas cancer with reduced survival. *Cancer Cell*. 25:719-734.
- Pan, F.C. and C. Wright. **2011**. Pancreas organogenesis: from bud to plexus to gland. *Dev Dyn*. 240:530-565.
- Pardoll, D.M. **2012**. The blockade of immune checkpoints in cancer immunotherapy. *Nat Rev Cancer*. 12:252-264.
- Parsa, A.T., J.S. Waldron, A. Panner, C.A. Crane, I.F. Parney, J.J. Barry, K.E. Cachola, J.C. Murray, T. Tihan, M.C. Jensen, P.S. Mischel, D. Stokoe and R.O. Pieper. **2007**. Loss of tumor suppressor PTEN function increases B7-H1 expression and immunoresistance in glioma. *Nat Med*. 13:84-88.

- Pello, O.M., M. De Pizzol, M. Mirolo, L. Soucek, L. Zammataro, A. Amabile, A. Doni, M. Nebuloni, L.B. Swigart, G.I. Evan, A. Mantovani and M. Locati. **2012**. Role of c-MYC in alternative activation of human macrophages and tumor-associated macrophage biology. *Blood*. 119:411-421.
- Porembka, M.R., J.B. Mitchem, B.A. Belt, C.S. Hsieh, H.M. Lee, J. Herndon, W.E. Gillanders, D.C. Linehan and P. Goedegebuure. **2012**. Pancreatic adenocarcinoma induces bone marrow mobilization of myeloid-derived suppressor cells which promote primary tumor growth. *Cancer Immunol Immunother*. 61:1373-1385.
- Provenzano, P.P., C. Cuevas, A.E. Chang, V.K. Goel, D.D. Von Hoff and S.R. Hingorani. **2012**. Enzymatic targeting of the stroma ablates physical barriers to treatment of pancreatic ductal adenocarcinoma. *Cancer Cell*. 21:418-429.
- Qian, B.Z. and J.W. Pollard. **2010**. Macrophage diversity enhances tumor progression and metastasis. *Cell*. 141:39-51.
- Qin, H., A.T. Holdbrooks, Y. Liu, S.L. Reynolds, L.L. Yanagisawa and E.N. Benveniste. **2012**. SOCS3 deficiency promotes M1 macrophage polarization and inflammation. *J Immunol*. 189:3439-3448.
- Rahib, L., B.D. Smith, R. Aizenberg, A.B. Rosenzweig, J.M. Fleshman and L.M. Matrisian. **2014**. Projecting cancer incidence and deaths to 2030: the unexpected burden of thyroid, liver, and pancreas cancers in the United States. *Cancer Res*. 74:2913-2921.
- Ren, G., X. Zhao, Y. Wang, X. Zhang, X. Chen, C. Xu, Z.R. Yuan, A.I. Roberts, L. Zhang, B. Zheng, T. Wen, Y. Han, A.B. Rabson, J.A. Tischfield, C. Shao and Y. Shi. **2012**. CCR2-dependent recruitment of macrophages by tumor-educated mesenchymal stromal cells promotes tumor development and is mimicked by TNFalpha. *Cell Stem Cell*. 11:812-824.
- Renaudineau, Y., E. Bariller and J. Olivier Pers. **2001**. B1- and CD5-Positive B Cells. *In* eLS. John Wiley & Sons, Ltd.
- Restifo, N.P., M.E. Dudley and S.A. Rosenberg. **2012**. Adoptive immunotherapy for cancer: harnessing the T cell response. *Nat Rev Immunol*. 12:269-281.
- Rhim, A.D., P.E. Oberstein, D.H. Thomas, E.T. Mirek, C.F. Palermo, S.A. Sastra, E.N. Dekleva, T. Saunders, C.P. Becerra, I.W. Tattersall, C.B. Westphalen, J. Kitajewski, M.G. Fernandez-Barrena, M.E. Fernandez-Zapico, C. Iacobuzio-Donahue, K.P. Olive and B.Z. Stanger. **2014**. Stromal elements act to restrain, rather than support, pancreatic ductal adenocarcinoma. *Cancer Cell*. 25:735-747.
- Royal, R.E., C. Levy, K. Turner, A. Mathur, M. Hughes, U.S. Kammula, R.M. Sherry, S.L. Topalian, J.C. Yang, I. Lowy and S.A. Rosenberg. **2010**. Phase 2 trial of single agent Ipilimumab (anti-CTLA-4) for locally advanced or metastatic pancreatic adenocarcinoma. *J Immunother*. 33:828-833.

- Ryan, D.P., T.S. Hong and N. Bardeesy. **2014**. Pancreatic adenocarcinoma. *N Engl J Med*. 371:1039-1049.
- Sanford, D.E., B.A. Belt, R.Z. Panni, A. Mayer, A.D. Deshpande, D. Carpenter, J.B. Mitchem, S.M. Plambeck-Suess, L.A. Worley, B.D. Goetz, A. Wang-Gillam, T.J. Eberlein, D.G. Denardo, S.P. Goedegebuure and D.C. Linehan. **2013**. Inflammatory monocyte mobilization decreases patient survival in pancreatic cancer: a role for targeting the CCL2/CCR2 axis. *Clin Cancer Res*. 19:3404-3415.
- Schmidt, A., N. Oberle and P.H. Krammer. **2012**. Molecular mechanisms of treg-mediated T cell suppression. *Front Immunol*. 3:51.
- Schonhuber, N., B. Seidler, K. Schuck, C. Veltkamp, C. Schachtler, M. Zukowska, S. Eser, T.B. Feyerabend, M.C. Paul, P. Eser, S. Klein, A.M. Lowy, R. Banerjee, F. Yang, C.L. Lee, E.J. Moding, D.G. Kirsch, A. Scheideler, D.R. Alessi, I. Varela, A. Bradley, A. Kind, A.E. Schnieke, H.R. Rodewald, R. Rad, R.M. Schmid, G. Schneider and D. Saur. **2014**. A next-generation dual-recombinase system for time- and host-specific targeting of pancreatic cancer. *Nat Med*. 20:1340-1347.
- Schreiber, R.D., L.J. Old and M.J. Smyth. **2011**. Cancer immunoediting: integrating immunity's roles in cancer suppression and promotion. *Science*. 331:1565-1570.
- Shevach, E.M. **2009**. Mechanisms of foxp3+ T regulatory cell-mediated suppression. *Immunity*. 30:636-645.
- Shevchenko, I., S. Karakhanova, S. Soltek, J. Link, J. Bayry, J. Werner, V. Umansky and A.V. Bazhin. **2013**. Low-dose gemcitabine depletes regulatory T cells and improves survival in the orthotopic Panc02 model of pancreatic cancer. *Int J Cancer*. 133:98-107.
- Sica, A. and A. Mantovani. **2012**. Macrophage plasticity and polarization: in vivo veritas. *J Clin Invest*. 122:787-795.
- Sica, A., T. Schioppa, A. Mantovani and P. Allavena. **2006**. Tumour-associated macrophages are a distinct M2 polarised population promoting tumour progression: potential targets of anti-cancer therapy. *Eur J Cancer*. 42:717-727.
- Siegel, R., D. Naishadham and A. Jemal. 2012. Cancer statistics, **2012**. *CA Cancer J Clin*. 62:10-29.
- Spaner, D. **2011**. B Lymphocytes in Cancer Immunology. In *Experimental and Applied Immunotherapy*. M.J.a.F. D., editor. Humana Press. 37-57.
- Stanley, E.R., K.L. Berg, D.B. Einstein, P.S. Lee and Y.G. Yeung. **1994**. The biology and action of colony stimulating factor-1. *Stem Cells*. 12 Suppl 1:15-24; discussion 25.

- Sternberg, N. and D. Hamilton. **1981**. Bacteriophage P1 site-specific recombination. I. Recombination between loxP sites. *J Mol Biol.* 150:467-486.
- Stromnes, I.M., J.S. Brockenbrough, K. Izeradjene, M.A. Carlson, C. Cuevas, R.M. Simmons, P.D. Greenberg and S.R. Hingorani. **2014**. Targeted depletion of an MDSC subset unmasks pancreatic ductal adenocarcinoma to adaptive immunity. *Gut.* 63:1769-1781.
- Sun, J.C., J.N. Beilke and L.L. Lanier. **2009**. Adaptive immune features of natural killer cells. *Nature.* 457:557-561.
- Suzuki, E., V. Kapoor, A.S. Jassar, L.R. Kaiser and S.M. Albelda. **2005**. Gemcitabine selectively eliminates splenic Gr-1+/CD11b+ myeloid suppressor cells in tumor-bearing animals and enhances antitumor immune activity. *Clin Cancer Res.* 11:6713-6721.
- Talmadge, J.E. and D.I. Gabrilovich. **2013**. History of myeloid-derived suppressor cells. *Nat Rev Cancer.* 13:739-752.
- Tanaka, Y., C.T. Morita, E. Nieves, M.B. Brenner and B.R. Bloom. **1995**. Natural and synthetic non-peptide antigens recognized by human gamma delta T cells. *Nature.* 375:155-158.
- Tanaka, Y., S. Sano, E. Nieves, G. De Libero, D. Rosa, R.L. Modlin, M.B. Brenner, B.R. Bloom and C.T. Morita. **1994**. Nonpeptide ligands for human gamma delta T cells. *Proc Natl Acad Sci U S A.* 91:8175-8179.
- Topalian, S.L., F.S. Hodi, J.R. Brahmer, S.N. Gettinger, D.C. Smith, D.F. McDermott, J.D. Powderly, R.D. Carvajal, J.A. Sosman, M.B. Atkins, P.D. Leming, D.R. Spigel, S.J. Antonia, L. Horn, C.G. Drake, D.M. Pardoll, L. Chen, W.H. Sharfman, R.A. Anders, J.M. Taube, T.L. McMiller, H. Xu, A.J. Korman, M. Jure-Kunkel, S. Agrawal, D. McDonald, G.D. Kollia, A. Gupta, J.M. Wigginton and M. Sznol. **2012**. Safety, activity, and immune correlates of anti-PD-1 antibody in cancer. *N Engl J Med.* 366:2443-2454.
- van de Laar, L., P.J. Coffey and A.M. Woltman. **2012**. Regulation of dendritic cell development by GM-CSF: molecular control and implications for immune homeostasis and therapy. *Blood.* 119:3383-3393.
- Vincent, A., J. Herman, R. Schulick, R.H. Hruban and M. Goggins. **2011**. Pancreatic cancer. *Lancet.* 378:607-620.
- Vivier, E., S. Ugolini, D. Blaise, C. Chabannon and L. Brossay. **2012**. Targeting natural killer cells and natural killer T cells in cancer. *Nat Rev Immunol.* 12:239-252.

- von Bernstorff, W., M. Voss, S. Freichel, A. Schmid, I. Vogel, C. Johnk, D. Henne-Bruns, B. Kremer and H. Kalthoff. **2001**. Systemic and local immunosuppression in pancreatic cancer patients. *Clin Cancer Res.* 7:925s-932s.
- Vonderheide, R.H. and L.J. Bayne. **2013**. Inflammatory networks and immune surveillance of pancreatic carcinoma. *Curr Opin Immunol.* 25:200-205.
- Vonlaufen, A., S. Joshi, C. Qu, P.A. Phillips, Z. Xu, N.R. Parker, C.S. Toi, R.C. Pirola, J.S. Wilson, D. Goldstein and M.V. Apte. **2008**. Pancreatic stellate cells: partners in crime with pancreatic cancer cells. *Cancer Res.* 68:2085-2093.
- Wang, Y.C., F. He, F. Feng, X.W. Liu, G.Y. Dong, H.Y. Qin, X.B. Hu, M.H. Zheng, L. Liang, L. Feng, Y.M. Liang and H. Han. **2010**. Notch signaling determines the M1 versus M2 polarization of macrophages in antitumor immune responses. *Cancer Res.* 70:4840-4849.
- Wolf, M.J., A. Hoos, J. Bauer, S. Boettcher, M. Knust, A. Weber, N. Simonavicius, C. Schneider, M. Lang, M. Sturzl, R.S. Croner, A. Konrad, M.G. Manz, H. Moch, A. Aguzzi, G. van Loo, M. Pasparakis, M. Prinz, L. Borsig and M. Heikenwalder. **2012**. Endothelial CCR2 signaling induced by colon carcinoma cells enables extravasation via the JAK2-Stat5 and p38MAPK pathway. *Cancer Cell.* 22:91-105.
- Xu, H., J. Zhu, S. Smith, J. Foldi, B. Zhao, A.Y. Chung, H. Outtz, J. Kitajewski, C. Shi, S. Weber, P. Saftig, Y. Li, K. Ozato, C.P. Blobel, L.B. Ivashkiv and X. Hu. **2012**. Notch-RBP-J signaling regulates the transcription factor IRF8 to promote inflammatory macrophage polarization. *Nat Immunol.* 13:642-650.
- Yanaba, K., J.D. Bouaziz, K.M. Haas, J.C. Poe, M. Fujimoto and T.F. Tedder. **2008**. A regulatory B cell subset with a unique CD1dhiCD5+ phenotype controls T cell-dependent inflammatory responses. *Immunity.* 28:639-650.
- Yoshikawa, K., S. Mitsunaga, T. Kinoshita, M. Konishi, S. Takahashi, N. Gotohda, Y. Kato, M. Aizawa and A. Ochiai. **2012**. Impact of tumor-associated macrophages on invasive ductal carcinoma of the pancreas head. *Cancer Sci.* 103:2012-2020.
- Zou, W. **2006**. Regulatory T cells, tumour immunity and immunotherapy. *Nat Rev Immunol.* 6:295-307.
- Zou, W. and N.P. Restifo. **2010**. T(H)17 cells in tumour immunity and immunotherapy. *Nat Rev Immunol.* 10:248-256.

6 APPENDIX

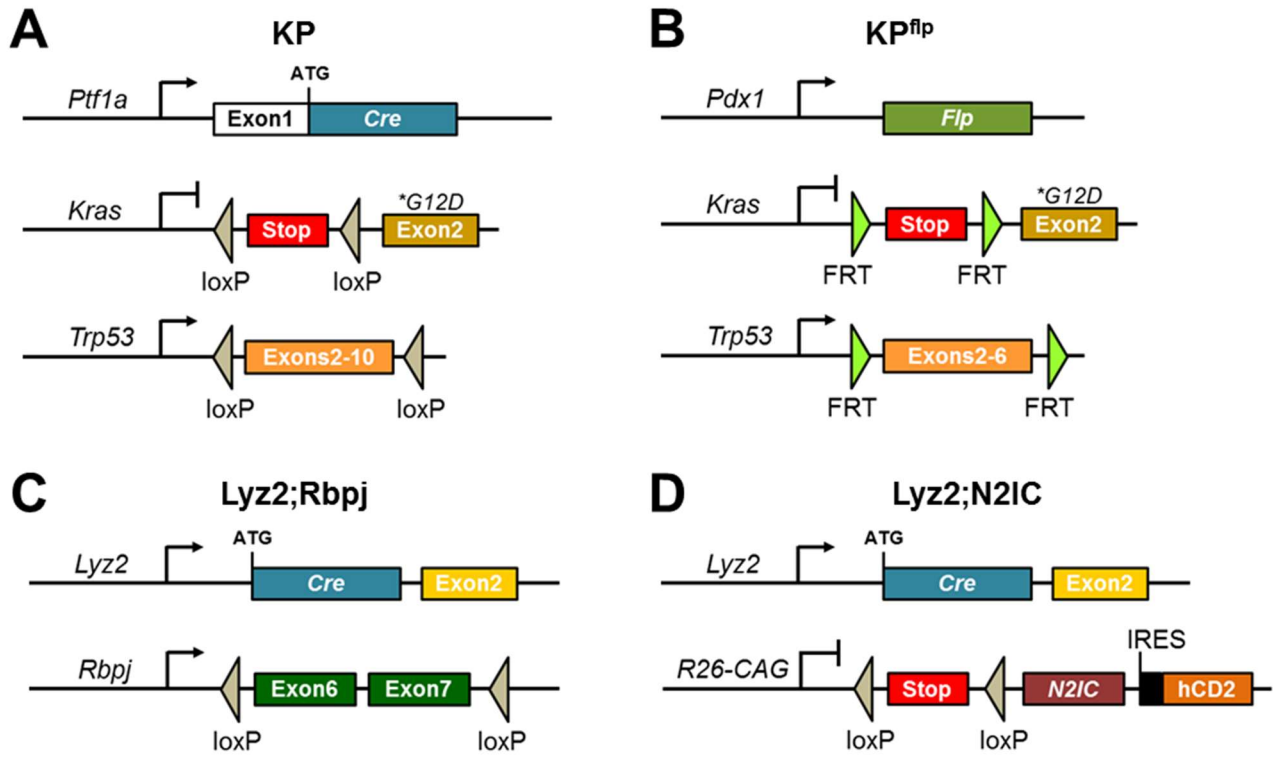


Figure A.1: Mouse crossing strategy. (A) KP mouse model. (B) KP^{flp} mouse model. (C) Lyz2;Rbpj mouse model. (D) Lyz2;N2IC mouse model. KP^{flp} line (B) was crossed to Lyz2;Rbpj (C) generating KP^{flp};Lyz2;Rbpj or to Lyz2;N2IC (D) generating the KP^{flp};Lyz2;N2IC line. IRES: internal ribosomal entry site.

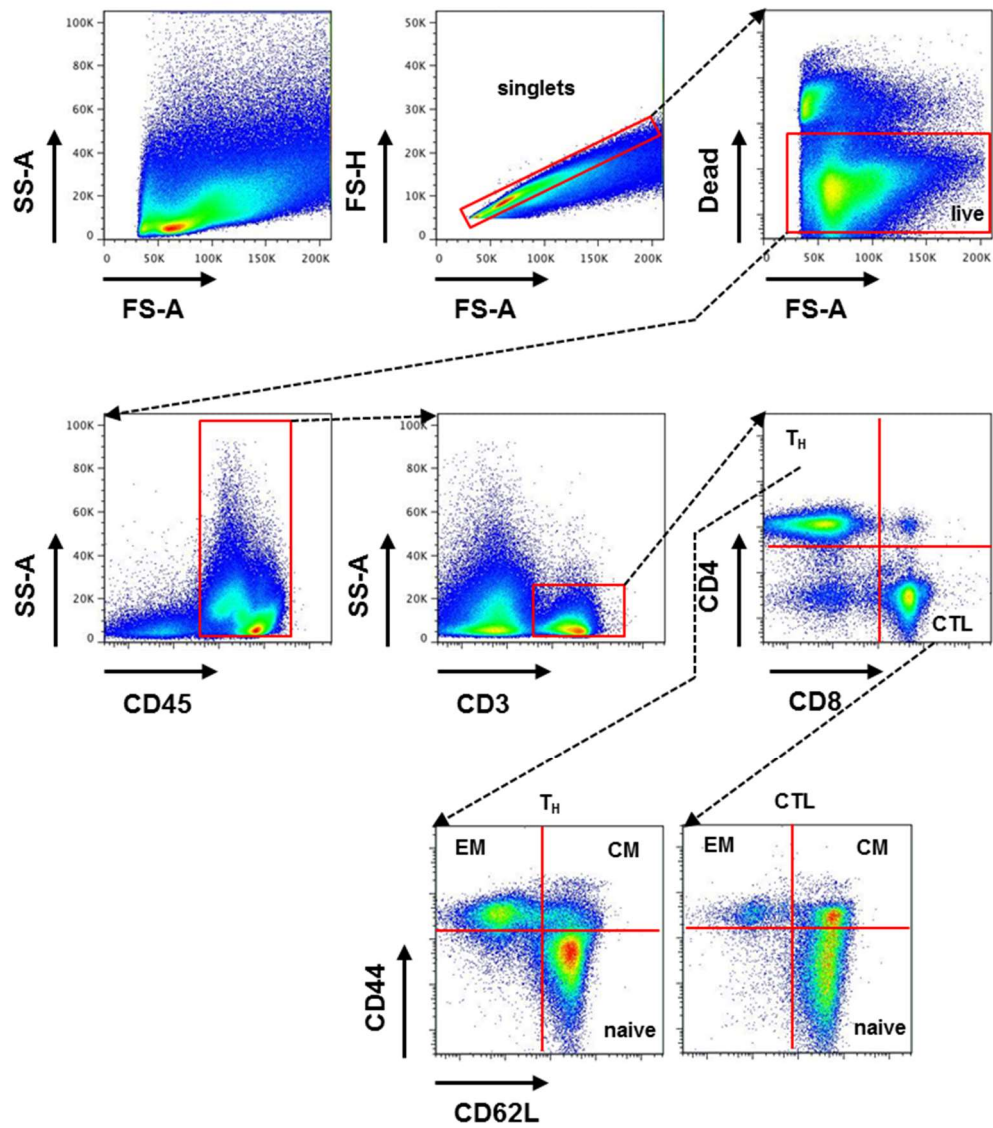


Figure A.2: T cell gating strategy. Example from spleen sample.

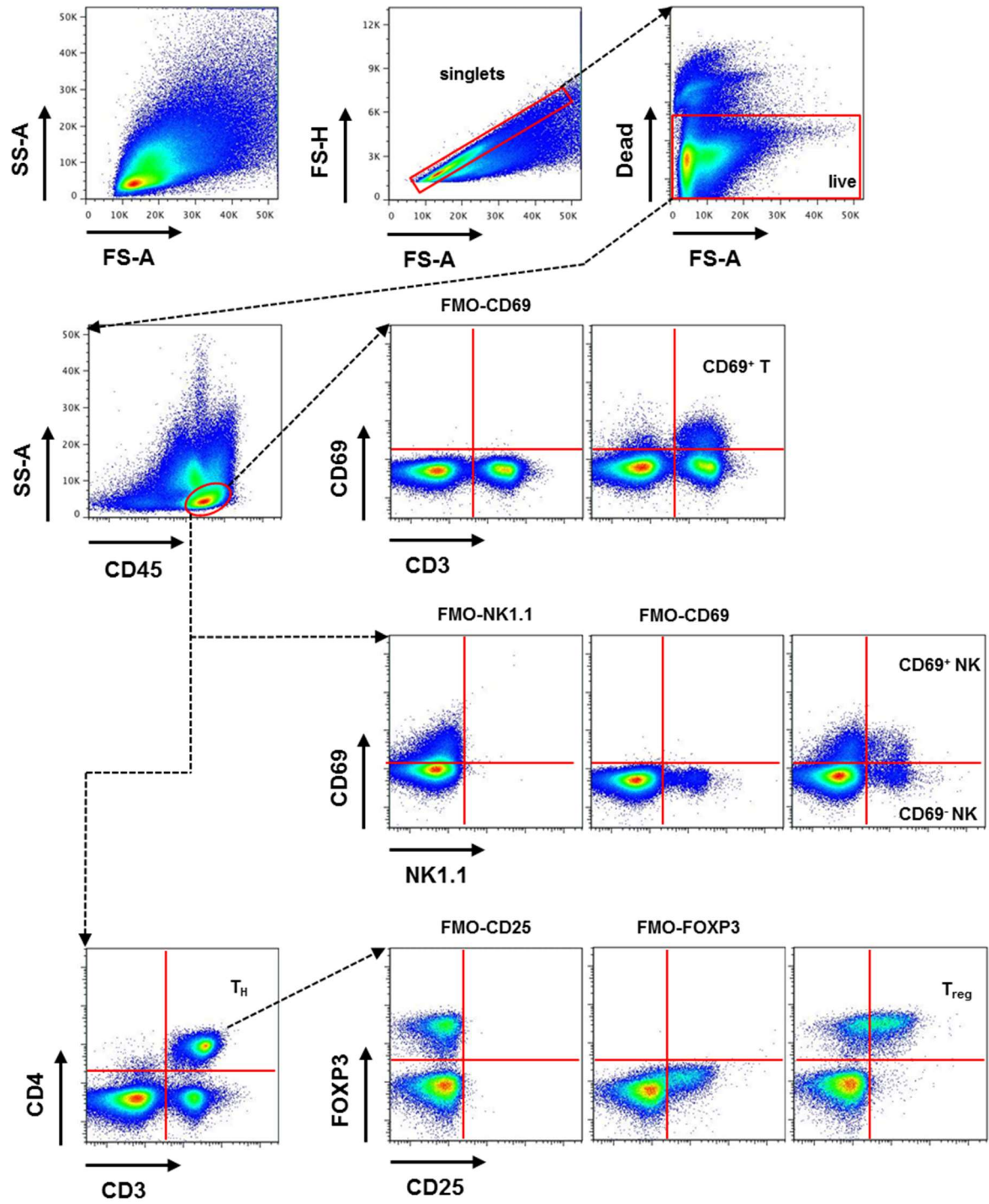


Figure A.3: NK and Treg gating strategy. Example from spleen sample.

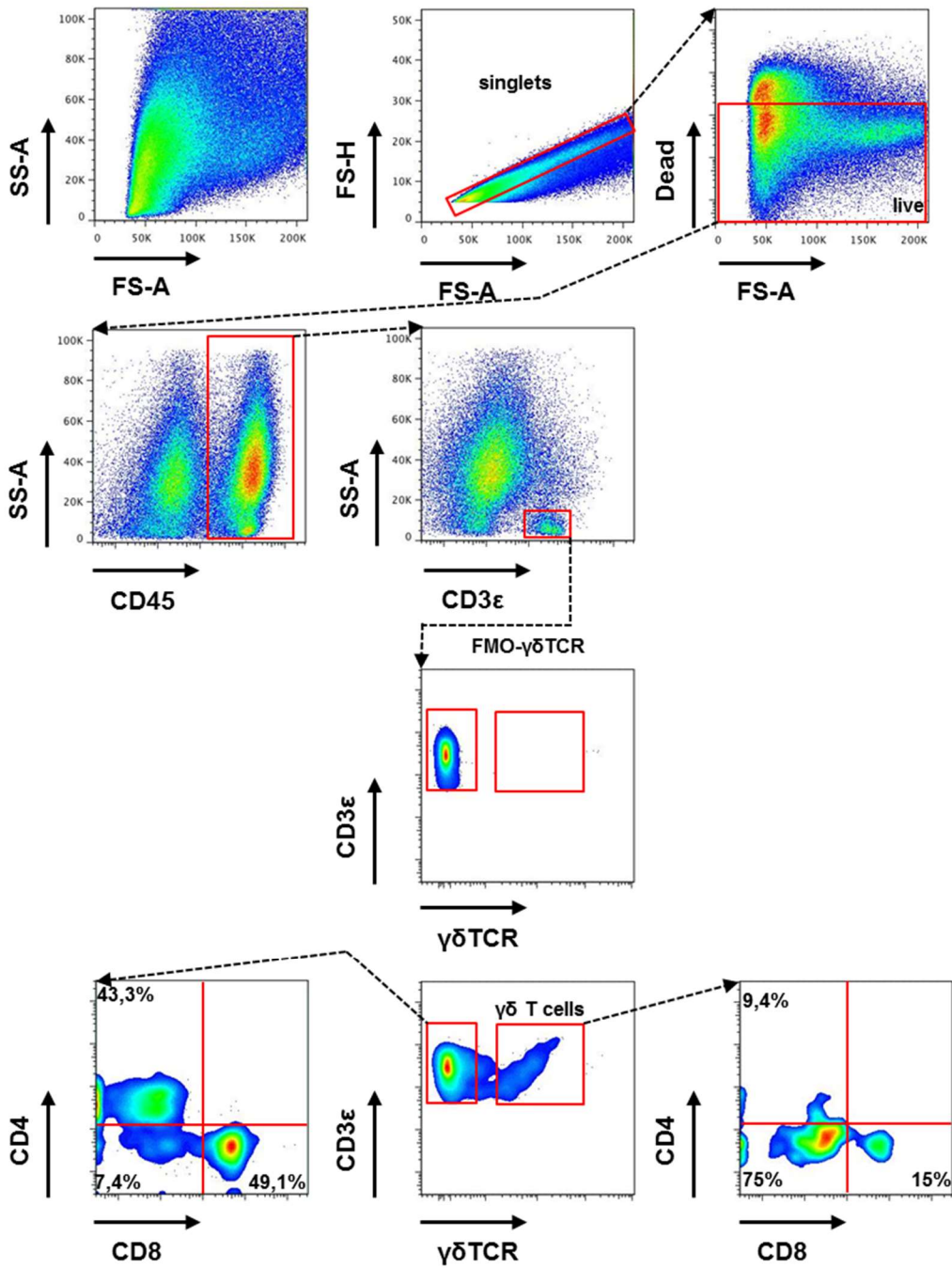


Figure A.4: $\gamma\delta$ T cell gating strategy. Example from tumor sample.

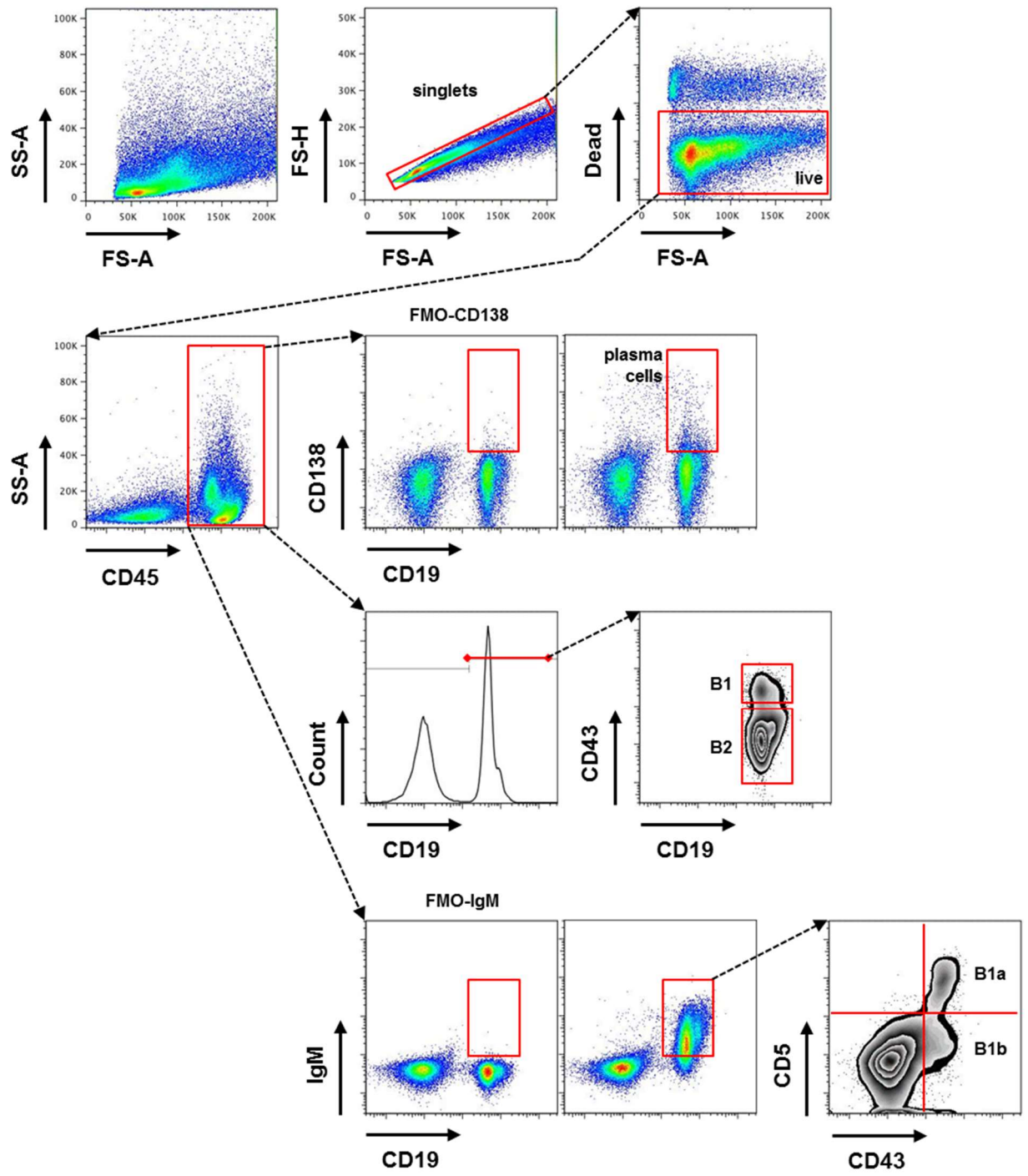


Figure A.5: B cell gating strategy. Example from spleen sample.

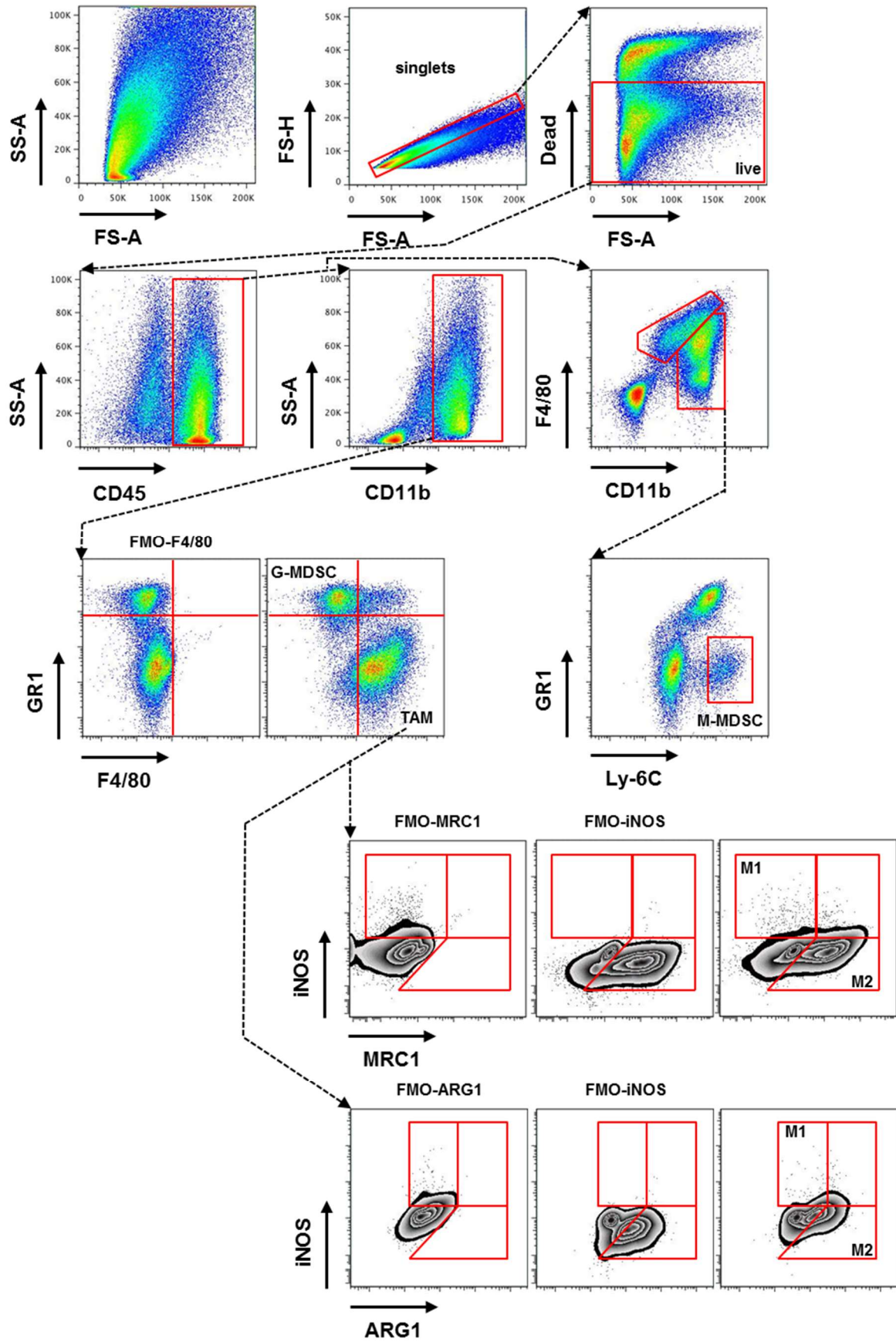


Figure A.6: Myeloid cell gating strategy. Example from tumor sample.

CV

Persönliche Daten

Name	Florian Neff
Geburtsdatum	04. Juli 1985
Geburtsort	Groß-Umstadt
Nationalität	deutsch

Hochschulbildung

09/2011 - heute	Promotion zum Dr. rer. nat. Klinikum rechts der Isar der Technischen Universität München Dissertation: <i>“Exploring the immune environment of pancreatic ductal adenocarcinoma”</i>
10/2006 - 06/2011	Studium der Molekularen Medizin Universität Erlangen-Nürnberg Abschluss: Diplom (1,0) Akademischer Grad: Diplom Molekularmediziner Univ. Diplomarbeit: <i>„Untersuchung des Entstehungsmechanismus N-terminal trunkierter Aβ-Peptide in Astrozyten“</i>

Schulbildung

08/1998 - 07/2005	Max-Planck-Gymnasium, Groß-Umstadt Abschluss: Allgemeine Hochschulreife (1,2)
-------------------	---

Konferenzbeiträge

06/2015	Cell Symposium Cancer, Inflammation, and Immunity Sitges, Spanien, Posterpräsentation
03/2015	2 nd Immunotherapy of Cancer Conference, ITOC2 München, Deutschland, Posterpräsentation
12/2014	AACR Tumor Immunology and Immunotherapy: A new chapter Orlando, USA, Posterpräsentation
09/2014	3 rd International Conference on Tumor Microenvironment and Cellular Stress. Mykonos, Griechenland, Posterpräsentation

Forschungsaufenthalte

- 11/2009 - 01/2010 **University College London**
UCL Cancer Institute
Cancer Research UK Viral Oncology Group
Prof. Christopher Boshoff
- 02/2009 - 08/2011 **Universitätsklinikum Erlangen**
Psychiatrische und Psychotherapeutische Klinik
Abteilung für Molekulare Neurobiologie
Dr. Manuel Maler
- 02 - 04/2008 **Universitätsklinikum Erlangen**
Institut für Klinische und Molekulare Virologie
Nationales Referenzzentrum für Retroviren
Dr. Karin Metzner
- 06 - 08/2006 **Robert Koch Institut, Berlin**
Bundesinstitut für Infektionskrankheiten
und nicht übertragbare Krankheiten
Projektgruppe Neurodegenerative Erkrankungen
Dr. Michael Baier
- 07 - 08/2005 **Paul Ehrlich Institut, Langen**
Bundesinstitut für Sera und Impfstoffe
Abteilung für Mikrobielle Sicherheit und Parasitologie
Dr. Thomas Montag-Lessing

Veröffentlichungen

Mazur PK, Herner A, **Neff F**, Siveke JT, *Current methods in mouse models of pancreatic cancer*. *Methods Mol Biol*, 2015. 1267: pp 185-215.

Oberstein TJ, Spitzer P, Klafki HW, Linning P, **Neff F**, Knölker HJ, Lewczuk P, Wiltfang J, Kornhuber J, Maler JM, *Astrocytes and microglia but not neurons preferentially generate N-terminally truncated A β peptides*. *Neurobiol Dis*, 2015. 73: pp 24-35.

DANKSAGUNG

Zahlreichen Personen gilt Dank für ihre Unterstützung beim Gelingen dieser Arbeit:

Prof. Jens Siveke für die Vergabe des Forschungsthemas und seine Bereitschaft das Projekt jederzeit finanziell zu fördern – auch in Zeiten, als Erfolge auf sich warten ließen.

Frau Prof. Aphrodite Kapurniotu für ihre Mitwirkung als Gutachterin.

Prof. Mathias Heikenwälder für exzellente experimentelle Unterstützung durch seine Arbeitsgruppe, seinen fortwährenden Ideenreichtum und die Mitwirkung im Thesis Advisory Committee.

Prof. Marc Schmidt-Supprian für die Überlassung rekombinanter NLS-TAT-CRE und diskussionsfreudiger Teilnahme am Thesis Advisory Committee, Prof. Roland Schmid für seine Mitwirkung im Thesis Advisory Committee und die finanzielle Unterstützung bei einer Kongressteilnahme, Prof. Alexander Bazhin und Svetlana Karakhanova für die Zusammenarbeit und Expertise im B7H1 Projekt, Ruth Hillermann und Daniel Kull für ihre hochprofessionelle Unterstützung in der Immunhistochemie, dem DKTK Standort München für die Möglichkeit der Benutzung der FACS Einrichtung.

Der Internationalen Max Planck Research School for Molecular and Cellular Life Sciences für ein sechsmonatiges Stipendium, weitreichende Finanzierung mehrerer Kongressreisen und exzellente überfachlicher Qualifizierung. Hans Jörg Schäffer, Ingrid Wolf, Maximiliane Reif, Katharina Frank und Ruth Willmot, durch sie alle lebt und funktioniert eine Graduiertenschule, wie es keine zweite gibt - hoch professional und immer *für* den Doktoranden.

Allen gegenwärtigen und früheren Mitgliedern der Arbeitsgruppe Siveke und Mitarbeitern aller Forschungsgruppen der II. Medizinische Klinik.

Meinem Freund Thomas, meiner Familie und Freunden, die im Hintergrund wirkten und die letzten vier Jahre zu lebenswerten Jahren gemacht haben.